METABOLIC REGULATION OF TRANSCRIPTION

THROUGH COMPARTMENTALIZED NAD^+ BIOSYNTHESIS

APPROVED BY SUPERVISORY COMMITTEE

W. Lee Kraus, Ph.D.

Ralph Deberardinis, M.D., Ph.D.

Joel Elmquist, D.V.M., Ph.D.

David Mangelsdorf, Ph.D.

DEDICATION

TO ALL THE PEOPLE I LOVE, ESPECAILLY TO MY GRANDMOTHER

METABOLIC REGULATION OF TRANSCRIPTION

THROUGH COMPARTMENTALIZED NAD^+ BIOSYTNEHSIS

by

KEUN WOO RYU

DISSERTATION

Presented to the Faculty of the Graduate School of Biomedical Sciences

The University of Texas Southwestern Medical Center at Dallas

In Partial Fulfillment of the Requirements

For the Degree of

DOCTOR OF PHILOSOPHY

The University of Texas Southwestern Medical Center at Dallas

Dallas, Texas

December 2017

ACKNOWLEDGMEN

I would thank my supervisor, Dr. W. Lee Kraus, for his constant supports throughout my time in the graduate school. As a graduate student in Kraus Lab, I learned how to carry out a research project and how to be an independent scientist. He fully supported me to develop my own ideas and test the hypothesis with various cutting-edge techniques. I also want to thank him for giving me wonderful opportunities to attend and present my work at the numerous conferences that allowed me to meet and interact with the leading scientists in the field. I believe my time in the Kraus lab helped me to become a better scientist and I appreciate Lee for all the support.

I would also like to thank to the members of my thesis committee, Dr. Ralph Deberardinis, Dr. David Mangelsdorf and Dr. Joel Elmuqist for the oversight on my progress, insightful scientific comments and advice throughout my graduate school. I also want to express my sincere gratitude to Dr. Sue-Goo Rhee, for his mentoring and encouragement during my time in Ewha University. His enthusiasm towards science always inspired me and led me to pursue my career in the biological science. I also want to thank Dr. Ji Yeon Kim and Dr. Rana Gupta for all the insightful discussions and helpful collaboration related to my thesis project.

My time in graduate school would have not been the same without my friends and colleagues. I would like to thank all the past and current Kraus lab and Green Center members for their helps throughout my graduate school. Thanks to Bryan Gibson and Xin Luo for the thoughtful and exciting scientific discussion over various topics. I also want to

thank Tulip Nandu for his computational support. I also want to give my thanks to Rebecca Gupte, Sara Martire, Melodi Tastemel, Ziying Liu, Balaji Parameswaran, Shrikanth Gadad, and Dae-Seok Kim for their wonderful companionship and kind support.

I would like to express my very special thanks to Anna Lee for all the support, patience, and caring. I feel very lucky that I could go through my time in graduate school with her. I am truly grateful about all the moments that we spent together and all the support she gave me.

Lastly, and most importantly, I want to thank my family for their endless love and support. I am deeply grateful to my parents for having faith in me all the time. They are my life-long role models and they mean more than anything to me. I also want to thank my sister for all the support. I want to express my biggest love and appreciation to my grandmother, who was waiting for this moment more than anyone. No matter where I am, she is always going to be in my heart.

Graduate school was a long journey. I couldn't be here without all the support that I got from all the people around me. I wish all and each of them the best for their future careers and lives.

BIOGRAPHICAL SKETCH

Keun Woo Ryu was born in Daejeon, South Korea, but spend most of his childhood in Pohang, South Korea. He started her undergraduate education at the Seoul National University in 2003, where he learned fundamentals of biology and chemistry. During his undergraduate education, he served 2 years of military service in army. After receiving his B.S. degree with cum laude in 2009, he joined the laboratory of Dr. Sue-Goo Rhee in Ewha University as a research technician. During his time as a research technician, he worked on independent project to understand the mechanism of how cytosolic Sulfiredoxin (Srx) regulates mitochondrial antioxidant enzyme Pereoxiredoxin 3 (Prx3). In 2010, he started his graduate study in Genes, Development and Disease program at the University of Texas Southwestern Medical Center at Dallas. In 2011, he joined the laboratory of Dr. W. Lee Kraus for his dissertation study to understand how compartmentalized NAD^+ synthesis regulates signal-dependent gene expression. Using cell-based, genomic and molecular approaches, his work provided a novel insight on the molecular mechanisms of NAD^+-dependent transcriptional regulation. In 2017, he completed his thesis study and received Ph.D. in biomedical sciences.

METABOLIC REGULATION OF TRANSCRIPTION

THROUGH COMPARTMENTALIZED NAD$^+$ BIOSYTNEHSIS

Publication No._____

Keun Woo Ryu, Ph.D.

The University of Texas Southwestern Medical Center at Dallas, 2017

Supervising Professor: W. Lee Kraus, Ph.D.

Extracellular signaling and nutrient availability are major factors for the cell fate decision. Responds to extracellular information requires metabolic alterations and differential gene expression. Recently emerging concept of metabolic regulation of transcription reveals that fluctuation of metabolite levels could modulate the activities of enzymes involved in gene regulation, which require substrates or cofactors that are intermediates of cell metabolism. However, how cells integrate extracellular signals (e.g. hormones) and cellular metabolic status to coordinate transcriptional outcome is poorly understood.

Nicotinamide adenine dinucleotide (NAD^+) is an essential small molecule co-factor in metabolic redox reactions as well as a substrate for many NAD^+-dependent enzymes, such as poly(ADP-ribose) polymerases (PARPs; e.g., PARP-1) or sirtuins (SIRTs; e.g., SIRT-1), which many of them are known to play an important role in gene regulation. In mammalian cells, NAD^+ is synthesized from nicotinamide mononucleotide (NMN) and ATP, by the family of enzymes known as nicotinamide mononucleotide adenylyl transferases (NMNATs). NMNATs exhibit unique subcellular localizations: NMNAT-1 in the nucleus NMNAT-2 in the cytosol and Golgi, and NMNAT-3 in the mitochondria, suggesting the compartmentalized regulation of NAD^+ biosynthesis within the cell. However, the biological role of this compartmentalized NAD^+ synthesis is largely unknown. Interestingly, NAD^+ synthesizing enzymes localize at the subcellular compartment where the transcription (nucleus) or the cellular metabolism (cytoplasm and mitochondria) occurs. Using adipogenesis as a model, we found that compartmentalized NAD^+ synthesis acts to integrate cellular glucose metabolism and the adipogenic transcription program during adipocyte differentiation. Nuclear NAD^+ is depleted by the induction of cytoplasmic NMNAT-2, whose levels rapidly increase concomitantly with glucose metabolism during differentiation. Competition between nuclear NMNAT-1 and cytoplasmic NMNAT-2 for the common substrate, nicotinamide mononucleotide (NMN), leads to a precipitous reduction in nuclear NAD+ synthesis by NMNAT-1. This inhibits the catalytic activity of poly(ADP-ribose) polymerase 1 (PARP-1), an NAD^+-dependent nuclear enzyme that ADP-ribosylates and inhibits the adipogenic transcription factor, C/EBPβ. Subsequent reversal of PARP-1-mediated repression and enhanced binding of C/EBPβ to adipogenic target genes drives

differentiation. Thus, compartmentalized NAD^+ synthesis functions as an integrator of cellular metabolism and signal-dependent transcriptional programs.

TABLE OF CONTENTS

PRIOR PUBLICATIONS

Luo, X.*, **Ryu, K.W.***, Kim, D.S., Nandu, T., Medina, C.J., Gupte, R., Gibson, B.A., Soccio, R.E., Yu, Y., Gupta, R.K., et al. (2017). PARP-1 Controls the Adipogenic Transcriptional Program by PARylating C/EBPbeta and Modulating Its Transcriptional Activity. ***Molecular Cell*** 65, 260-271. ***Co-first author**

Ryu, K.W., and Kraus, W.L. (2016). Who Put the "A" in ATP? Generation of ATP from ADP-Ribose in the Nucleus for Hormone-Dependent Gene Regulation. ***Molecular Cell*** 63, 349-351.

Kil, I.S., **Ryu, K.W.**, Lee, S.K., Kim, J.Y., Chu, S.Y., Kim, J.H., Park, S., and Rhee, S.G. (2015). Circadian Oscillation of Sulfiredoxin in the Mitochondria. ***Molecular Cell*** 59, 651-663.

Ryu, K.W.*, Kim, D.S.*, and Kraus, W.L. (2015). New facets in the regulation of gene expression by ADP-ribosylation and poly(ADP-ribose) polymerases. ***Chemical Reviews*** 115, 2453-2481. ***Co-first author**

Kil, I.S., Lee, S.K., **Ryu, K.W.**, Woo, H.A., Hu, M.C., Bae, S.H., and Rhee, S.G. (2012). Feedback control of adrenal steroidogenesis via H2O2-dependent, reversible inactivation of peroxiredoxin III in mitochondria. ***Molecular Cell*** 46, 584-594.

Zhang, T., Berrocal, J.G., Yao, J., DuMond, M.E., Krishnakumar, R., Ruhl, D.D., **Ryu, K.W.**, Gamble, M.J., and Kraus, W.L. (2012). Regulation of poly(ADP-ribose) polymerase-1-dependent gene expression through promoter-directed recruitment of a nuclear NAD+ synthase. ***The Journal of Biological Chemistry*** 287, 12405-12416.

LIST OF FIGURES

LIST OF ABBREVIATION

3T3 cells – Cell lines established from the primary mouse embryonic fibroblast cells from Swiss mouse embryo tissue cultured by "3-day transfer, inoculum 3 x 105 cells"

3T3-L1 – A cell line derived from Swiss 3T3 cells that have a potential to differentiate into adipocyte upon adipogenic stimuli

4-OHT – 4-Hydroxytamoxifen

5hmC – 5-Hydroxymethylcytosine

5mC – 5-methylcytosine

Adipoq – Adiponectin

ALC1 – Amplified in liver cancer 1

APLF – Aprataxin PNK-like factor

ATP – Adenosine Triphosphate

BRCT – BRCA1 C-terminal

C/EBPα (Cebpa) – CCAAT-enhancer-binding protein alpha

C/EBPβ (Cebpb) – CCAAT-enhancer-binding protein beta

C/EBPδ (Cebpd) – CCAAT-enhancer-binding protein delta

CBP – CREB binding protein

Cdk8 – Cyclin-dependent kinase 8

CHFR – Checkpoint protein with FHA and RING domains

ChIP – Chromatin immunoprecipitation

CLOCK – Circadian locomotor output cycles kaput

Dnmt1 – DNA methyltransferase 1

Dox – Doxycycline

Elk1 – ETS transcription factor 1

ER – Estrogen receptor

Fabp4 – Fatty acid binding protein 4

FACT – Facilitates chromatin transcription

FXR – Farnesoid X receptor

GTeX – Genotype-Tissue Expression Consortium Project

H2A – Histone H2A

H2Av – *Drosophila* Histone H2A variant (a homolog of mammalian H2Az and H2Ax)

H2AX – Histone H2AX

H3 – Histone H3

H4 – Histone H4

HAT – Histone acetyltransferase

HDAC3 – Histone deacetylase

HES1 – Hairy and enhancer of split-1

IBMX – 3-isobutyl-1-methylxanthine

ISWI – Chromatin remodeling complex ATPase chain Iswi

KDM4D – Lysine demethylase 4D

KDM5B – Lysine demethylase 5B

LAP – Liver-enriched activator protein

LIP – Liver-enriched inhibitory protein

MacroH2A – Histone H2A variant containing macro domain

MCF-7 – Human breast adenocarcinoma cell line

NA – Nicotinic Acid

NAD^+ – Nicotinamide adenine dinucleotide (Oxidized form)

NADH – Nicotinamide adenine dinucleotide (Reduced form)

NADS – NAD synthetase

NAM – Nicotinamide

NaMN – Nicotinic acid mononucleotide

NAMPT – Nicotinamide phosphoribosyltransferase

NAPRT – Nicotinic acid phosphoribosyltransferase

NAR – Nicotinic acid riboside

NCoR – Nuclear receptor co-repressor

NELF-E – Negative elongation factor E

NF-κB – Nuclear factor kappa-light-chain-enhancer of activated B cells

NFAT – Nuclear factor of activated T-cells

NIH/3T3 – Mouse embryo fibroblast cell line

NLS – Nuclear localization sequence

NMN – Nicotinamide Mononucleotide

NMNAT – Nicotinamide mononucleotide adenylyl transferase

$Nmnat1^{loxp/loxp}$ – Nuclear factor of activated T-cells

NR – Nicotinamide riboside

NRK – Nicotinamide riboside kinases

NuRD – Nucleosome remodeling deacetylase

OB fold – Oligonucleotide/Oligosaccharide-binding Fold

p300 – E1A binding protein p300

PAR – Poly(ADP-ribose)

PARG – Poly(ADP-ribose) glycohydrolase

PARP – Poly(ADP-ribose) polymerase

PBZ – PAR-Binding Zinc finger

$PPAR_Y$ (Pparg2) – Peroxisome proliferator-activated receptor gamma

qPCR – Quantitative PCR

RNF146 – Ring finger protein 146

SG – Stress granules

shRNA – Short hairpin RNA

SIRT – Sirtuin

Smad – SMA-and MAD-related protein

Sox2 – SRY (sex determining region Y)-box 2 transcription factor

Sp1 – Specificity protein 1

SSB1 – Ribosome-associated molecular chaperone

ssDNA – Single-stranded DNA

SVF – Stromal vascular fraction

Tet2 – Tet methylcytosine dioxygenase 2

TLE1 – Transducin-like enhancer protein 1

TopoII – DNA topoisomerase 2-beta

Ub24B – Ubiquitylation assembly factor 4B

WGR – Tryptophan-, glycine-, arginine-rich

Wlds – Wallerian degeneration slow

WWE – Tryptophan-tryptophan-glutamate

XRCC1 – X-ray repair cross-complementing protein 1

YY1 – Yin Yang 1 transcriptional repressor protein

CHAPTER ONE

Introduction

The Information described in this chapter is selected sections from the prior publication in Ryu, KW et al., Chemical Reviews 2015.

1.1 Summary

Extracellular signaling and nutrient availability are major factors for the cell fate determination (Lu and Thompson, 2012). Responds to extracellular information requires metabolic alterations and differential gene expression (Boukouris et al., 2016). Metabolic regulation of transcription rely on the fluctuation of metabolite levels, which are often intermediates of cell metabolism, to modulate the activities of enzymes involved in gene regulation (Lu and Thompson, 2012). However, it is still unclear how cells integrate cellular metabolic status and signal-dependent transcription. NAD^+ is an essential small molecule co-factor that involves in various cellular metabolic pathways as well as a substrate for many NAD^+-dependent enzymes, such as PARPs or SIRTs that are known to play an important role in gene regulation. NAD^+ is synthesized in distinct cellular compartment by the family of enzymes NMNATs, which exhibits unique cellular localization. Using adipogenesis as a model system, I ought to investigate the molecular mechanisms of how compartmentalized NAD^+ synthesis integrate cellular metabolism and signal-dependent gene regulation.

1.2 NAD^+ as a Signaling Moleucle

More than a century ago, nicotine adenine dinucleotide (oxidized form, NAD^+) was first discovered as a cofactor in fermentation (Berger et al., 2004). Subsequent years of study have revealed it to be a universal energy-carrying molecule that acts as a cofactor in multiple cellular redox reactions. In these reactions, this pyridine nucleotide is reversibly oxidized (NAD^+) or reduced (NADH) by various oxidoreductases, yet the total pool remains unaltered.

A novel aspect of NAD^+ as a signaling molecule has emerged more recently, with the identification of NAD^+-dependent enzymes, such as PARPs and SIRTs. These enzymes use NAD^+ as a substrate to catalyze their respective enzymatic reactions. However, unlike oxidoreductases, NAD^+-dependent enzymes irreversibly degrade NAD^+, which can lead to the depletion of cellular NAD^+ contents (Chiarugi et al., 2012). Thus, the regeneration and maintenance of nuclear NAD^+ is crucial for maintaining cellular signaling function.

1.2.1 NAD^+ Biosynthesis Pathways

NAD^+ can be synthesized from L-tryptophan via the *de novo* pathway or from other nucleotides via the salvage pathway (**Figure 1.1**) (Chiarugi et al., 2012). In the *de novo* pathway, tryptophan is converted to quinolinic acid, which is subsequently processed by quinolinate phosphoribosyltransferase (QPRT) to form nicotinic acid mononucleotide (NaMN), a pyridine mononucleotide precursor for NAD^+ (Houtkooper et al., 2010). Alternatively, the salvage pathway utilizes the nucleobases, nicotinic acid (NA) and nicotinamide (NAM), and nucleosides, nicotinamide riboside (NR) and nicotinic acid riboside (NAR), to generate a pyridine mononucleotide (Chiarugi et al., 2012). Nicotinic acid phosphoribosyltransferase (NAPRT) converts NA to NaMN, while nicotinamide phosphoribosyltransferase (NAMPT) and nicotinamide riboside kinases (NRKs) use NAM and NR, respectively, to generate nicotinamide mononucleotide (NMN), another pyridine mononucleotide precursor for NAD^+ (Chiarugi et al., 2012).

The only enzyme shared by both NAD^+ synthesis pathways is NMNAT, which condenses ATP and a pyridine mononucleotide, NMN or NaMN, to generate pyridine

dinucleotide NAD^+ or $NaAD^+$, respectively, and $NaAD^+$ is further catalyzed by NAD synthetase (NADS) to produce NAD^+ (Petrelli et al., 2011). Given that NMNAT is the only enzyme known to catalyze such reactions and is the only common enzyme between both the *de novo* and salvage pathways, NMNAT is considered an indispensible enzyme for NAD^+ biosynthesis.

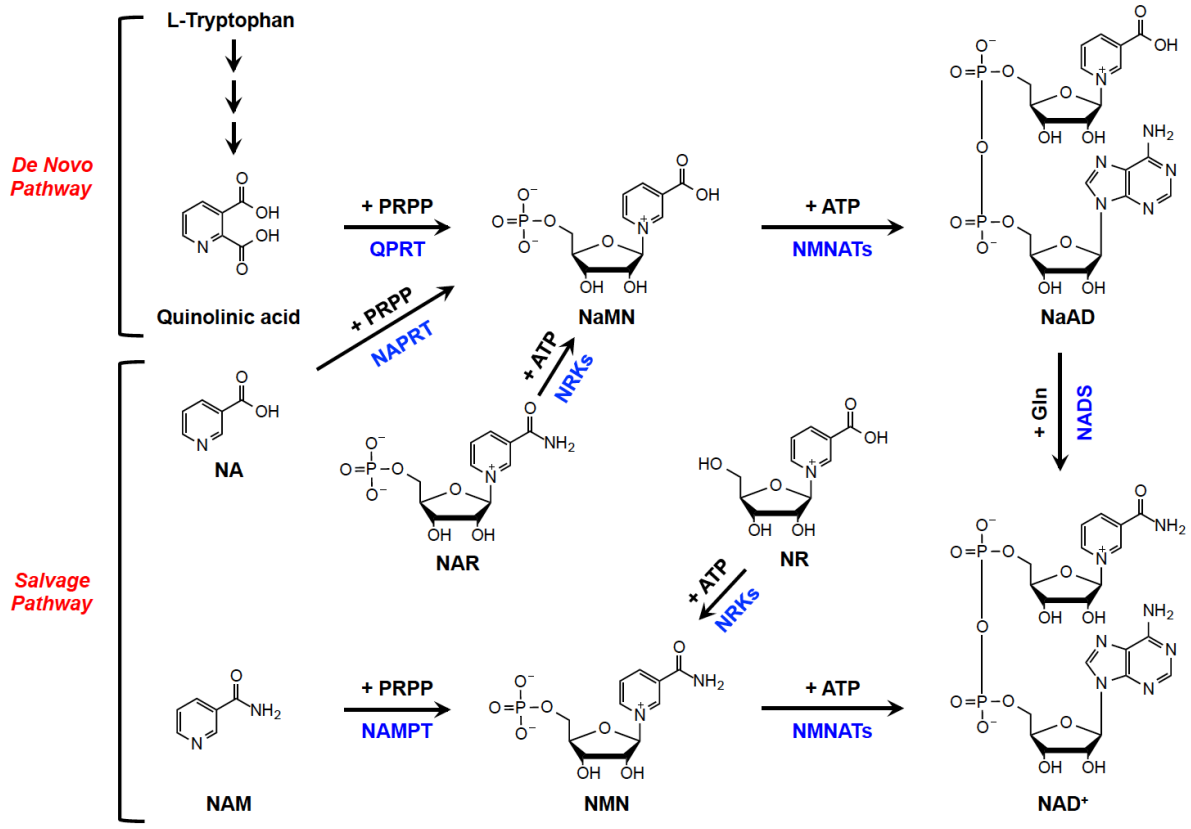

Figure 1.1. NAD^+ biosynthetic pathways.
In mammals, NAD^+ can be synthesized *de novo* from L-tryptophan (the *de novo* pathway) or from other nucleotides such as nucleobases or nucleosides (the salvage pathway).

1.2.2 NMNATs

The enzymatic activity of NMNATs was first discovered in the 1950s by Arthur Kornberg, who detected an enzymatic activity in yeast extracts that catalyzes the synthesis of NAD^+ from NMN and ATP (Kornberg, 1948). Additional studies revealed that NMNAT transfers the adenylyl moiety from ATP to NMN or NaMN and releases pyrophosphate and also catalyzes a reversible reaction through its NAD^+ pyrophosphorylase activity (Kornberg and Pricer, 1951). *In vitro*, equilibrium favors the reverse reaction (Berger et al., 2005), but under physiological conditions, NAD^+ synthesis is preferred, possibly due to abundant ATP levels and limited pyrophosphate concentrations.

Human NMNAT (hNMNAT) belongs to the nucleotidyl transferase superfamily and exists as three isoforms (NMNAT-1, NMNAT-2, and NMNAT-3), which are numbered according to the order in which they were cloned (Emanuelli et al., 2001; Raffaelli et al., 2002; Zhang et al., 2003), These NMNAT isoforms exhibit different tissue expression patterns and, more interestingly, unique subcellular localizations: NMNAT-1 in the nucleus (Berger et al., 2005; Schweiger et al., 2001), NMNAT-2 in the cytosol and Golgi (Berger et al., 2005; Zhang et al., 2003), and NMNAT-3 in the cytosol and mitochondria (Berger et al., 2005; Zhang et al., 2003). Although evidence to support the contention that cells have a compartmentalized pool of NAD^+ is limited, mainly due to the lack of *in vivo* NAD^+ detection methods, this unique subcellular localization of NMNATs suggests that NAD+ biosynthesis and subsequently, pool of NAD^+ is also compartmentalized within the cell. Indeed, overexpression of hNMNAT-1 in MCF7 cells increased NAD(P)H levels only in the nucleus while having no effect on the cytosolic or mitochondrial pool of NAD(P)H (Wang et

al., 2012). Additionally, depletion of NMNAT-1 in primary myoblasts decreased mitochondrial DNA contents in the cell, where NMNAT-2 or NMNAT-3 depletion didn't, indicating the distinct role of nuclear NAD^+ synthesis by NMNAT-1 in the regulation of cellular process (Gomes et al., 2013). Moreover, *Nmnat1* null mice have been reported to be embryonic lethal (Conforti et al., 2011), indicating that the cytosolic or mitochondrial pool of NAD^+ cannot compensate for the loss of nuclear NAD^+ production during embryonic development. These data support the possibility that NAD^+ is compartmentalized; however, additional studies are needed, and a key step in determining the compartmentalization of NAD^+ will be to establish technologies that allow direct detection of NAD^+.

Structural analyses have revealed clearer insight into how hNMNAT utilizes pyridine mononucleotides and ATP to generate NAD^+. Three independent groups solved crystal structures of hNMNAT-1 and found the enzyme to be a homo-hexameric protein (**Figure 1.2A**) (Garavaglia et al., 2002; Werner et al., 2002; Zhou et al., 2002). Each monomer contains six parallel β-sheets flanked by α-helices containing the mononucleotide-binding motif (Garavaglia et al., 2002; Werner et al., 2002; Zhou et al., 2002). Ligand binding of hNMNAT-1 is mediated by a number of conserved amino acids. Trp169 (conserved in all NMNAT sequences) stacks against the pyridine ring of nicotinamide, and Trp92 (conserved among the human NMNATs) interacts with the pyridine ring in face-to-edge fashion on the other side (Werner et al., 2002; Zhou et al., 2002), Trp92, together with Glu94, also interacts with the ribose oxygen, while Ser16 and Lys57 contact the ribose phosphate (Werner et al., 2002). An interesting feature of the hNMNAT-1 active site compared with bacterial and archaeal NMNAT is the presence of structural water molecules (ω), which together with

Asp173 can subtly change the electrostatic distribution within the substrate-binding site, allowing hNMNAT-1 to bind NMN and NaMN without conformational changes (Zhou et al., 2002).

1.3 Overview of PARPs

In 1963, Chambon *et al.* reported the detection of a nicotinamide mononucleotide-activated, DNA-dependent enzymatic activity in rat liver extracts that catalyzed the synthesis of a polyadenylic acid (Chambon et al., 1963). The product of this reaction was later identified as poly(ADP-ribose) or PAR, a polymer of ADP-ribose (ADPR) monomers derived from the oxidized form of NAD^+ (Futai et al., 1967; Nishizuka et al., 1967; Reeder et al., 1967; Shimizu et al., 1967; Sugimura et al., 1967). These initial studies have led to half a century of research on the chemistry, enzymology, structure, function, biology, physiology, and pathology of ADPR, PAR, and their derivatives, as well as the enzymes that catalyze their synthesis and degradation, and the effector proteins that interact with or are posttranslationally modified by them.

1.3.1 The PARP Family

The synthesis of PAR from NAD^+ is catalyzed by poly(ADP-ribose) polymerase (PARP) enzymes belonging to the PARP family (EC 2.4.2.30), which contains at least 17 distinct proteins (Hanai et al., 2004; Schreiber et al., 2006). Not all PARP family members are enzymatically active, and some may function as mono(ADP-ribosyl)transferases rather

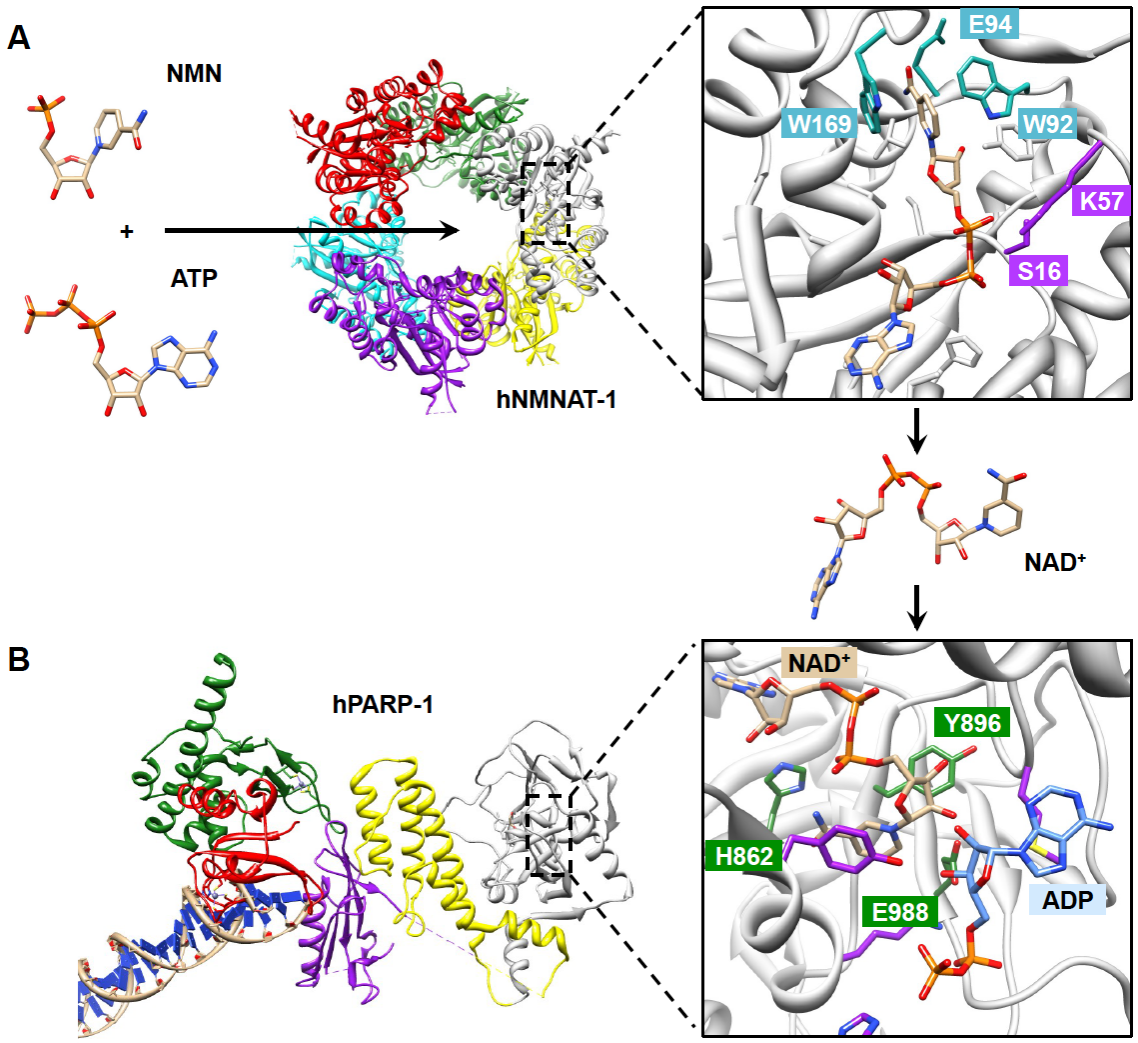

Figure 1.2. Mechanisms of NAD^+ synthesis and utilization.
(A) NAD^+ synthesis by NMNAT-1. NMN and ATP bind to the mononucleotide-binding motif of NMNAT-1, which catalyzes generation of NAD^+. The crystal structure of hNMNAT-1 bound by NAD^+ reveals conserved amino acid residues (W169, W92, and E94 in cyan, S16 and K57 in purple) that mediate its catalytic reaction (PDB: 1KQN) (Zhou et al., 2002). (B) The structure of hPARP-1 bound to DNA (PDB: 4DQY) (Langelier et al., 2012). PARP-1 utilizes NAD^+ to generate PAR polymers. NAD^+ (left, shown in light brown) was positioned into the catalytic domain of hPARP-1 bound by carba-NAD (cNAD (PDB: 1A26))(Ruf et al., 1998) by homology modeling with NAD^+ bound diphtheria toxin (PDB: 1TOX). The triad of conserved residues, H-Y-E (H862, Y896, and E988, shown in green), is required for NAD^+ binding. ADP from cNAD (right, shown in blue) represents the terminal region of the PAR chain. Conserved residues from acceptor sites (purple) interact with ADP from the terminal ADP-ribose.

than PARPs (Vyas et al., 2014). As a consequence, a new nomenclature describing PARPs more accurately as ADP-ribosyltransferases (ARTs) has been proposed (Asher et al., 2010). The 17 PARP family members can be subdivided into four subfamilies based on their domain architectures (Hanai et al., 2004; Schreiber et al., 2006). These include: (1) DNA dependent PARPs (PARP-1, PARP-2, and PARP-3), which are activated by discontinuous DNA structures (for PARPs 1 and 2, through their amino-terminal DNA binding domains) (**Figure 1.3**); (2) tankyrases, including PARP5a (tankyrase-1) and PARP-5b (tankyrase-2), which contain large ankyrin domain repeats that mediate protein-protein interactions; (3) CCCH PARPs, including PARP-7 (tiPARP), PARP-12, PARP13.1, and PARP13.2, which contain Cys-Cys-Cys-His zinc fingers that bind to RNA, as well as WWE domains, which can exhibit PAR binding activity; and (4) macroPARPs, including PARP-9 (BAL1), PARP14 (BAL2, CoaSt6), and PARP-15 (BAL3), which contain macrodomain folds that can bind ADPR and derivatives. As these examples illustrate, nature through the course of evolution has modified the PARP catalytic domain and functionalized it with a variety of other protein domains to create a set of proteins with varied activities, subcellular locations, and functions.

PARP-1 (ARDT1) is the prototypical and founding member of the PARP family. It is a 116 kDa protein containing a set of well characterized structural and functional domains (**Figure 1.3**, *top*) (Hanai et al., 2004; Schreiber et al., 2006). These include (from the amino to carboxyl termini of the protein): (1) an amino-terminal DNA binding domain containing two zinc finger motifs, a zinc binding domain, and a nuclear localization signal (NLS); (2) an automodification domain containing a BRCA1 C-terminus (BRCT) motif; (3) a WGR (Trp-

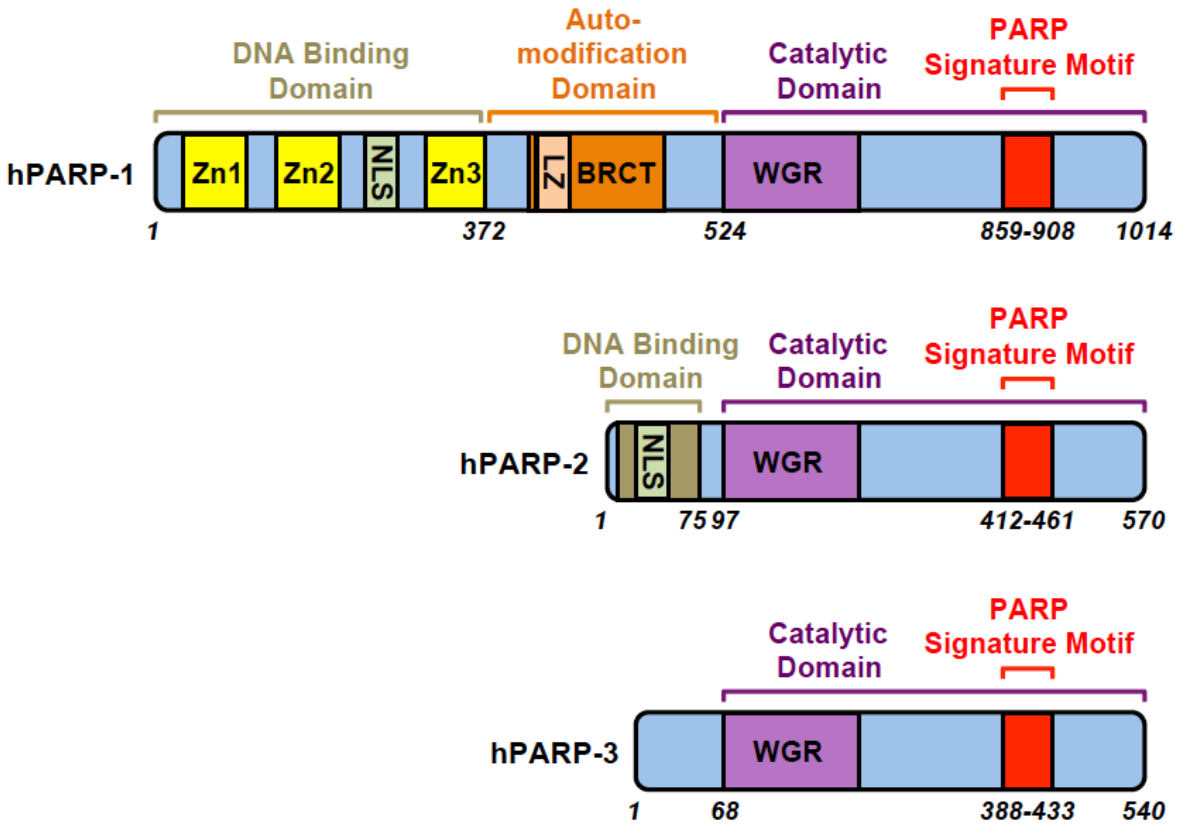

Figure 1.3. Structural and functional organization of nuclear DNA-dependent PARPs. PARPs 1, 2, and 3 comprise a subset of nuclear PARPs whose catalytic activity is stimulated by discontinuous DNA structures. In the case of PARPs 1 and 2, this activation by DNA occurs through their N-terminal DNA binding domains. Unlike PARPs 1 and 3, PARP-3 does not have a well defined DNA-binding domain, but it can interact with chromatin and to bind to DNA in vitro (Rouleau et al., 2007; Rulten et al., 2011). PARPs 1 and 2 are poly(ADP-ribosyl) transferases, while PARP-3 is a mono(ADP-ribosyl) transferase. Abbreviations as are follows: Zn1, Zn2, Zn3 = zinc binding domains 1-3; NLS = nuclear localization signal; LZ = leucine zipper motif (thought to function as a protein-protein interaction motif); BRCT = BRCA1 C-terminal motif (thought to function as a phosphopeptide binding motif); WGR = tryptophan-glycine-arginine-containing motif (may function as a nucleic acid binding motif).

Gly-Arg) motif; and (4) a carboxyl-terminal catalytic domain containing the highly conserved PARP signature motif, which forms the NAD^+ binding site and defines the PARP family of proteins. This collection of structural and functional domains comprises a ubiquitous and abundant protein that is ideally suited to carry out a wide variety of functions in the nucleus (Boamah et al., 2012; Krishnakumar and Kraus, 2010b). Many of the functional studies of PARP family members to date have been done with PARP-1. As such, many of the examples herein are derived from the PARP-1 literature.

1.3.2 Overview of The Molecular Functions of PAR and The PARP family

PARP family members exhibit a wide array of subcellular distributions and expression patterns, suggesting a broad and varied biology for this family (Hassa and Hottiger, 2008; Vyas et al., 2014). Although some PARP-mediated cellular responses may be independent of their catalytic activity, many of the best-characterized actions of PARP family members require PAR production and may involve distinct PAR-binding modules present in key regulatory proteins (see below). The functions of PARPs can be understood at (1) the molecular level, relating to the chemical biology of PAR, (2) the cellular level, relating to the cellular processes that they control, and (3) the biological level, relating to the physiological and pathological processes in which they play key roles. With respect to the first, three general types of regulatory mechanisms have been ascribed to PAR: inhibition of protein-protein interactions, formation of interaction scaffolds, and regulation of ubiquitylation (Gibson and Kraus, 2012). With respect to the second, PARPs have been shown to function as regulatory proteins in a wide array of cellular processes, from

transcription and DNA repair, to mitochondrial function and the formation of sub-organellar bodies (D'Amours et al., 1999; Gibson and Kraus, 2012; Hassa et al., 2006; Ji and Tulin, 2010; Kraus and Hottiger, 2013; Vyas et al., 2014). With respect to the third, PARPs have been shown to function as key components of stress responses, as well as other critical homeostatic mechanisms (Hottiger et al., 2011; Luo and Kraus, 2012; Rosado et al., 2013). Given the dependence of PARP catalytic activity on NAD^+, the functions of the PARP family members may be physically and functionally linked to cellular metabolic processes and the enzymes that control them (Kim et al., 2005; Zhang et al., 2012).

1.4 NAD^+ Utilization and Synthesis PAR Polymer by PARP-1

1.4.1 NAD^+ Binding and PAR Synthesis

PARP proteins utilize NAD^+ as a donor of ADP-ribose units and transfer these units to their target proteins. The NAD^+ binding pocket in the PARP-1 catalytic domain differs from well-known NAD^+-binding motifs that are known to exist in many other NAD^+-binding proteins (e.g., hNMNAT-1) (Gibson and Kraus, 2012). While the crystal structure of PARP-1 bound to NAD^+ has yet to be determined, however, the structure of PARP-1 catalytic domain with an inactive NAD^+ analogue (carba-NAD^+) (Ruf et al., 1998) and homolog diphtheria toxin bound with NAD^+ (Bell and Eisenberg, 1996) suggests that the conserved His, Tyr, and Glu residues are important for ligand binding (**Figure 1.2B**). Specifically, substrate pyrophosphate forms hydrogen bonds with His826 of PARP-1, and the hydroxyl group from the ribose forms hydrogen bonds with Tyr907 and Glu988 (Ruf et al., 1998). The latter

residue also forms hydrogen bonds with the hydroxyl group of the acceptor ribose (at the end of the PAR chain), which is a critical residue for adding new ADP-ribose units onto the acceptor ribose (Gibson and Kraus, 2012). Site-directed mutagenesis of these conserved residues significantly reduces PARP-1 poly(ADP-ribosyl)ation (PARylation) activity while maintaining mono-ADP-ribosylation activity (Ruf et al., 1998).

During ADP-ribose transfer reactions, one molecule of NAD^+ is catalyzed to generate ADP-ribose and nicotinamide. The ADP-ribose unit is then transferred to the Lys, Glu, and Asp residues of target proteins, releasing nicotinamide as a byproduct of the reaction. The ADP-ribose chain can grow by up to 200 units by repeated attachment of an ADP-ribose unit to the adenine-proximal ribose unit through an α (1-2) O-glycosidic bond at the end of the PAR chain (elongation) (**Figure 1.4A**). In addition to linear extension, the PAR polymer can also form branches every 20–50 ADP-ribose units by forming an α (1-2) glycosidic bond between two nicotinamide-proximal riboses (**Figure 1.4A**) (Kiehlbauch et al., 1993). Each PAR residue contains an adenine moiety with two phosphate groups that carry negative charges. Due to diverse elongation and branching processes, PAR forms strongly negatively charged heterogeneous polymers both *in vitro* and *in vivo*, although the significance of this heterogeneity has remained elusive.

Despite our understanding of how PAR is synthesized, it is still difficult to determine the specific protein targets of each individual PARP. This has been a challenging question in the field due to the common substrate (NAD^+) shared by PARP family proteins and the functional redundancy between them. A breakthrough approach to identifying proteome-wide PARP-1 targets has been recently reported by Carter-O'Connell *et al*. using an NAD^+

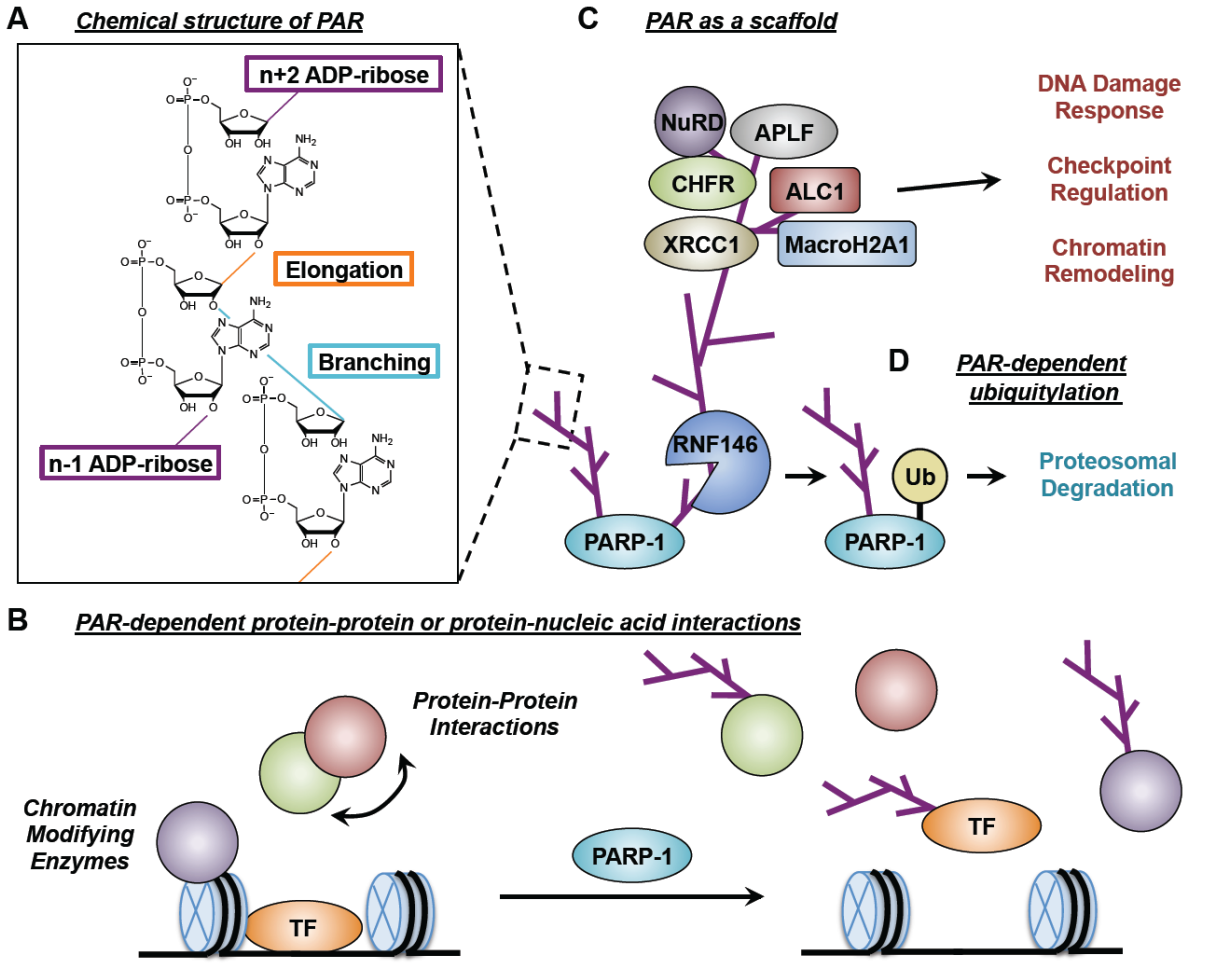

Figure 1.4. The structure of PAR and the mechanism of PAR action.
(A) Chemical structure of PAR illustrating elongation of the PAR chain by an α(1-2) O-glycosidic bond between riboses (elongation, orange line) and branching of the PAR chain by an α(1-2) glycosidic bond between two nicotinamide-proximal riboses (branching, blue line). (B) PARylation of a protein inhibits protein–protein or protein–nucleic acid interactions by masking interaction sites or introducing charge repulsion with strongly negatively charged polymers(Gibson and Kraus, 2012). (C) PAR recruits PAR-binding protein to its sites of action, serving as an interaction scaffold (Gibson and Kraus, 2012). (D) PARylation of PARP-1 triggers recruitment of the E3 ligase RNF146, which contains a PAR-binding WWE domain and brings about subsequent ubiquitylation and proteasome-mediated degradation of the target protein (Andrabi et al., 2011; Kang et al., 2011).

analogue and a mutant form of PARP-1, followed by copper-catalyzed conjugation to an azidoalkyl reporter (click chemistry) and tandem mass spectrometry (**Figure 1.5**) (Carter-O'Connell et al., 2014). In this study, the conserved catalytic lysine (K903) in PARP-1 is mutated to alanine, and 5-ethyl-6-alkyne-NAD^+ is used as a substrate for this mutant PARP-1. The NAD^+ analog can only be utilized by the mutant PARPs but not their wild-type counterparts, leading to the identification of specific targets for individual PARPs (PARP-1 and PARP-2)(Carter-O'Connell et al., 2014). However, the PARP-1 K903A mutant catalyzes only mono-ADP ribosylation rather than PARylation, which possibly affects the identification of proteome-wide PARP-1 targets. Therefore, improved methodologies will be required to overcome this limitation.

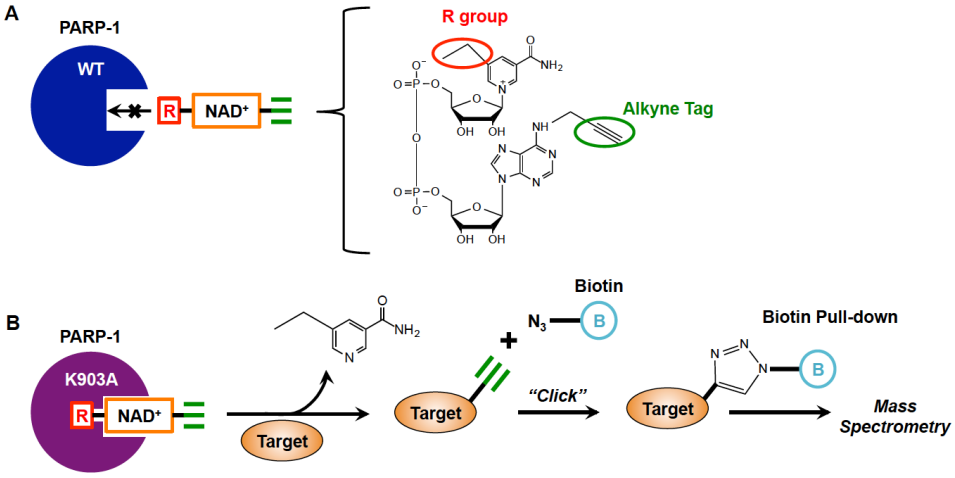

Figure 1.5. Strategy for defining proteome-wide PARP-1-specific targets.
The NAD^+ analogue (5-Et-6-a-NAD^+) and PARP-1 mutant (K903A) were used to identify specific targets for PARP-1 (Carter-O'Connell et al., 2014). Ethyl group and alkyne tags were added to the C-5 position of the nicotinamide ring and the N-6 position of adenosine ring, respectively, to generate the NAD^+ analogue, which can only be utilized by the K903A PARP-1 mutant and not by wild type PARP-1 or other PARP family members. Following conjugation with biotin azide and subsequent enrichment of biotinylated proteins, samples were subjected to LC-MS/MS to identify the proteome-wide targets of PARP-1. (A) NAD^+ analog with wild-type PARP-1 (WT). (B) NAD^+ analog with analog-sensitive mutant PARP-1 (K903A).

1.4.2 Mechanisms of PAR Action

The synthesis of a long, negatively charged polymer affects a wide array of biological processes through various mechanisms. PARylation of the protein alters its interaction with other binding partners, including proteins and nucleic acids (**Figure 1.4B**). For example, PARP-1 PARylates the chromatin remodeling factor FACT upon DNA damage and disrupts FACT–nucleosome interactions as well as FACT-mediated H2A/H2AX exchange(Heo et al., 2008; Huang et al., 2006). PARP-1 also modifies the ATP-dependent chromatin remodeler ISWI and histone demethylases KDM5B and KDM4D by reducing their binding to the nucleosome (Khoury-Haddad et al., 2014; Krishnakumar and Kraus, 2010b; Sala et al., 2008). PARP-1-dependent PARylation has also been shown to regulate many transcription factors in a similar manner, including, but not limited to, Sp1 (Zaniolo et al., 2007), NFAT (Olabisi et al., 2008), Sox2 (Gao et al., 2009; Weber et al., 2013), Smad (Lonn et al., 2010), and CLOCK (Asher et al., 2010) as well as nuclear receptors such as farnesoid X receptors (FXR) (Wang et al., 2013) and estrogen receptor (ER) (Zhang et al., 2013a) (see below). A plausible explanation for these effects could be that PARP-1-dependent PARylation masks protein–protein interaction sites or introduces charge repulsion with strongly negatively charged polymers.

PAR also acts as a scaffold to recruit other proteins (**Figure 1.4C**). The mechanism of scaffold function is well studied in the DNA damage response process. Upon laser-induced DNA damage, PARP-1 is rapidly activated, and PAR is accumulated at the site of damage (within seconds), followed by recruitment of scaffold proteins such as XRCC1 (El-Khamisy et al., 2003; Masson et al., 1998; Okano et al., 2003), which preferentially binds to

PARylated PARP-1 (Masson et al., 1998), and chemical inhibition of PAR synthesis or genetic depletion of PARP-1 abolishes XRCC1 recruitment (El-Khamisy et al., 2003; Masson et al., 1998; Okano et al., 2003). Additionally, PAR polymers direct polycomb complexes and the NuRD (nucleosome remodeling and histone deacetylase) complex to DNA damage sites. Recruitment of these complexes deposits repressive histone marks on the chromatin, allowing a transient repressive chromatin structure at the site of DNA damage that blocks transcription and facilitates DNA repair (Chou et al., 2010).

Recent studies have led to the further identification of PAR-dependent recruitment of proteins to their sites of action, mediated by PAR-binding domains (**Figure 1.6**). CHFR (checkpoint protein with FHA and RING domains) and APLF (aprataxin PNK-like factor) both contain the PAR-binding C2H2 zinc finger motif (PBZ) and are recruited in a PAR-dependent manner for checkpoint regulation (CHFR) and DNA damage response (APLF) (**Figure 1.4C**) (Ahel et al., 2008; Li et al., 2010). MacroH2A.1 and ALC1 (amplified in liver cancer 1) also require PAR in order to be recruited to their target (Ahel et al., 2009; Timinszky et al., 2009). However, these proteins contain a macrodomain, an ancient and highly conserved domain that recognizes PAR polymers in submicromolar affinities (Gibson and Kraus, 2012; Kraus, 2009). MacroH2A.1 and ALC1 interact with PAR chains through their macrodomains, and inhibition of PAR synthesis or mutation in the macrodomain fail to recruit these proteins to laser-induced DNA damage sites (Ahel et al., 2009; Timinszky et al., 2009). Moreover, human ssDNA-binding protein 1 (hSSB1) binds to PAR and is recruited to sites of DNA damage via its oligonucleotide/oligosaccharide-binding (OB) fold, a ssDNA or RNA binding motif found in prokaryote and eukaryotes (Zhang et al., 2014).

A

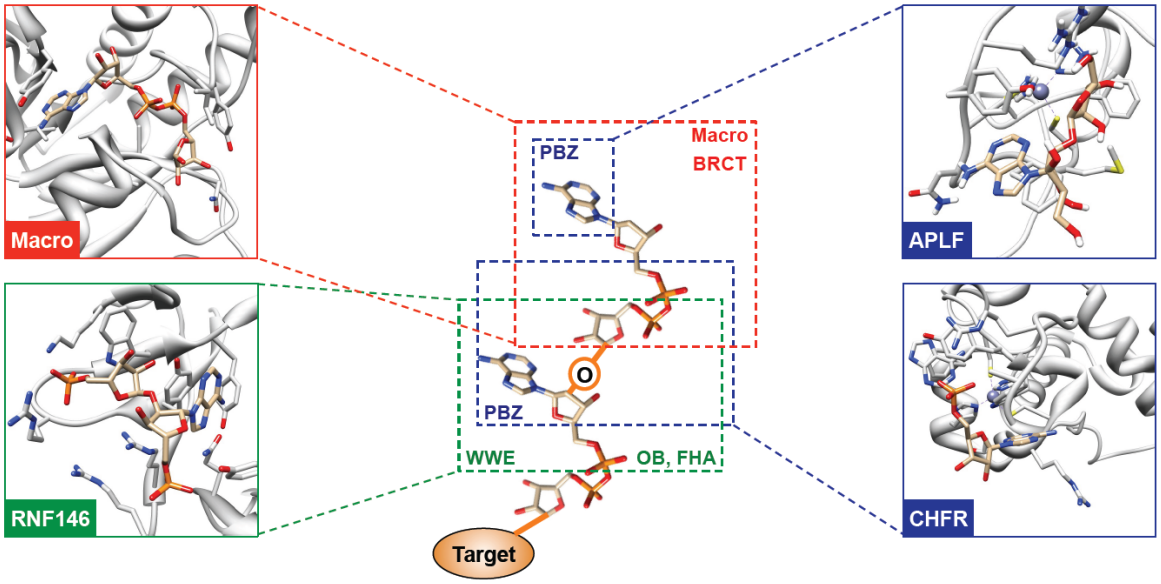

B

PAR-binding	Recognition	Factors
PBM	Unknown	XRCC1, ALF1
Macrodomains	Terminal ADP-ribose of PAR and mono-ADP-ribosylated protein	MacroH2A, PARP-14(mono)
PBZ domains	O-glycosidic bond between two ribose	APLF, CHFR
WWE domains	*Iso*-ADP-ribose	RNF146, PARP-11, PARP-14
OB fold	*Iso*-ADP-ribose	hSSB1
FHA	*Iso*-ADP-ribose	APTX, PNKP
BRCT	ADP-ribose from PAR chain	XRCC1, BARD1

Figure 1.6. Recognition of PAR chains by PAR-binding modules.
(A) PAR-binding proteins utilize various PAR-binding modules to recognize PAR. The PBZ domain (blue) uses a zinc-coordinated fold that recognizes the α(1→2) O-glycosidic bond between two ribose units (Gibson and Kraus, 2012). Solution structure of the first PBZ domain in a complex with ribofuranosyladenosine (upper right panel, PDB: 2KQD) (Eustermann et al., 2010) and CHFR bound to P(1)P(2)-diadenosine 5'-pyrophosphate (lower right panel, PDB: 2XOY) (Oberoi et al., 2010) are shown as examples. The macrodomain binds to the terminal ADP-ribose residue of PAR (red, upper left panel, PDB: 2BFQ) (Karras et al., 2005) or mono-ADP ribosylated protein (Forst et al., 2013), and the WWE domains recognize the *iso*-ADP-ribose residue (green). Human RNF146 WWE domain in complex with *iso*-ADP-ribose is shown as an example (lower left, PDB: 3V3L) (Wang et al., 2012). (B) A table summarizing different PAR-binding modules. PAR-binding motifs (PBM) are short amino acid sequences found in PAR-binding proteins such as XRCC1 (Gibson and Kraus, 2012). The OB fold is a ssDNA- or RNA-binding motif in prokaryotes and eukaryotes; however, the OB fold of human SSB1 recognizes *iso*-ADP-ribose (Zhang et al., 2014).

Another layer of biological process that PAR modulates is protein degradation through ubiquitylation. The mechanism of PAR-dependent ubiquitylation has been suggested to be through RNF146, in which the E3 ligase RNF146 binds to PAR through its WWE domain and subsequently ubiquitylates the Lys residue of the PARylated protein (**Figures 1.4D and 1.6**)(Kang et al., 2011). RNF146 protects against DNA damage-induced cell death by ubiquitylating PARP-1 in a PAR-dependent manner, leading to proteasomal degradation of PARP-1(Andrabi et al., 2011; Kang et al., 2011). Interestingly, RNF146 has also been shown to regulate the Wnt signaling pathway and downstream gene expression. In this case, Axin is PARylated by tankyrase (PARP-5), and RNF146 interacts with PARylated Axin and controls its degradation (Huang et al., 2009; Zhang et al., 2011). Regulation of the cellular signaling pathway through PAR-dependent protein degradation can be another interesting mechanism that PARP-1 might apply to regulate transcription, likely through controlling the stability of PARylated transcription factors or chromatin-modifying enzymes. However, whether PARP-1 adopts a similar mechanism in transcription regulation has yet to be determined.

1.5. Overview of The Mechanisms of PARP-1-Dependent Gene Expression

Although originally overlooked as an important aspect of PARP biology, roles for PARP-1 and other PARP family members are, by now, well established in the literature (Hassa and Hottiger, 2008; Ji and Tulin, 2010; Kraus, 2008; Kraus and Hottiger, 2013; Kraus and Lis, 2003; Krishnakumar and Kraus, 2010a). A survey of the literature reveals at least four distinct, but interrelated, ways in which PARP-1 acts to control the how genes are expressed and how the levels of gene products are maintained. They are: (1) modulation of

chromatin, (2) transcriptional coregulation, (3) modulation of DNA methylation, and (4) regulator of RNA.

1.5.1 PARP-1 as a Modulator of Chromatin

Chromatin, a repeating array of nucleosomes, is a protein-DNA complex that comprises genomic DNA, core histones (i.e., H2A, H2B, H3, and H4, or perhaps core histone variants), linker histones (e.g., H1), and other chromatin-associated proteins (Widom, 1998; Wolffe and Guschin, 2000). Many early studies on the nuclear functions of PARP-1 and PAR showed that can modulate chromatin structure, promoting the decompaction of chromatin by reducing interactions between nucleosomes and reducing nucleosome-dependent higher-order structures (D'Amours et al., 1999; Kraus and Lis, 2003). For example, in *Drosophila,* activation of dPARP (the PARP-1 homolog) promotes decondensation of chromatin in response to heat shock or other cellular signaling pathways (Petesch and Lis, 2011; Tulin and Spradling, 2003). Furthermore, PARP-1-dependent PARylation of native polynucleosomes promotes decondensation, mimicking the effects of linker histone H1 depletion (Poirier et al., 1982). These effects may be mediated by PARylation of H1 by PARP-1 (Poirier et al., 1982) or competition between PARP-1 and H1 for binding to nucleosomes (Kim et al., 2004; Krishnakumar et al., 2008a).

Other effects of PARP-1 on chromatin are mediated, in part, by its effects on core histones or core histone variants. PARP-1 has been shown to PARylate histones, as well as non-histone, chromatin-associated proteins (D'Amours et al., 1999; Kraus and Lis, 2003). Presumably, histone ADP-ribosylation (either mono- or poly-) affects the biochemical

properties of the histones, thus altering nucleosome structure, or promotes interactions with chromatin-modulating proteins that contain ADPR-binding modules (Gibson and Kraus, 2012; Kraus, 2009). Interestingly, proinflammatory signaling induces PARP-1 enzymatic activity and histone ADP-ribosylation at transcriptionally active and accessible chromatin regions in macrophages (Martinez-Zamudio and Ha, 2012), lending support to the idea that histones, as well as non-histone, chromatin-associated proteins, are PARylated at specific loci in vivo. Conversely, the amino-terminal tails of core histones have been shown to regulate PARP-1 enzymatic activity, which could serve a regulatory role for PARylation by chromatin-bound PARP-1 (D'Amours et al., 1999; Kraus and Lis, 2003; Pinnola et al., 2007).

Studies with the *Drosophila* H2A variant H2Av (a homolog of mammalian H2A variants H2Az and H2Ax) have shown that replacement of canonical H2A with H2Av alters the conformation of nucleosomes and promotes the binding of dPARP to H3 and H4(Kotova et al., 2011). Phosphorylation of H2Av in response to cellular signaling pathways exposes the H4 N-terminal tail even further to activate dPARP catalytic activity, which in turn directs heat-shock-induced transcriptional activation and genotoxic stress-induced DNA repair(Kotova et al., 2011; Pinnola et al., 2007). Studies with macroH2A, another H2A variant that has a macrodomain in its extended C-terminal domain, have shown that the 1.1 isoform, but not the 1.2 splice variant, binds both ADPR and PAR (Karras et al., 2005). The macrodomain may allow chromatin-bound macroH2A1.1 to bind to PAR produced locally by PARP-1, resulting in macroH2A1.1-dependent chromatin compaction (Timinszky et al., 2009).

In addition to its directs effects on components of chromatin, PARP-1 may also modulate the localization and activity of a broad array of histone-modifying and nucleosome remodeling enzymes. For example, PARylation of KDM5B, a histone lysine demethylase that acts on histone H3 lysine 4 trimethyl (H3K4me3), inhibits KDM5B binding and demethylase activity at specific sites in the genome (Krishnakumar and Kraus, 2010b). This leads to an increase in the levels of H3K4me3 at the promoters of PARP-1-regulated genes, supporting continued gene expression. Likewise, physical and functional interactions with PARP-1 can alter the activity of ATP-dependent nucleosome remodeling enzymes. For example, PARylation of *Drosophila* ISWI by dPARP inhibits ISWI nucleosome binding, ATPase, and chromatin condensation activities at heat-shock loci (Sala et al., 2008), In contrast, PAR-dependent interactions between PARP-1 and ALC1, a macrodomain-containing nucleosome remodeling enzyme, promote nucleosome remodeling by ALC1, as well as recruitment of ALC1 to specific loci in the genome (Ahel et al., 2009; Gottschalk et al., 2009). Thus, as illustrated here, PARP-1 (and potentially other nuclear PARPs, such as PARP-2 and PARP-3) can modulate gene expression by altering chromatin structure to affect transcriptional outcomes.

1.5.2. PARP-1 as a Transcriptional Coregulator

In addition to its role as a modulator of chromatin structure to control gene expression, PARP-1 has also been shown to act as classical transcription factor-dependent coregulatory protein. As a coregulator, PARP-1 functions with the basal transcription machinery, other coregulators with enzymatic activities (e.g., histone-modifying enzymes

and nucleosome remodelers), and sequence-specific DNA-binding transcription factors, such as NF-κB, HES1, Elk1, Sox2, and nuclear hormone receptors (D'Amours et al., 1999; Kraus, 2008; Kraus and Lis, 2003). In this regard, two types of coregulatory functions have been ascribed to PARP-1: (1) scaffold and (2) exchange factor.

With respect to the former (i.e., scaffold), PARP-1 may act as scaffold by interacting with and promoting the recruitment of other coregulators independent of its DNA binding and catalytic activities. In this regard, PARP-1 has been shown to interact with the protein arginine methyltransferase PRMT1 and the protein acetyltransferase p300/CBP to support NF-κB-dependent gene expression (Hassa et al., 2003; Hassa et al., 2008; Hassa et al., 2005). With respect to the latter (i.e., exchange factor), PARP-1 has been shown to promote the release of inhibitory factors and the recruitment of stimulatory factors to DNA-bound transcription factors. PARP-1-dependent exchange of opposing pairs of factors has been observed for: (1) inactive Cdk8-positive Mediator, which is exchanged for an active Cdk8-negative Mediator during retinoic acid-regulated activation (Pavri et al., 2005), (2) a TLE1-containing corepressor complex, which is exchanged for a HAT-containing coactivator complex during signal-dependent gene regulation in neuronal cells (Ju et al., 2004), and (3) a corepressor complex containing NCoR and HDAC3, which is exchanged for an activation complex containing topoisomerase IIβ (TopoIIβ) at steroid hormone-regulated promoters(Ju et al., 2006).

These examples illustrate a common theme of coregulation by PARP-1, namely the modulation of protein complex formation, which may occur as a result of PARP-1 scaffolding functions or PARP-1 enzymatic activity.

1.5.3 PARP-1 as a Modulator of DNA Methylation

An emerging literature over the past decade or so has shown that PARP-1 can alter the methylation of genomic DNA (Attwood et al., 2002; Caiafa and Zampieri, 2005). PARP-1 may mediate these effects by regulating the expression or activity of the DNA methyltransferase Dnmt1 (Caiafa et al., 2009; Caiafa and Zampieri, 2005). In this regard, PARP-1 may directly interact with Dnmt1 through newly synthesized PAR polymers to inhibit Dnmt1 DNA methyltransferase activity (Reale et al., 2005). PARP-1 has been shown to interact functionally with the methylcytosine dioxygenase Tet2, an enzyme that catalyzes the conversion of 5-methylcytosine (5mC) to 5-hydroxymethylcytosine (hmC) (Doege et al., 2012). These interactions may play a key role during somatic cell reprogramming, acting to promote an epigenetic program that directs transcriptional induction at pluripotency loci; PARP-1 regulates the 5mC modification, while Tet2 promotes the early generation of 5hmC by the oxidation of 5mC (Doege et al., 2012). As these examples show, modulation of DNA methylation by PARP-1 can impact the genome and affect gene expression outcomes.

1.5.4 PARP-1 as a Regulator of RNA

A growing body of evidence indicates that PARP-1 plays an important role in various aspects of RNA biology. First, PARP-1 binds and acts in concert with noncoding pRNA to retain the silent rDNA chromatin in the nucleolus (Guetg et al., 2012). Second, PARP-1 plays an essential role in ribosomal biogenesis in the nucleolus by PARylation of several nucleolar proteins in *Drosophila* (Boamah et al., 2012). Third, PARP-1 was identified as a novel mRNA binding protein (Castello et al., 2012), as well as a factor in the human pre-mRNA 3'-

end-processing complex (Di Giammartino et al., 2013). In addition, PARP-1 PARylates heterogeneous nuclear ribonucleoproteins (hnRNPs), which are involved in alternative splicing of pre-mRNAs and translation (Ji and Tulin, 2009). Fourth, six PARPs, two poly(ADP-ribose) glycohydrolase (PARG) isoforms, and PAR are required for the cytoplasmic posttranscriptional regulation of mRNA in stress granules (SGs) (Leung et al., 2011). Lastly, other PARP family members, such as PARP-13/ZAP and PARP-2, have been implicated in viral gene expression (Gao et al., 2002) and in nucleolar processes (Leger et al., 2014), respectively.

1.6. NAD^+-Dependent Regulation of PARP-1

An interesting aspect of the enzymatic reaction of NAD^+-dependent enzymes is the consumption of NAD^+ and the generation of NAM as a byproduct of the reaction. As described previously, NAM is a substrate for the NAD^+ salvage pathway but also a potent inhibitor of NAD^+-dependent enzymes, such as PARPs and SIRTs (Jackson et al., 1995; Preiss et al., 1971; Sauve and Schramm, 2003). This dual role indicates the possibility of a functional interplay between NAD^+ synthesis and consumption. In the nucleus, PARP-1 activity is a major NAD^+-consuming process. Upon activation, PARP-1 can rapidly use NAD^+, and when hyper-activated, PARP-1 can deplete the cellular NAD^+ pool (Schreiber et al., 2006). Therefore, appropriate synthesis of nuclear NAD^+ is required for the cells to maintain their enzymatic activity.

Among the three isoforms of NMNATs, NMNAT-1 is the only enzyme that resides exclusively in the nucleus (Berger et al., 2005). Its unique subcellular localization suggests

that it may be responsible for the regulation of nuclear NAD^+-dependent enzymes, such as PARP-1 or SIRT1. Functional interplay between NMNAT-1 and NAD^+-dependent enzymes was first suggested by the Wallerian degeneration slow (Wlds) mouse model, a dominant mouse mutation that can significantly delay axon degeneration (Coleman, 2005). The protein responsible for this phenotype was found to be a chimeric NMNAT-1 that consists of the N-terminal 70 amino acids of the Ub24B (ubiquitylation assembly factor 4B) and the full coding sequence of NMNAT-1 (Mack et al., 2001). It was proposed that this chimeric protein protects neuronal degeneration by increasing NAD^+, leading to the subsequent activation of SIRT1 (Araki et al., 2004; Press and Milbrandt, 2008). Although the clear mechanism of this neuroprotective effect still remains elusive, overexpression of NMNAT-1 or supplying NMN, NaMN, or NR supports a protective role for NAD^+ synthesis during the axonal degeneration process (Fang et al., 2014; Press and Milbrandt, 2008; Sasaki et al., 2006).

Until recently, it was unclear how enzymes involved in the NAD^+ synthesis pathway regulate PARP-1. The first biochemical evidence of the link between nuclear NAD^+ synthesis and PARP-1 was proposed by Berger and colleagues in relation to DNA damage, where NMNAT-1 interacts with PARP-1 in a PAR-dependent manner (Berger et al., 2007). Upon binding, NMNAT-1 stimulates PARP-1 enzymatic activity. The NMNAT-1–PARP-1 interaction is regulated through phosphorylation of NMNAT-1 by protein kinase C (PKC), which reduces NMNAT-1 binding to PARP-1 (Berger et al., 2007). Moreover, Zhang and colleagues suggested that there is functional interplay between NMNAT-1 and PARP-1 in the context of transcription regulation (Zhang et al., 2012). In MCF-7 cells, NMNAT-1 is recruited to promoters of the genes via PARP-1. This study also revealed that NMNAT-1

could enhance PARP-1 enzymatic activity upon binding, although the interaction was rather direct, instead of through the PAR polymer. Moreover, the enzymatic activity of NMNAT-1 was required for PARP-1-dependent PARylation at the promoters, indicating that NMNAT-1 regulates PARP-1 through protein–protein interactions as well as providing the PARP-1 substrate, NAD^+ (Zhang et al., 2012). Although the functional link between NMNAT-1 and PARP-1 has been established, how this interplay affects biological processes requires further study.

1.7 References

Ahel, D., Horejsi, Z., Wiechens, N., Polo, S.E., Garcia-Wilson, E., Ahel, I., Flynn, H., Skehel, M., West, S.C., Jackson, S.P.*, et al.* (2009). Poly(ADP-ribose)-dependent regulation of DNA repair by the chromatin remodeling enzyme ALC1. Science *325*, 1240-1243.

Ahel, I., Ahel, D., Matsusaka, T., Clark, A.J., Pines, J., Boulton, S.J., and West, S.C. (2008). Poly(ADP-ribose)-binding zinc finger motifs in DNA repair/checkpoint proteins. Nature *451*, 81-85.

Andrabi, S.A., Kang, H.C., Haince, J.F., Lee, Y.I., Zhang, J., Chi, Z., West, A.B., Koehler, R.C., Poirier, G.G., Dawson, T.M.*, et al.* (2011). Iduna protects the brain from glutamate excitotoxicity and stroke by interfering with poly(ADP-ribose) polymer-induced cell death. Nature medicine *17*, 692-699.

Araki, T., Sasaki, Y., and Milbrandt, J. (2004). Increased nuclear NAD biosynthesis and SIRT1 activation prevent axonal degeneration. Science *305*, 1010-1013.

Asher, G., Reinke, H., Altmeyer, M., Gutierrez-Arcelus, M., Hottiger, M.O., and Schibler, U. (2010). Poly(ADP-ribose) polymerase 1 participates in the phase entrainment of circadian clocks to feeding. Cell *142*, 943-953.

Attwood, J.T., Yung, R.L., and Richardson, B.C. (2002). DNA methylation and the regulation of gene transcription. Cellular and molecular life sciences : CMLS *59*, 241-257.

Bell, C.E., and Eisenberg, D. (1996). Crystal structure of diphtheria toxin bound to nicotinamide adenine dinucleotide. Biochemistry *35*, 1137-1149.

Berger, F., Lau, C., Dahlmann, M., and Ziegler, M. (2005). Subcellular compartmentation and differential catalytic properties of the three human nicotinamide mononucleotide adenylyltransferase isoforms. The Journal of biological chemistry *280*, 36334-36341.

Berger, F., Lau, C., and Ziegler, M. (2007). Regulation of poly(ADP-ribose) polymerase 1 activity by the phosphorylation state of the nuclear NAD biosynthetic enzyme NMN adenylyl transferase 1. Proceedings of the National Academy of Sciences of the United States of America *104*, 3765-3770.

Berger, F., Ramirez-Hernandez, M.H., and Ziegler, M. (2004). The new life of a centenarian: signalling functions of NAD(P). Trends in biochemical sciences *29*, 111-118.

Boamah, E.K., Kotova, E., Garabedian, M., Jarnik, M., and Tulin, A.V. (2012). Poly(ADP-Ribose) polymerase 1 (PARP-1) regulates ribosomal biogenesis in Drosophila nucleoli. PLoS genetics *8*, e1002442.

Boukouris, A.E., Zervopoulos, S.D., and Michelakis, E.D. (2016). Metabolic Enzymes Moonlighting in the Nucleus: Metabolic Regulation of Gene Transcription. Trends in biochemical sciences *41*, 712-730.

Caiafa, P., Guastafierro, T., and Zampieri, M. (2009). Epigenetics: poly(ADP-ribosyl)ation of PARP-1 regulates genomic methylation patterns. FASEB journal : official publication of the Federation of American Societies for Experimental Biology *23*, 672-678.

Caiafa, P., and Zampieri, M. (2005). DNA methylation and chromatin structure: the puzzling CpG islands. Journal of cellular biochemistry *94*, 257-265.

Carter-O'Connell, I., Jin, H., Morgan, R.K., David, L.L., and Cohen, M.S. (2014). Engineering the substrate specificity of ADP-ribosyltransferases for identifying direct protein targets. Journal of the American Chemical Society *136*, 5201-5204.

Castello, A., Fischer, B., Eichelbaum, K., Horos, R., Beckmann, B.M., Strein, C., Davey, N.E., Humphreys, D.T., Preiss, T., Steinmetz, L.M.*, et al.* (2012). Insights into RNA biology from an atlas of mammalian mRNA-binding proteins. Cell *149*, 1393-1406.

Chambon, P., Weill, J.D., and Mandel, P. (1963). Nicotinamide mononucleotide activation of new DNA-dependent polyadenylic acid synthesizing nuclear enzyme. Biochemical and biophysical research communications *11*, 39-43.

Chiarugi, A., Dolle, C., Felici, R., and Ziegler, M. (2012). The NAD metabolome--a key determinant of cancer cell biology. Nature reviews Cancer *12*, 741-752.

Chou, D.M., Adamson, B., Dephoure, N.E., Tan, X., Nottke, A.C., Hurov, K.E., Gygi, S.P., Colaiacovo, M.P., and Elledge, S.J. (2010). A chromatin localization screen reveals poly (ADP ribose)-regulated recruitment of the repressive polycomb and NuRD complexes to sites of DNA damage. Proceedings of the National Academy of Sciences of the United States of America *107*, 18475-18480.

Coleman, M. (2005). Axon degeneration mechanisms: commonality amid diversity. Nature reviews Neuroscience *6*, 889-898.

Conforti, L., Janeckova, L., Wagner, D., Mazzola, F., Cialabrini, L., Di Stefano, M., Orsomando, G., Magni, G., Bendotti, C., Smyth, N.*, et al.* (2011). Reducing expression of NAD+ synthesizing enzyme NMNAT1 does not affect the rate of Wallerian degeneration. The FEBS journal *278*, 2666-2679.

D'Amours, D., Desnoyers, S., D'Silva, I., and Poirier, G.G. (1999). Poly(ADP-ribosyl)ation reactions in the regulation of nuclear functions. The Biochemical journal *342 (Pt 2)*, 249-268.

Di Giammartino, D.C., Shi, Y., and Manley, J.L. (2013). PARP1 represses PAP and inhibits polyadenylation during heat shock. Molecular cell *49*, 7-17.

Doege, C.A., Inoue, K., Yamashita, T., Rhee, D.B., Travis, S., Fujita, R., Guarnieri, P., Bhagat, G., Vanti, W.B., Shih, A.*, et al.* (2012). Early-stage epigenetic modification during somatic cell reprogramming by Parp1 and Tet2. Nature *488*, 652-655.

El-Khamisy, S.F., Masutani, M., Suzuki, H., and Caldecott, K.W. (2003). A requirement for PARP-1 for the assembly or stability of XRCC1 nuclear foci at sites of oxidative DNA damage. Nucleic acids research *31*, 5526-5533.

Emanuelli, M., Carnevali, F., Saccucci, F., Pierella, F., Amici, A., Raffaelli, N., and Magni, G. (2001). Molecular cloning, chromosomal localization, tissue mRNA levels, bacterial expression, and enzymatic properties of human NMN adenylyltransferase. The Journal of biological chemistry *276*, 406-412.

Eustermann, S., Brockmann, C., Mehrotra, P.V., Yang, J.C., Loakes, D., West, S.C., Ahel, I., and Neuhaus, D. (2010). Solution structures of the two PBZ domains from human APLF and their interaction with poly(ADP-ribose). Nature structural & molecular biology *17*, 241-243.

Fang, E.F., Scheibye-Knudsen, M., Brace, L.E., Kassahun, H., Sengupta, T., Nilsen, H., Mitchell, J.R., Croteau, D.L., and Bohr, V.A. (2014). Defective Mitophagy in XPA via PARP-1 Hyperactivation and NAD(+)/SIRT1 Reduction. Cell *157*, 882-896.

Forst, A.H., Karlberg, T., Herzog, N., Thorsell, A.G., Gross, A., Feijs, K.L., Verheugd, P., Kursula, P., Nijmeijer, B., Kremmer, E.*, et al.* (2013). Recognition of mono-ADP-ribosylated ARTD10 substrates by ARTD8 macrodomains. Structure *21*, 462-475.

Futai, M., Mizuno, D., and Sugimura, T. (1967). Hydrolysis of the polymer formed from NAD with rat liver phosphodiesterase yielding nucleoside 5'monophosphate. Biochemical and biophysical research communications *28*, 395-399.

Gao, F., Kwon, S.W., Zhao, Y., and Jin, Y. (2009). PARP1 poly(ADP-ribosyl)ates Sox2 to control Sox2 protein levels and FGF4 expression during embryonic stem cell differentiation. The Journal of biological chemistry *284*, 22263-22273.

Gao, G., Guo, X., and Goff, S.P. (2002). Inhibition of retroviral RNA production by ZAP, a CCCH-type zinc finger protein. Science *297*, 1703-1706.

Garavaglia, S., D'Angelo, I., Emanuelli, M., Carnevali, F., Pierella, F., Magni, G., and Rizzi, M. (2002). Structure of human NMN adenylyltransferase. A key nuclear enzyme for NAD homeostasis. The Journal of biological chemistry *277*, 8524-8530.

Gibson, B.A., and Kraus, W.L. (2012). New insights into the molecular and cellular functions of poly(ADP-ribose) and PARPs. Nature reviews Molecular cell biology *13*, 411-424.

Gomes, A.P., Price, N.L., Ling, A.J., Moslehi, J.J., Montgomery, M.K., Rajman, L., White, J.P., Teodoro, J.S., Wrann, C.D., Hubbard, B.P.*, et al.* (2013). Declining NAD(+) induces a pseudohypoxic state disrupting nuclear-mitochondrial communication during aging. Cell *155*, 1624-1638.

Gottschalk, A.J., Timinszky, G., Kong, S.E., Jin, J., Cai, Y., Swanson, S.K., Washburn, M.P., Florens, L., Ladurner, A.G., Conaway, J.W.*, et al.* (2009). Poly(ADP-ribosyl)ation directs recruitment and activation of an ATP-dependent chromatin remodeler. Proceedings of the National Academy of Sciences of the United States of America *106*, 13770-13774.

Guetg, C., Scheifele, F., Rosenthal, F., Hottiger, M.O., and Santoro, R. (2012). Inheritance of silent rDNA chromatin is mediated by PARP1 via noncoding RNA. Molecular cell *45*, 790-800.

Hanai, S., Kanai, M., Ohashi, S., Okamoto, K., Yamada, M., Takahashi, H., and Miwa, M. (2004). Loss of poly(ADP-ribose) glycohydrolase causes progressive neurodegeneration in Drosophila melanogaster. Proceedings of the National Academy of Sciences of the United States of America *101*, 82-86.

Hassa, P.O., Buerki, C., Lombardi, C., Imhof, R., and Hottiger, M.O. (2003). Transcriptional coactivation of nuclear factor-kappaB-dependent gene expression by p300 is regulated by poly(ADP)-ribose polymerase-1. The Journal of biological chemistry *278*, 45145-45153.

Hassa, P.O., Covic, M., Bedford, M.T., and Hottiger, M.O. (2008). Protein arginine methyltransferase 1 coactivates NF-kappaB-dependent gene expression synergistically with CARM1 and PARP1. Journal of molecular biology *377*, 668-678.

Hassa, P.O., Haenni, S.S., Buerki, C., Meier, N.I., Lane, W.S., Owen, H., Gersbach, M., Imhof, R., and Hottiger, M.O. (2005). Acetylation of poly(ADP-ribose) polymerase-1 by p300/CREB-binding protein regulates coactivation of NF-kappaB-dependent transcription. The Journal of biological chemistry *280*, 40450-40464.

Hassa, P.O., Haenni, S.S., Elser, M., and Hottiger, M.O. (2006). Nuclear ADP-ribosylation reactions in mammalian cells: where are we today and where are we going? Microbiol Mol Biol Rev *70*, 789-829.

Hassa, P.O., and Hottiger, M.O. (2008). The diverse biological roles of mammalian PARPS, a small but powerful family of poly-ADP-ribose polymerases. Front Biosci *13*, 3046-3082.

Heo, K., Kim, H., Choi, S.H., Choi, J., Kim, K., Gu, J., Lieber, M.R., Yang, A.S., and An, W. (2008). FACT-mediated exchange of histone variant H2AX regulated by phosphorylation of H2AX and ADP-ribosylation of Spt16. Molecular cell *30*, 86-97.

Hottiger, M.O., Boothby, M., Koch-Nolte, F., Luscher, B., Martin, N.M., Plummer, R., Wang, Z.Q., and Ziegler, M. (2011). Progress in the function and regulation of ADP-Ribosylation. Sci Signal *4*, mr5.

Houtkooper, R.H., Canto, C., Wanders, R.J., and Auwerx, J. (2010). The secret life of NAD+: an old metabolite controlling new metabolic signaling pathways. Endocrine reviews *31*, 194-223.

Huang, J.Y., Chen, W.H., Chang, Y.L., Wang, H.T., Chuang, W.T., and Lee, S.C. (2006). Modulation of nucleosome-binding activity of FACT by poly(ADP-ribosyl)ation. Nucleic acids research *34*, 2398-2407.

Huang, S.M., Mishina, Y.M., Liu, S., Cheung, A., Stegmeier, F., Michaud, G.A., Charlat, O., Wiellette, E., Zhang, Y., Wiessner, S.*, et al.* (2009). Tankyrase inhibition stabilizes axin and antagonizes Wnt signalling. Nature *461*, 614-620.

Jackson, T.M., Rawling, J.M., Roebuck, B.D., and Kirkland, J.B. (1995). Large supplements of nicotinic acid and nicotinamide increase tissue NAD+ and poly(ADP-ribose) levels but do not affect diethylnitrosamine-induced altered hepatic foci in Fischer-344 rats. The Journal of nutrition *125*, 1455-1461.

Ji, Y., and Tulin, A.V. (2009). Poly(ADP-ribosyl)ation of heterogeneous nuclear ribonucleoproteins modulates splicing. Nucleic acids research *37*, 3501-3513.

Ji, Y., and Tulin, A.V. (2010). The roles of PARP1 in gene control and cell differentiation. Current opinion in genetics & development *20*, 512-518.

Ju, B.G., Lunyak, V.V., Perissi, V., Garcia-Bassets, I., Rose, D.W., Glass, C.K., and Rosenfeld, M.G. (2006). A topoisomerase IIbeta-mediated dsDNA break required for regulated transcription. Science *312*, 1798-1802.

Ju, B.G., Solum, D., Song, E.J., Lee, K.J., Rose, D.W., Glass, C.K., and Rosenfeld, M.G. (2004). Activating the PARP-1 sensor component of the groucho/ TLE1 corepressor complex mediates a CaMKinase IIdelta-dependent neurogenic gene activation pathway. Cell *119*, 815-829.

Kang, H.C., Lee, Y.I., Shin, J.H., Andrabi, S.A., Chi, Z., Gagne, J.P., Lee, Y., Ko, H.S., Lee, B.D., Poirier, G.G*., et al.* (2011). Iduna is a poly(ADP-ribose) (PAR)-dependent E3 ubiquitin ligase that regulates DNA damage. Proceedings of the National Academy of Sciences of the United States of America *108*, 14103-14108.

Karras, G.I., Kustatscher, G., Buhecha, H.R., Allen, M.D., Pugieux, C., Sait, F., Bycroft, M., and Ladurner, A.G. (2005). The macro domain is an ADP-ribose binding module. The EMBO journal *24*, 1911-1920.

Khoury-Haddad, H., Guttmann-Raviv, N., Ipenberg, I., Huggins, D., Jeyasekharan, A.D., and Ayoub, N. (2014). PARP1-dependent recruitment of KDM4D histone demethylase to DNA damage sites promotes double-strand break repair. Proceedings of the National Academy of Sciences of the United States of America *111*, E728-737.

Kiehlbauch, C.C., Aboul-Ela, N., Jacobson, E.L., Ringer, D.P., and Jacobson, M.K. (1993). High resolution fractionation and characterization of ADP-ribose polymers. Analytical biochemistry *208*, 26-34.

Kim, M.Y., Mauro, S., Gevry, N., Lis, J.T., and Kraus, W.L. (2004). NAD+-dependent modulation of chromatin structure and transcription by nucleosome binding properties of PARP-1. Cell *119*, 803-814.

Kim, M.Y., Zhang, T., and Kraus, W.L. (2005). Poly(ADP-ribosyl)ation by PARP-1: 'PAR-laying' NAD+ into a nuclear signal. Genes & development *19*, 1951-1967.

Kornberg, A. (1948). The participation of inorganic pyrophosphate in the reversible enzymatic synthesis of diphosphopyridine nucleotide. The Journal of biological chemistry *176*, 1475.

Kornberg, A., and Pricer, W.E., Jr. (1951). Enzymatic cleavage of diphosphopyridine nucleotide with radioactive pyrophosphate. The Journal of biological chemistry *191*, 535-541.

Kotova, E., Lodhi, N., Jarnik, M., Pinnola, A.D., Ji, Y., and Tulin, A.V. (2011). Drosophila histone H2A variant (H2Av) controls poly(ADP-ribose) polymerase 1 (PARP1) activation in chromatin. Proceedings of the National Academy of Sciences of the United States of America *108*, 6205-6210.

Kraus, W.L. (2008). Transcriptional control by PARP-1: chromatin modulation, enhancer-binding, coregulation, and insulation. Current opinion in cell biology *20*, 294-302.

Kraus, W.L. (2009). New functions for an ancient domain. Nature structural & molecular biology *16*, 904-907.

Kraus, W.L., and Hottiger, M.O. (2013). PARP-1 and gene regulation: progress and puzzles. Molecular aspects of medicine *34*, 1109-1123.

Kraus, W.L., and Lis, J.T. (2003). PARP goes transcription. Cell *113*, 677-683.

Krishnakumar, R., Gamble, M., Frizzell, K., Berrocal, J., Kininis, M., and Kraus, W. (2008). Reciprocal binding of PARP-1 and histone H1 at promoters specifies transcriptional outcomes. Science *319*, 819-821.

Krishnakumar, R., and Kraus, W.L. (2010a). The PARP side of the nucleus: molecular actions, physiological outcomes, and clinical targets. Molecular cell *39*, 8-24.

Krishnakumar, R., and Kraus, W.L. (2010b). PARP-1 regulates chromatin structure and transcription through a KDM5B-dependent pathway. Molecular cell *39*, 736-749.

Langelier, M.F., Planck, J.L., Roy, S., and Pascal, J.M. (2012). Structural basis for DNA damage-dependent poly(ADP-ribosyl)ation by human PARP-1. Science *336*, 728-732.

Leger, K., Bar, D., Savic, N., Santoro, R., and Hottiger, M.O. (2014). ARTD2 activity is stimulated by RNA. Nucleic acids research *42*, 5072-5082.

Leung, A.K., Vyas, S., Rood, J.E., Bhutkar, A., Sharp, P.A., and Chang, P. (2011). Poly(ADP-ribose) regulates stress responses and microRNA activity in the cytoplasm. Molecular cell *42*, 489-499.

Li, G.Y., McCulloch, R.D., Fenton, A.L., Cheung, M., Meng, L., Ikura, M., and Koch, C.A. (2010). Structure and identification of ADP-ribose recognition motifs of APLF and role in the DNA damage response. Proceedings of the National Academy of Sciences of the United States of America *107*, 9129-9134.

Lonn, P., van der Heide, L.P., Dahl, M., Hellman, U., Heldin, C.H., and Moustakas, A. (2010). PARP-1 attenuates Smad-mediated transcription. Molecular cell *40*, 521-532.

Lu, C., and Thompson, C.B. (2012). Metabolic regulation of epigenetics. Cell metabolism *16*, 9-17.

Luo, X., and Kraus, W.L. (2012). On PAR with PARP: cellular stress signaling through poly(ADP-ribose) and PARP-1. Genes & development *26*, 417-432.

Mack, T.G., Reiner, M., Beirowski, B., Mi, W., Emanuelli, M., Wagner, D., Thomson, D., Gillingwater, T., Court, F., Conforti, L.*, et al.* (2001). Wallerian degeneration of injured axons and synapses is delayed by a Ube4b/Nmnat chimeric gene. Nature neuroscience *4*, 1199-1206.

Martinez-Zamudio, R., and Ha, H.C. (2012). Histone ADP-ribosylation facilitates gene transcription by directly remodeling nucleosomes. Molecular and cellular biology *32*, 2490-2502.

Masson, M., Niedergang, C., Schreiber, V., Muller, S., Menissier-de Murcia, J., and de Murcia, G. (1998). XRCC1 is specifically associated with poly(ADP-ribose) polymerase and negatively regulates its activity following DNA damage. Molecular and cellular biology *18*, 3563-3571.

Nishizuka, Y., Ueda, K., Nakazawa, K., and Hayaishi, O. (1967). Studies on the polymer of adenosine diphosphate ribose. I. Enzymic formation from nicotinamide adenine dinuclotide in mammalian nuclei. The Journal of biological chemistry *242*, 3164-3171.

Oberoi, J., Richards, M.W., Crumpler, S., Brown, N., Blagg, J., and Bayliss, R. (2010). Structural basis of poly(ADP-ribose) recognition by the multizinc binding domain of checkpoint with forkhead-associated and RING Domains (CHFR). The Journal of biological chemistry *285*, 39348-39358.

Okano, S., Lan, L., Caldecott, K.W., Mori, T., and Yasui, A. (2003). Spatial and temporal cellular responses to single-strand breaks in human cells. Molecular and cellular biology *23*, 3974-3981.

Olabisi, O.A., Soto-Nieves, N., Nieves, E., Yang, T.T., Yang, X., Yu, R.Y., Suk, H.Y., Macian, F., and Chow, C.W. (2008). Regulation of transcription factor NFAT by ADP-ribosylation. Molecular and cellular biology *28*, 2860-2871.

Pavri, R., Lewis, B., Kim, T.K., Dilworth, F.J., Erdjument-Bromage, H., Tempst, P., de Murcia, G., Evans, R., Chambon, P., and Reinberg, D. (2005). PARP-1 determines specificity in a retinoid signaling pathway via direct modulation of mediator. Molecular cell *18*, 83-96.

Petesch, S.J., and Lis, J.T. (2011). Activator-induced spread of poly(ADP-ribose) polymerase promotes nucleosome loss at Hsp70. Molecular cell.

Petrelli, R., Felczak, K., and Cappellacci, L. (2011). NMN/NaMN adenylyltransferase (NMNAT) and NAD kinase (NADK) inhibitors: chemistry and potential therapeutic applications. Current medicinal chemistry *18*, 1973-1992.

Pinnola, A., Naumova, N., Shah, M., and Tulin, A.V. (2007). Nucleosomal core histones mediate dynamic regulation of poly(ADP-ribose) polymerase 1 protein binding to chromatin and induction of its enzymatic activity. The Journal of biological chemistry *282*, 32511-32519.

Poirier, G.G., de Murcia, G., Jongstra-Bilen, J., Niedergang, C., and Mandel, P. (1982). Poly(ADP-ribosyl)ation of polynucleosomes causes relaxation of chromatin structure. Proceedings of the National Academy of Sciences of the United States of America *79*, 3423-3427.

Preiss, J., Schlaeger, R., and Hilz, H. (1971). Specific inhibition of poly adpribose polymerase by thymidine and nicotinamide in HeLa cells. FEBS letters *19*, 244-246.

Press, C., and Milbrandt, J. (2008). Nmnat delays axonal degeneration caused by mitochondrial and oxidative stress. The Journal of neuroscience : the official journal of the Society for Neuroscience *28*, 4861-4871.

Raffaelli, N., Sorci, L., Amici, A., Emanuelli, M., Mazzola, F., and Magni, G. (2002). Identification of a novel human nicotinamide mononucleotide adenylyltransferase. Biochemical and biophysical research communications *297*, 835-840.

Reale, A., Matteis, G.D., Galleazzi, G., Zampieri, M., and Caiafa, P. (2005). Modulation of DNMT1 activity by ADP-ribose polymers. Oncogene *24*, 13-19.

Reeder, R.H., Ueda, K., Honjo, T., Nishizuka, Y., and Hayaishi, O. (1967). Studies on the polymer of adenosine diphosphate ribose. II. Characterization of the polymer. The Journal of biological chemistry *242*, 3172-3179.

Rosado, M.M., Bennici, E., Novelli, F., and Pioli, C. (2013). Beyond DNA repair, the immunological role of PARP-1 and its siblings. Immunology *139*, 428-437.

Rouleau, M., McDonald, D., Gagne, P., Ouellet, M.E., Droit, A., Hunter, J.M., Dutertre, S., Prigent, C., Hendzel, M.J., and Poirier, G.G. (2007). PARP-3 associates with polycomb group bodies and with components of the DNA damage repair machinery. Journal of cellular biochemistry *100*, 385-401.

Ruf, A., Rolli, V., de Murcia, G., and Schulz, G.E. (1998). The mechanism of the elongation and branching reaction of poly(ADP-ribose) polymerase as derived from crystal structures and mutagenesis. Journal of molecular biology *278*, 57-65.

Rulten, S.L., Fisher, A.E., Robert, I., Zuma, M.C., Rouleau, M., Ju, L., Poirier, G., Reina-San-Martin, B., and Caldecott, K.W. (2011). PARP-3 and APLF function together to accelerate nonhomologous end-joining. Molecular cell *41*, 33-45.

Sala, A., La Rocca, G., Burgio, G., Kotova, E., Di Gesu, D., Collesano, M., Ingrassia, A.M., Tulin, A.V., and Corona, D.F. (2008). The nucleosome-remodeling ATPase ISWI is regulated by poly-ADP-ribosylation. PLoS biology *6*, e252.

Sasaki, Y., Araki, T., and Milbrandt, J. (2006). Stimulation of nicotinamide adenine dinucleotide biosynthetic pathways delays axonal degeneration after axotomy. The Journal of neuroscience : the official journal of the Society for Neuroscience *26*, 8484-8491.

Sauve, A.A., and Schramm, V.L. (2003). Sir2 regulation by nicotinamide results from switching between base exchange and deacetylation chemistry. Biochemistry *42*, 9249-9256.

Schreiber, V., Dantzer, F., Ame, J.C., and de Murcia, G. (2006). Poly(ADP-ribose): novel functions for an old molecule. Nature reviews Molecular cell biology *7*, 517-528.

Schweiger, M., Hennig, K., Lerner, F., Niere, M., Hirsch-Kauffmann, M., Specht, T., Weise, C., Oei, S.L., and Ziegler, M. (2001). Characterization of recombinant human nicotinamide mononucleotide adenylyl transferase (NMNAT), a nuclear enzyme essential for NAD synthesis. FEBS letters *492*, 95-100.

Shimizu, Y., Hasegawa, S., Fujimura, S., and Sugimura, T. (1967). Solubilization of enzyme forming ADPR polymer from NAD. Biochemical and biophysical research communications *29*, 80-83.

Sugimura, T., Fujimura, S., Hasegawa, S., and Kawamura, Y. (1967). Polymerization of the adenosine 5'-diphosphate ribose moiety of NAD by rat liver nuclear enzyme. Biochimica et biophysica acta *138*, 438-441.

Timinszky, G., Till, S., Hassa, P.O., Hothorn, M., Kustatscher, G., Nijmeijer, B., Colombelli, J., Altmeyer, M., Stelzer, E.H., Scheffzek, K.*, et al.* (2009). A macrodomain-containing histone rearranges chromatin upon sensing PARP1 activation. Nature structural & molecular biology *16*, 923-929.

Tulin, A., and Spradling, A. (2003). Chromatin loosening by poly(ADP)-ribose polymerase (PARP) at Drosophila puff loci. Science *299*, 560-562.

Vyas, S., Matic, I., Uchima, L., Rood, J., Zaja, R., Hay, R.T., Ahel, I., and Chang, P. (2014). Family-wide analysis of poly(ADP-ribose) polymerase activity. Nature communications *5*, 4426.

Wang, C., Zhang, F., Wang, L., Zhang, Y., Li, X., Huang, K., Du, M., Liu, F., Huang, S., Guan, Y.*, et al.* (2013). Poly(ADP-ribose) polymerase 1 promotes oxidative-stress-induced liver cell death via suppressing farnesoid X receptor alpha. Molecular and cellular biology *33*, 4492-4503.

Wang, Z., Michaud, G.A., Cheng, Z., Zhang, Y., Hinds, T.R., Fan, E., Cong, F., and Xu, W. (2012). Recognition of the iso-ADP-ribose moiety in poly(ADP-ribose) by WWE domains suggests a general mechanism for poly(ADP-ribosyl)ation-dependent ubiquitination. Genes & development *26*, 235-240.

Weber, F.A., Bartolomei, G., Hottiger, M.O., and Cinelli, P. (2013). Artd1/Parp1 regulates reprogramming by transcriptional regulation of Fgf4 via Sox2 ADP-ribosylation. Stem Cells *31*, 2364-2373.

Werner, E., Ziegler, M., Lerner, F., Schweiger, M., and Heinemann, U. (2002). Crystal structure of human nicotinamide mononucleotide adenylyltransferase in complex with NMN. FEBS letters *516*, 239-244.

Widom, J. (1998). Chromatin structure: linking structure to function with histone H1. Current biology : CB *8*, R788-791.

Wolffe, A.P., and Guschin, D. (2000). Review: chromatin structural features and targets that regulate transcription. J Struct Biol *129*, 102-122.

Zaniolo, K., Desnoyers, S., Leclerc, S., and Guerin, S.L. (2007). Regulation of poly(ADP-ribose) polymerase-1 (PARP-1) gene expression through the post-translational modification of Sp1: a nuclear target protein of PARP-1. BMC molecular biology *8*, 96.

Zhang, F., Chen, Y., Li, M., and Yu, X. (2014). The oligonucleotide/oligosaccharide-binding fold motif is a poly(ADP-ribose)-binding domain that mediates DNA damage response. Proceedings of the National Academy of Sciences of the United States of America *111*, 7278-7283.

Zhang, F., Wang, Y., Wang, L., Luo, X., Huang, K., Wang, C., Du, M., Liu, F., Luo, T., Huang, D.*, et al.* (2013). Poly(ADP-ribose) polymerase 1 is a key regulator of estrogen

receptor alpha-dependent gene transcription. The Journal of biological chemistry *288*, 11348-11357.

Zhang, T., Berrocal, J.G., Yao, J., DuMond, M.E., Krishnakumar, R., Ruhl, D.D., Ryu, K.W., Gamble, M.J., and Kraus, W.L. (2012). Regulation of poly(ADP-ribose) polymerase-1-dependent gene expression through promoter-directed recruitment of a nuclear NAD+ synthase. The Journal of biological chemistry *287*, 12405-12416.

Zhang, X., Kurnasov, O.V., Karthikeyan, S., Grishin, N.V., Osterman, A.L., and Zhang, H. (2003). Structural characterization of a human cytosolic NMN/NaMN adenylyltransferase and implication in human NAD biosynthesis. The Journal of biological chemistry *278*, 13503-13511.

Zhang, Y., Liu, S., Mickanin, C., Feng, Y., Charlat, O., Michaud, G.A., Schirle, M., Shi, X., Hild, M., Bauer, A.*, et al.* (2011). RNF146 is a poly(ADP-ribose)-directed E3 ligase that regulates axin degradation and Wnt signalling. Nature cell biology *13*, 623-629.

Zhou, T., Kurnasov, O., Tomchick, D.R., Binns, D.D., Grishin, N.V., Marquez, V.E., Osterman, A.L., and Zhang, H. (2002). Structure of human nicotinamide/nicotinic acid mononucleotide adenylyltransferase. Basis for the dual substrate specificity and activation of the oncolytic agent tiazofurin. The Journal of biological chemistry *277*, 13148-13154.

CHAPTER TWO

PARP-1 Controls the Adipogenic Transcriptional Program by PARylating C/EBPβ and Modulating Its Transcriptional Activity

The study described in this chapter is selected sections from the prior publication in Luo, X and Ryu, KW et al., Molecular Cell 2017. This chapter highlights the study with the sections with my contributions. The study herein was conducted in collaboration with Xin Luo, Ph.D., Rebecca Gupte, Ph.D., Tulip Nandu, M.S.. X.L. initiated the study, performed molecular biology experiments for the Figure 2.3A, Figure 2.4C, 2.4D, and Figure 2.5. I designed and performed all the rest of molecular biology assays and generated ChIP-seq library. R.G. generated *Parp1* floxed mice and derivatives. T.N. performed bioinformatics analysis on the ChIP-seq dataset.

2.1 Summary

Poly(ADP-ribosyl)ation (PARylation) is a post-translational modification of proteins mediated by PARP family members, such as PARP-1. Although PARylation has been studied extensively, few examples of definitive biological roles for site-specific PARylation have been reported. Here we show that C/EBPβ, a key pro-adipogenic transcription factor, is PARylated by PARP-1 on three amino acids in a conserved regulatory domain. PARylation at these sites inhibits C/EBPβ's DNA binding and transcriptional activities, and attenuates adipogenesis in various genetic and cell-based models. Interestingly, PARP-1 catalytic activity drops precipitously during the first 48 hours of differentiation, corresponding to a release of C/EBPβ from PARylation-mediated inhibition. This promotes the binding of C/EBPβ at enhancers controlling the expression of pro-adipogenic target genes and continued differentiation. Depletion or chemical inhibition of PARP-1, or mutation of the PARylation sites on C/EBPβ, enhances these early adipogenic events. Collectively, our results provide a clear example of how site-specific PARylation drives biological outcomes.

2.2 Introduction

Poly(ADP-ribose) polymerase-1 (PARP-1) (a.k.a ARDT1) is an abundant nuclear protein involved in a variety of nuclear processes, including transcription, RNA processing, and DNA repair (Gibson and Kraus, 2012; Ryu et al., 2015). It is the founding member of the PARP family of proteins, which share a conserved "PARP domain" that catalyzes the transfer of ADP-ribose moieties from NAD^+ to target proteins, in either poly- or mono(ADP-ribosyl)ation reactions (Gibson and Kraus, 2012). PARP proteins are located in most cellular

compartments and play key roles in an array of cellular processes (Gibson and Kraus, 2012; Ryu et al., 2015; Vyas et al., 2013). Among the nuclear PARP proteins, PARP-1 has a well established role in gene regulation, although the mechanisms by which it controls the transcription of target genes remain enigmatic, with both catalytic-dependent and -independent mechanisms described (Kraus and Hottiger, 2013; Krishnakumar and Kraus, 2010a).

Essential steps toward understanding the catalytic-dependent biological roles of PARPs include (1) identifying the target proteins of individual family members, as well as the specific sites at which they are ADP-ribosylated, and (2) determining how ADP-ribosylation of the target proteins affects their biochemical and molecular functions, as well as their biological roles. PARP-1 has been shown to poly(ADP-ribosyl)ate (PARylate) a variety of histone-modifying enzymes and transcription factors to modify their activities (Gao et al., 2009; Gibson et al., 2016; Kanai et al., 2007; Krishnakumar and Kraus, 2010a, b; Olabisi et al., 2008). In most cases, however, detailed analysis of these processes has been hampered by the limited information available on the specific amino acid residues that are PARylated. In this regard, methods for assessing site-specific ADP-ribosylation of proteins have recently been developed (reviewed in (Daniels et al., 2015)) and definitive examples of functional consequences of site-specific ADP-ribosylation are beginning to emerge (Gibson et al., 2016; Kanai et al., 2007; Olabisi et al., 2008).

Previous studies have connected PARP-1 catalytic activity to metabolic outcomes, including adipogenesis, in cell-based model systems, as well as in vivo in mice (Bai et al., 2011; Devalaraja-Narashimha and Padanilam, 2010; Erener et al., 2012a; Erener et al., 2012b;

Lehmann et al., 2015; Luo and Kraus, 2011). The site-specific targets of PARP-1 catalytic activity in these processes, however, have not been determined. In the studies described herein, we link PARP-1-mediated site-specific PARylation of C/EBPβ, a key pro-adipogenic transcription factor, to the regulation of adipogenesis. Adipogenesis is controlled by two sequential waves of transcription factor activation (e.g., C/EBPβ and C/EBPδ in the first wave, and C/EBPα and PPARγ2 in the second wave) (Farmer, 2006; Siersbaek et al., 2012). Once expressed and activated, CEBPβ and C/EBPδ drive the expression of the genes encoding the late transcription factors C/EBPα and PPARγ2, which activate downstream adipocyte-specific genes to control terminal differentiation into mature adipocytes (Farmer, 2006; Siersbaek et al., 2012).

Although the transcriptional control of adipogenesis by pro-adipogenic transcription factors is relatively well understood, the molecular mechanisms controlling the sequential waves of transcriptional activity are still poorly understood. Several post-transcriptional modifications of adipogenic transcription factors, such as C/EBPβ, are thought to link hormonal signaling to the transcriptional regulation program (Nerlov, 2008). Here we show that PARylation of mouse C/EBPβ at three amino acids located in a key regulatory domain inhibits C/EBPβ's DNA binding and transcriptional activities, and attenuates adipogenesis. Our results provide a clear example of how PARylation of specific amino acids in a key transcriptional regulatory protein can affect the molecular and biochemical functions of a protein, as well as the biological outcomes that it controls.

2.3 Results

Genetic depletion of PARP-1 enhances adipogenesis in primary preadipocytes

PARP-1 plays important roles in a wide variety of functionally interconnected tissues that control metabolic outcomes and fat metabolism, including liver, muscle, adipose, pancreas, and the central nervous system (Luo and Kraus, 2011, 2012), making it difficult to separate the effects of PARP-1 in one tissue from effects in other tissues. Thus, studies with whole body *Parp1* null mice where PARP-1 is depleted throughout development have often yielded conflicting results (Bai et al., 2011; Devalaraja-Narashimha and Padanilam, 2010; Erener et al., 2012b; Lehmann et al., 2015; Luo and Kraus, 2011, 2012). To avoid these complications while examining the role of PARP-1 in adipogenesis, we developed a mouse line with a conditional ('floxed') allele of *Parp1* (*Parp1*$^{loxP/loxP}$) (**Fig. 2.1 and 2.2A**). We then crossed the *Parp1*$^{loxP/loxP}$ mice with transgenic mice containing a *Pdgfra-cre/ERT* cassette to generate a Tamoxifen-inducible conditional allele of *Parp1* (*Parp1*$^{loxP/loxP}$*;Pdgfra-cre/ERT*) (**Fig. 2.2B**).

To explore the specific role of PARP-1 in adipogenesis, separated from any potential complicating developmental effects of *Parp1* deletion, we isolated primary preadipocytes from the stromal-vascular fraction (SVF) of adipose tissue (Rodeheffer et al., 2008; Van et al., 1976) collected from *Parp1*$^{loxP/loxP}$ and *Parp1*$^{loxP/loxP}$*;Pdgfra-cre/ERT* mice. When then treated the SVF cells in culture with adenovirus-Cre (Adv-Cre) (**Fig. 2.2A**) or 4-hydroxytamoxifen (4-OHT) (**Fig. 2.2B**) to induce the depletion of PARP-1, which resulted in a dramatic reduction in total cellular PAR levels, as determined by Western blotting (**Fig. 2.2, C and D**). The cells were induced to differentiate with a cocktail of differentiation agents (MDI), containing IBMX, dexamethasone, and insulin. To assess the effects of PARP-1

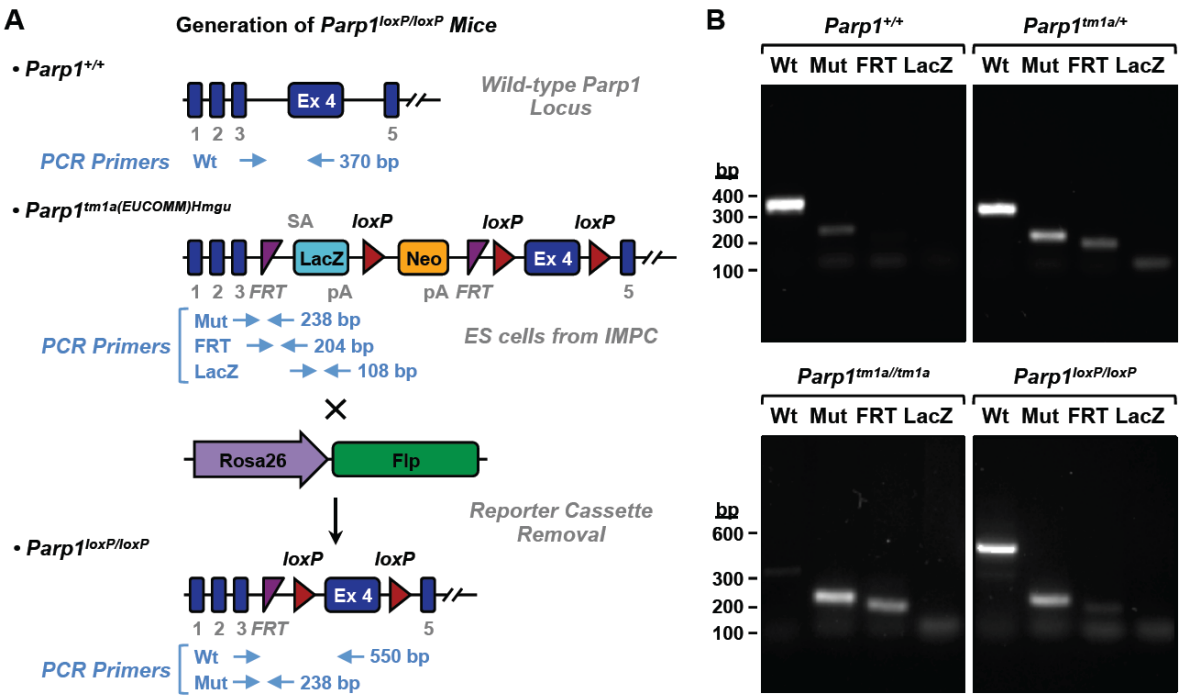

Figure 2.1. Generation of *Parp1*$^{loxP/loxP}$ mice.
(A) Schematic diagram showing a flow chart for the generation of *Parp1*$^{loxP/loxP}$ mice on a C57BL/6N background. The PCR primer pairs used for genotyping at each step are indicated.
(B) Ethidium bromide-stained agarose gels showing the diagnostic PCR products used for genotyping at each step in the generation of *Parp1*$^{loxP/loxP}$ mice. The PCR products are indicated by the PCR primer sets shown in (A). Size markers in base pairs (bp) are shown.

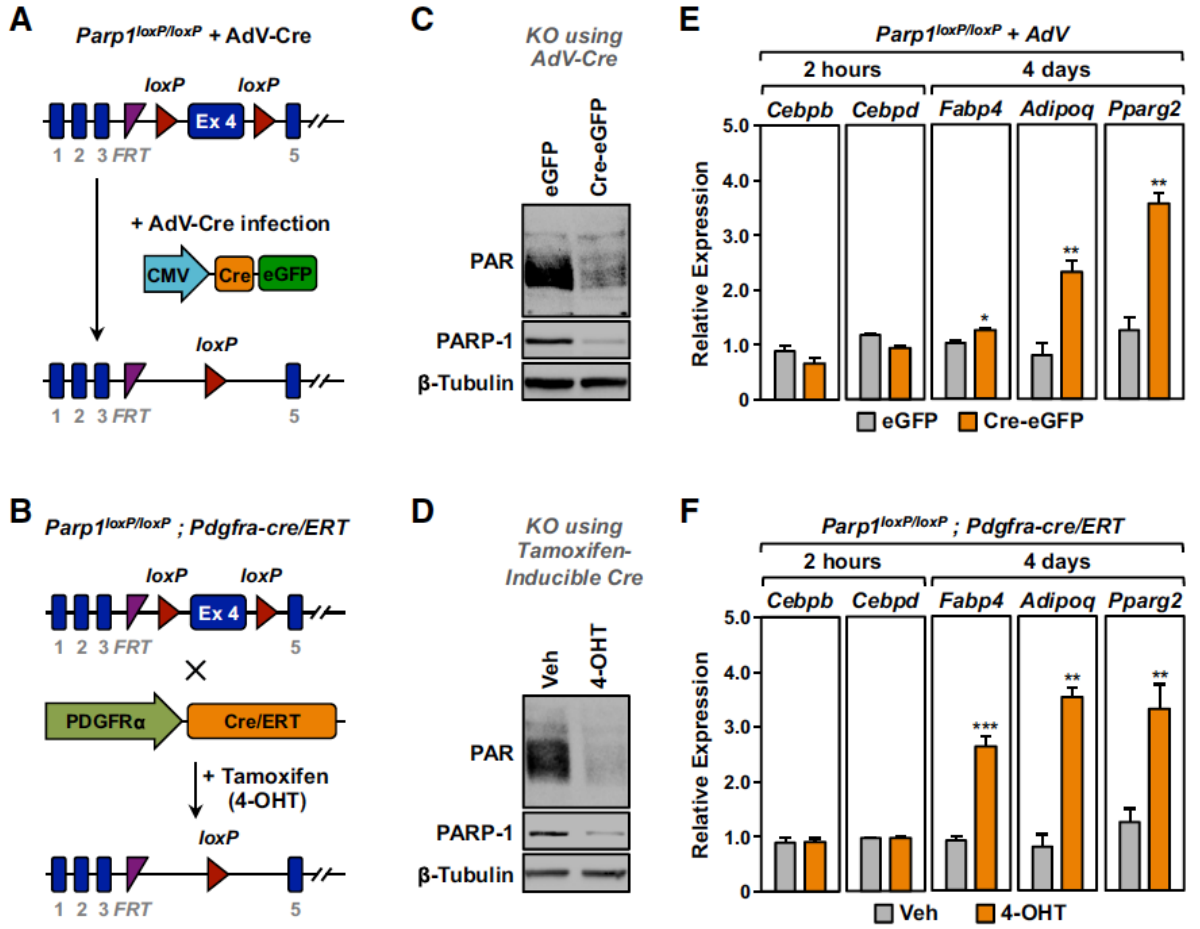

Figure 2.2. Genetic depletion of PARP-1 promotes the differentiation of primary preadipocytes from the stromal-vascular fraction (SVF).
(A and B) Primary SVF preadipocytes isolated from (A) *Parp1*$^{loxP/loxP}$ mice or (B) *Parp1*$^{loxP/loxP}$*;Pdgfra-cre/ERT* mice were subjected to deletion of *Parp1* in culture using adenovirus-Cre (AdV-Cre) or 4-OHT, respectively.
(C and D) Western blots showing the relative levels of PARP-1 and PAR in primary SVF preadipocytes with or without deletion of *Parp1*. β-tubulin was used as a loading control.
(E and F) SVF preadipocytes were subjected to *Parp1* deletion using (E) AdV-Cre or (F) 4-OHT as shown in (A) and (B), respectively, prior to differentiation with MDI. Two hours or 4 days later, the relative expression of various adipocyte marker genes was assayed by RT-qPCR. Each bar represents the mean + SEM for three replicates. Bars marked with asterisks are statistically different from the control (Student's t-test; *** p-value < 0.001 ** p-value < 0.01 or * p-value < 0.05).

depletion on adipogenesis, we monitored the expression of genes associated with adipogenesis by RT-qPCR: (1) 'early' genes, *Cebpb* and *Cebpd*, and (2) 'late' genes *Fabp4*, *Adipoq*, and *Pparg2*, which were assessed 2 hours or 4 days after treatment with MDI, respectively. We observed a significant increase in the expression of *Fabp4*, *Adipoq*, and *Pparg2*, which serve as markers of adipogenesis, upon PARP-1 depletion in both genetic models (**Fig. 2.2, E and F**). These results indicate that PARP-1 acts to attenuate adipogenesis, a conclusion that differs from previous results using *Parp1* null mice and other cell-based models ((Erener et al., 2012a; Erener et al., 2012b; Lehmann et al., 2015); discussed in more detail below).

PARP-1 catalytic activity attenuates adipogenesis

To explore the role of PARP-1 and its catalytic activity in the transcriptional events leading to adipogenesis more broadly, we examined the effect of PARP inhibitors in three mouse cell-based models of adipogenesis: (1) primary SVF preadipocytes (described above), (2) NIH/3T3 fibroblasts (Todaro and Green, 1963), and (3) 3T3-L1 committed preadipocytes (Green and Kehinde, 1975). All three of these cell types can be induced to differentiate using the MDI cocktail described above. Both the PARP-1-selective inhibitor, BYK204165, and a broader spectrum PARP inhibitor, PJ34, promoted adipogenesis in all three cell types, as assessed by increased expression of mRNAs encoding markers of mature adipocytes, *Fabp4* and *AdipoQ* (**Figs. 2.3A**). The effect of BYK204165 on *Fabp4* and *AdipoQ* expression was observed by day 4 post-MDI treatment and persisted until day 8 (**Fig. 2.3B**), indicating that PARP-1's effects on early adipogenic events impact the formation of mature adipocytes.

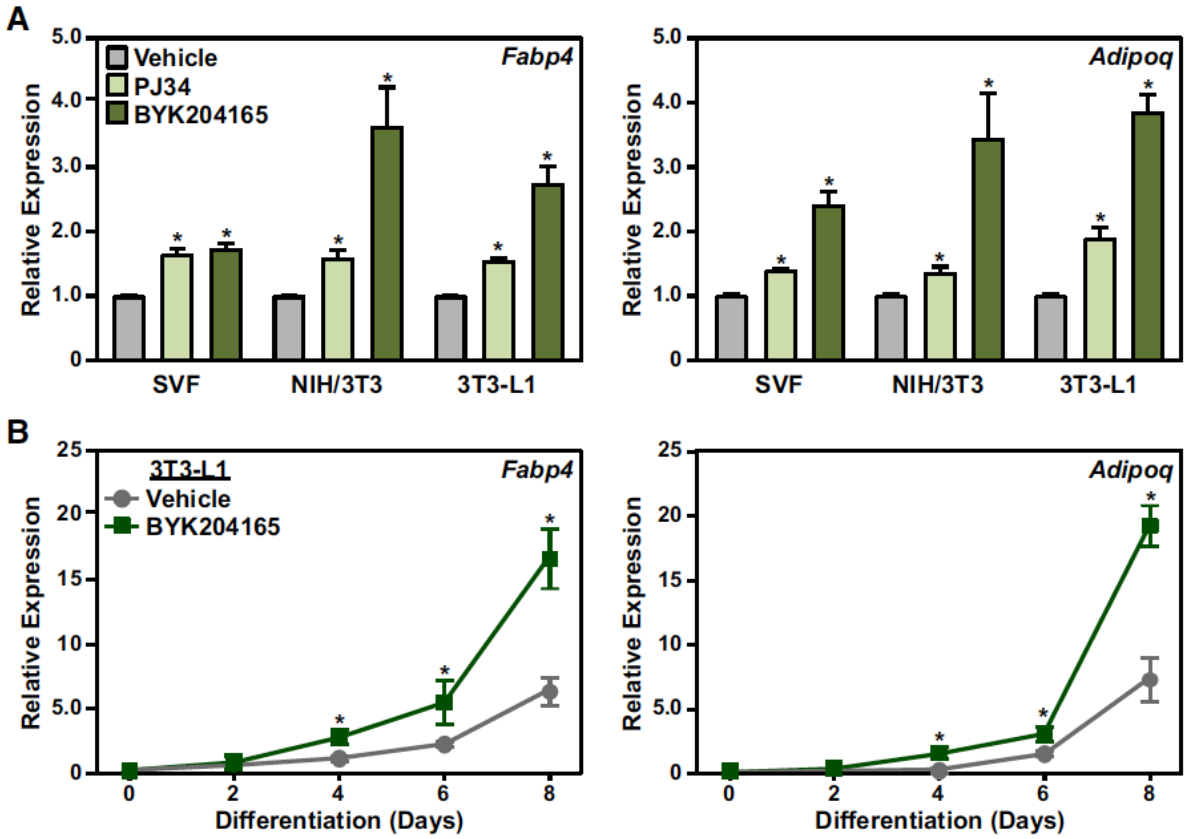

Figure 2.3. Inhibition or depletion of PARP-1 promotes the differentiation of preadipocytes.

(A) SVF, NIH/3T3, and 3T3-L1 cells were treated with 5 μM PJ34 or 20 μM BYK204165 prior to differentiation with MDI. Four days later, the relative expression of adipocyte marker genes *Fabp4* and *AdipoQ* was assayed by RT-qPCR. Each bar represents the mean + SEM for three replicates. Bars marked with an asterisk are statistically different from the control (Student's t-test; p-value < 0.05).

(B) Time course of differentiation in 3T3-L1 cells in response to MDI ± 20 μM BYK204165. The relative expression of adipocyte marker genes *Fabp4* and *AdipoQ* was assayed by RT-qPCR every two days. Each point represents the mean ± SEM for three replicates. Points marked with an asterisk are statistically different from the vehicle-treated control (Student's t-test; p-value < 0.05).

Together, these initial experiments implicate PARP-1 and its catalytic activity in the attenuation of adipogenesis.

Nuclear PAR levels fluctuate during adipogenesis, demarcating the transition between two distinct waves of transcription

To gain mechanistic insights into the regulation of adipogenesis by PARP-1, we conducted additional experiments using 3T3-L1 cells. Consistent with previous studies (Janssen and Hilz, 1989; Pekala et al., 1981), we observed a reduction in nuclear PAR levels (as detected by Western blotting for PAR) during the first two days of adipogenesis (i.e., post-differentiation with MDI), followed by an increase in PAR levels when the cells undergo terminal differentiation (**Fig. 2.4, A and B**). These changes in nuclear PAR levels, however, are not due to alterations in the levels of PARP-1, which remain constant throughout adipogenesis (**Fig. 2.4A**), suggesting instead that they may be due to fluctuations in the activity of PARP-1. Interestingly, the inflection point for the changes in nuclear PAR levels at 48 hours post-differentiation corresponds with two well-characterized cellular states during adipogenesis: proliferation and differentiation. These cellular states are driven by two distinct waves of transcription factor activation (C/EBPβ and C/EBPδ early, C/EBPα and PPARγ2 late) (Farmer, 2006; Siersbaek et al., 2012).

With this in mind, we determined the effects of PARP-1 knockdown on the expression of mRNAs encoding two early adipogenic transcription factors (i.e., C/EBPβ and C/EBPδ) in the first wave of transcription (at 2 hours), and two late adipogenic transcription factors (i.e., C/EBPα and PPARγ2) in the second wave of transcription (at 4 days). Changes

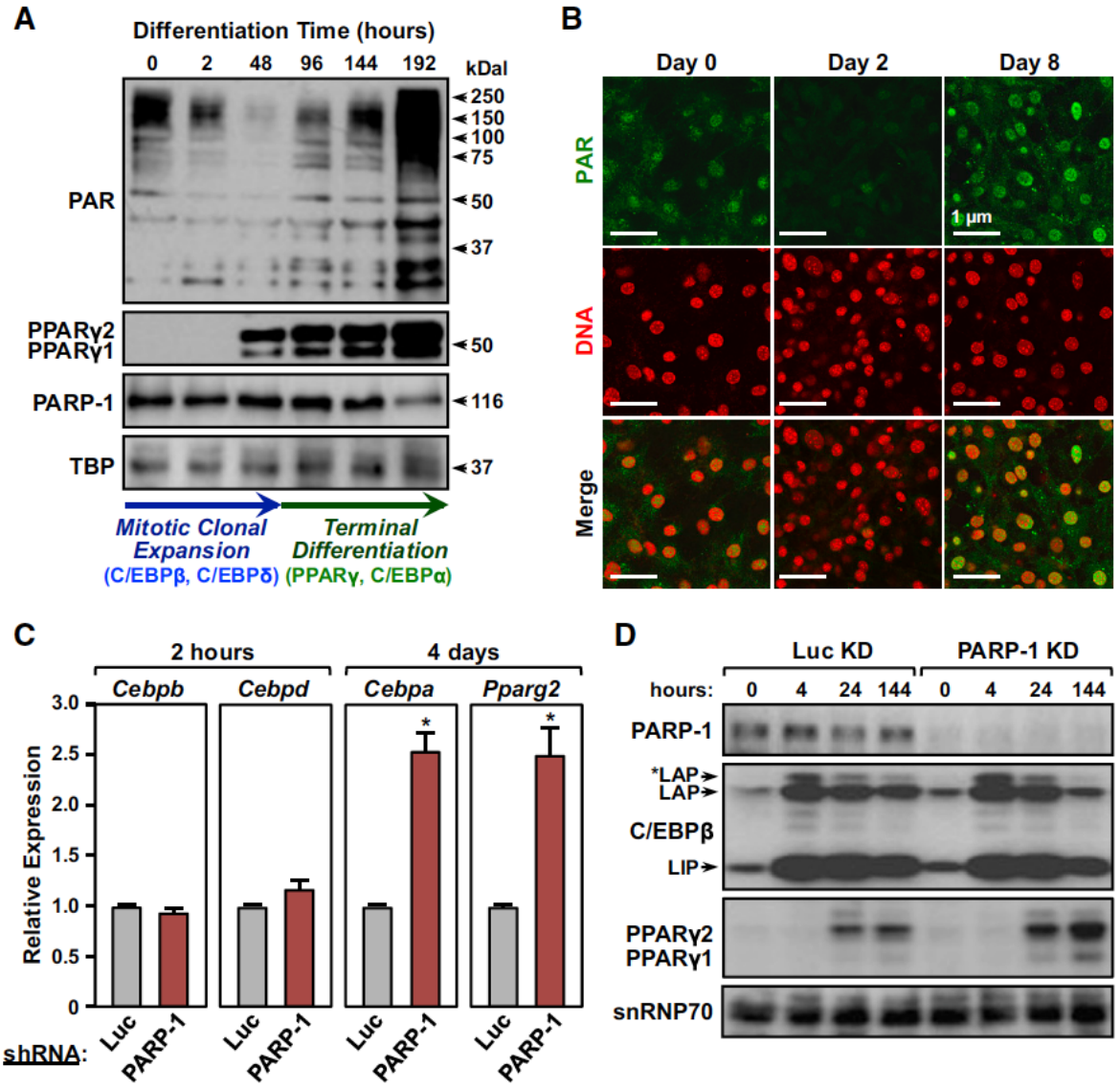

Figure 2.4. Nuclear PAR levels fluctuate and demarcate the transition between two distinct waves of transcription during adipogenesis.

(A) (*Top*) Western blots showing the levels of PAR, PPARγ1, PPARγ2, and PARP-1 in nuclear extracts from 3T3-L1 cells during a time course of differentiation with MDI. TBP was used as a loading control. (*Bottom*) The arrows indicate two distinct phases of adipogenesis: (1) mitotic clonal expansion (0 to 48 hours post MDI; elevated C/EBPβ and C/EBPδ; blue) and (2) terminal differentiation (>48 hours post MDI; elevated PPARγ and C/EBPα; green).

(B) Immunofluorescent staining of 3T3-L1 cells for PAR (green) and DNA (red) during a time course of differentiation with MDI.

(C) RT-qPCR analysis showing the expression of early transcription factors (2 hours post MDI; *Cebpb*, *Cebpd*), and late transcription factors (4 days post MDI; *Cebpa*, *Pparg2*) in 3T3-L1 cells ± knockdown using shRNAs targeting PARP-1 or luciferase (Luc, as a control). Each bar represents the mean + SEM for three replicates. Bars marked with an asterisk are statistically different from the control (Student's t-test; p-value < 0.05).
(D) Western blots showing the expression of PARP-1, C/EBPβ, and PPARγ in 3T3-L1 cells ± knockdown using shRNAs targeting PARP-1 or luciferase (Luc, as a control) during a time course of differentiation with MDI. snRNP70 was used as a loading control.

in expression were observed for *Cebpa* and *Pparg2* (encoding late transcription factors), but not for *Cebpb* and *Cebpd* (encoding early transcription factors) (**Fig. 2.4C**). Although the levels of PPARγ2 increased upon PARP-1 knockdown, the overall levels and distribution of the three isoforms of C/EBPβ (LIP, LAP, and *LAP) were not affected by PARP-1 knockdown during the adipogenesis (**Fig. 2.4D**), consistent with the mRNA expression. Together, these results indicate that hormonal signals may promote the differential regulation of PARP-1 activity at different stages of adipogenesis, leading to sequential regulation of adipogenic transcription factors and the adipogenic transcription program.

PARP-1 and PARylation regulate C/EBPβ-dependent expression of genes encoding late transcription factors

In the sequential model of adipogenic gene expression, early transcription factors, such as C/EBPβ, control the expression of genes encoding late transcription factors, such as *Cebpa* and *Pparg2* (Farmer, 2006; Siersbaek et al., 2012). Thus, we hypothesized that the effects of PARP-1 depletion or inhibition on the expression of *Cebpa* and *Pparg2* that we observed in 3T3-L1 cells might be mediated through C/EBPβ. In this regard, we observed an enrichment of both PARP-1 and C/EBPβ at the promoters of the *Cebpa* and *Pparg2* genes in

3T3-L1 cells 24 hours after MDI-induced differentiation (**Fig. 2.5, A and B**). Furthermore, we observed a significant increase in C/EBPβ at both promoters upon knockdown of PARP-1 (**Fig. 2.5A**) or inhibition of PARP-1 catalytic activity (**Fig. 2.5B**). The latter occurred without a loss of PARP-1 binding at the promoters (**Fig. 2.5B**). Together, these results connect the localization and function of PARP-1 and C/EBPβ to the expression of genes encoding late transcription factors.

C/EBPβ is PARylated by PARP-1 in Preadipocytes

Given the observed requirement of PARP-1 catalytic activity for the attenuation of adipogenesis in preadipocytes (primary, NIH/3T3, and 3T3-L1) (**Fig. 2.3A**), as well as the inverse relationship between PARP-1 activity and C/EBPβ enrichment at the promoters of genes encoding late transcription factors (**Figs. 2.5**), we surmised that PARP-1 may directly antagonize the activity of C/EBPβ at those promoters. More specifically, we hypothesized that PARP-1 might PARylate C/EBPβ to inhibit its DNA binding and transcriptional activity. To test this hypothesis, we first determined if C/EBPβ is PARylated by PARP-1. The PARylation of C/EBPβ was confirmed in C/EBPβ-containing immunoprecipitates from 3T3-L1 cells ectopically expressing doxycycline (Dox)-inducible HA-tagged C/EBPβ (**Fig. 2.6 and Fig. 2.7**). In the latter, we observed a precipitous reduction in C/EBPβ PARylation after 24 hours of MDI-induced differentiation (**Fig. 2.7B**), corresponding to a similar reduction in total cellular PAR levels in early differentiation (**Fig. 2.4A**). Together, these results demonstrate that C/EBPβ is PARylated by PARP-1.

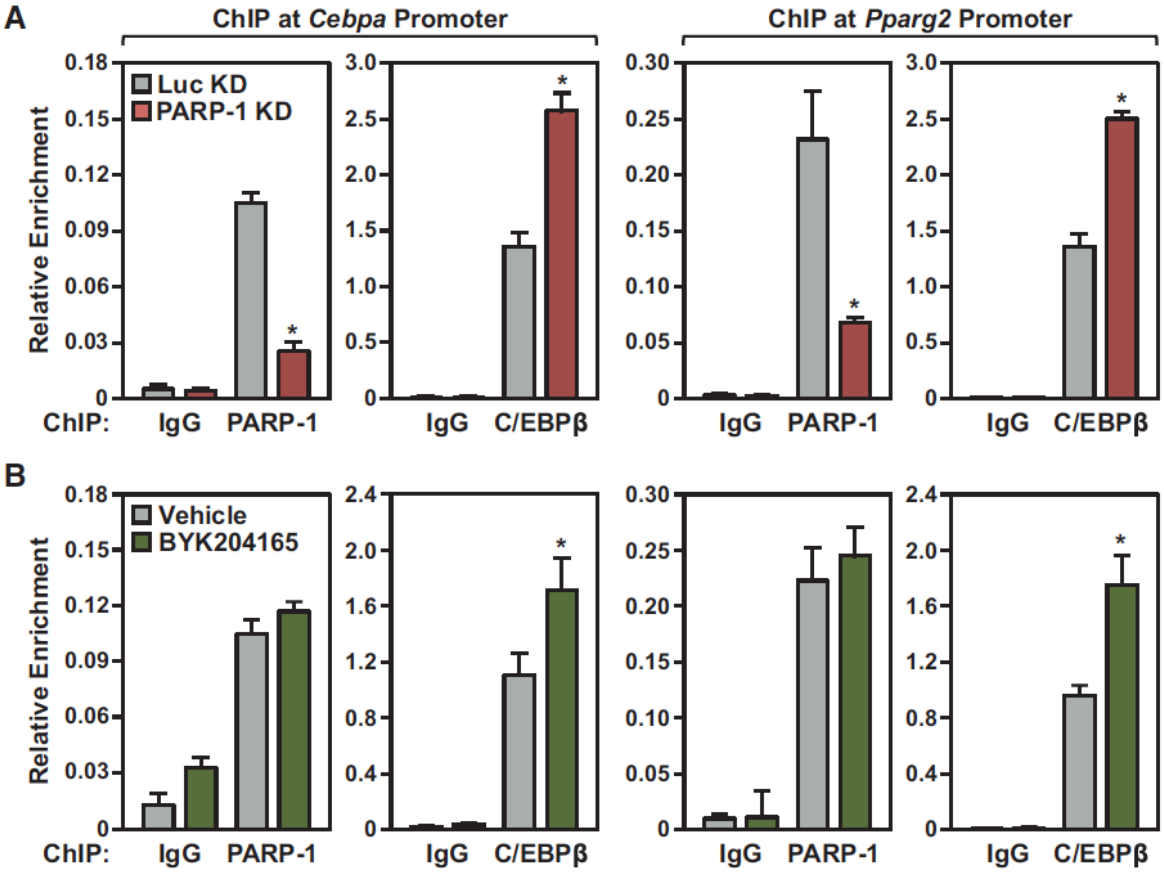

Figure 2.5. PARP-1 and PARylation modulate the binding of C/EBPβ to the promoters of C/EBPβ target genes encoding late transcription factors in 3T3-L1 cells.
(A and B) Results from ChIP-qPCR assays for PARP-1 or C/EBPβ (as indicated) binding at the *Cebpa* (*left*) and *Pparg2* (*right*) gene promoters performed in 3T3-L1 cells 24 hours after differentiation with MDI. The assays were performed (A) with knockdown using shRNAs targeting PARP-1 or luciferase (Luc, as a control), or (B) ± 20 μM BYK204165 (1 hour pretreatment, followed by 24 hours of treatment after adding MDI). Each bar represents the mean + SEM for three replicates. Bars marked with an asterisk are statistically different from the control (Student's t-test; p-value < 0.05).

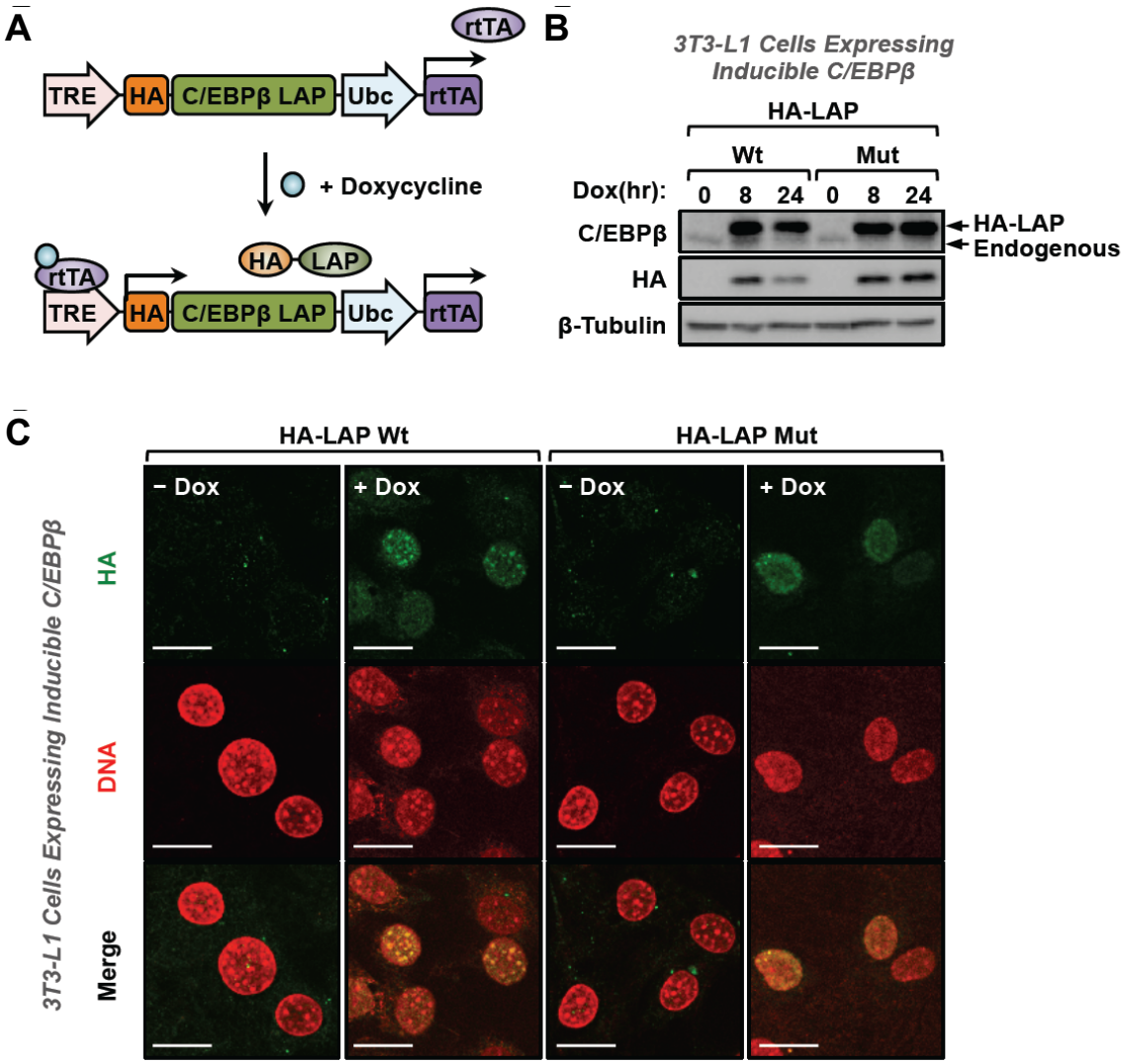

Figure 2.6. Inducible expression of C/EBPβ in 3T3-L1 cells.
(A) Schematic of the system used for doxycycline (Dox)-inducible expression of HA-tagged full-length mouse C/EBPβ in 3T3-L1 cells. The system contains the following: (1) the Tet response element (TRE) linked to the Cytomegalovirus (CMV) promoter, (2) a cDNA encoding HA-tagged full-length mouse C/EBPβ (LAP), and (3) the *Ubc* promoter driving expression of a cDNA encoding the reverse tetracycline-controlled transactivator (rtTA).
(B) Western blots showing Dox-inducible expression of HA-tagged wild-type or ADP-ribosylation site mutant (K133A, E135A, E139A) mouse C/EBPβ in 3T3-L1 cells using the expression system described in (A).
(C) Immunofluorescent staining showing Dox-inducible expression of HA-tagged wild-type or ADP-ribosylation site mutant (K133A, E135A, E139A) mouse C/EBPβ in 3T3-L1 cells using the expression system described in (B). Expression was induced for 8 hours. The signals for the HA tag and DNA (TO-PRO-3) are shown, along with the merged image.

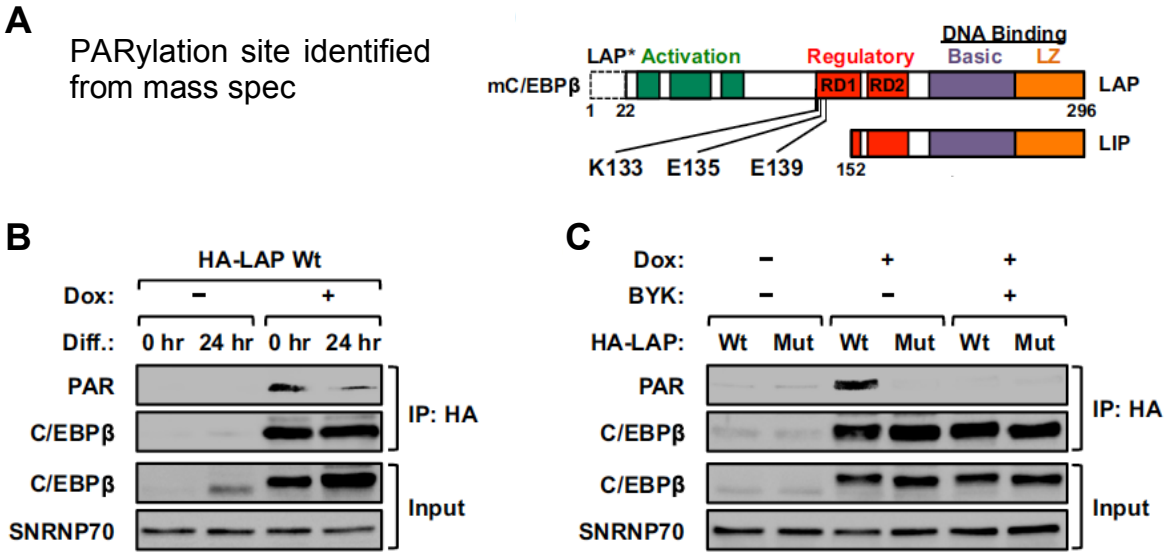

Figure 2.7. PARP-1 PARylates C/EBPβ at specific sites in 3T3-L1 cells.
(**A**) Schematic diagram of mouse C/EBPβ showing the ADP-ribosylation site determined by mass spectrometry (E135), as well as two adjacent sites determined by mutagenesis (K133, E139). C/EBPβ isoforms: LAP, common full-length, LAP*, 22 amino acid N-terminal extension; LIP, N-terminally truncated.
(**B**) Reduced PARylation of C/EBPβ in 3T3-L1 cells upon differentiation. Expression of HA-tagged mouse C/EBPβ was induced from a transgene by treatment with Dox. The cells were then differentiated with MDI for 24 hours and subjected to immunoprecipitation with an anti-HA antibody. The input and the immunoprecipitate (IP) were analyzed by Western blotting for C/EBPβ and PAR as indicated. snRNP70 was used as a loading control.
(**C**) A PARylation site mutant of C/EBPβ is not PARylated in 3T3-L1 cells. The expression of HA-tagged wild-type (Wt) or PARylation site mutant (K133A/E135A/E139A; Mut) mouse C/EBPβ was induced from a transgene by treatment with Dox. The cells were induced to differentiate with MDI for 24 hours ± 20 μM BYK204165 (BYK) and then subjected to immunoprecipitation (IP) with an anti-HA antibody. The input and the immunoprecipitated material were analyzed by Western blotting for C/EBPβ and PAR. snRNP70 was used as a loading control.

To explore the sites at which C/EBPβ is PARylated by PARP-1, we mined an existing mass spectrometry database of experimentally-determined site-specific ADP-ribosylation, which identified glutamate 175 (Glu175 or E175) in human C/EBPβ as a major site of ADP-ribosylation (Zhang et al., 2013b). This amino acid, which is homologous to glutamate 135 (Glu135 or E135) in mouse C/EBPβ, is located within a conserved regulatory domain (RD1) (Abdou et al., 2013; Williams et al., 1995) (**Fig. 2.7A**). Thus, we focused our subsequent functional analyses on E135 to explore the function of C/EBPβ PARylation in adipogenesis. In addition, since previous analyses have shown the PARP-1 is promiscuous in its site selection, particularly when primary target sites are altered by mutagenesis (Altmeyer et al., 2009), we also considered potential secondary PARylation sites located adjacent to E135, including a nearby lysine (lysine 133; K133) and glutamate (glutamate 139; E139) residues (**Fig. 2.7A**).

To verify that these residues are PARylated in cells, we generated a triple mutant with alanine substitutions at K133, E135, and E139. We then expressed either wild type or triple mutant forms of C/EBPβ in 3T3-L1 cells and immunoprecipitate them to check the PARylation level. In 3T3-L1 cells, the triple point mutant (K133/E135/E139) showed no detectable PARylation (**Fig. 2.7C**). Furthermore, the PARylation of wild-type C/EBPβ was completed inhibited by treating the cells with BYK204165 (**Fig. 2.7C**). These results indicate that E135 and adjacent amino acids (K133 and E139) in C/EBPβ can be PARylated by PARP-1 in preadipocytes.

PARylation of C/EBPβ by PARP-1 inhibits its DNA binding activity in vitro and in vivo

Next, we sought to determine the mechanisms by which PARylation of C/EBPβ inhibits its activity. The ChIP-qPCR results shown in Figs. 2.5 demonstrate that PARP-1 can attenuate the binding of C/EBPβ to the promoters of its target genes, suggesting that PARylation of C/EBPβ may inhibit its DNA binding activity. To determine the effects of PARylation on C/EBPβ binding to its cognate enhancers in cells, we performed ChIP-seq for C/EBPβ in 3T3-L1 cells ectopically expressing doxycycline (Dox)-inducible wild-type C/EBPβ or the K133A/E135A/E139A triple point mutant. We observed a dramatic increase in C/EBPβ binding at enhancers near the *Cebpa* and *Pparg* genes with the triple point mutant compared to wild-type C/EBPβ (**Fig. 2.8A**). Furthermore, treatment of the cells with BYK204165 enhanced the binding of wild-type C/EBPβ to the same enhancers (**Fig. 2.8A**). Globally, the significant peaks of C/EBPβ binding in the three conditions (Wt C/EBPβ, Mut C/EBPβ, and Wt C/EBPβ + BYK204165) showed considerable overlap (~2/3 of the sites), although unique sites were observed in all conditions (**Fig. 2.8B**). For the common sites, Mut C/EBPβ and Wt C/EBPβ + BYK204165 showed ~2-fold more binding than Wt C/EBPβ (**Fig. 2.8, C and D**). Together, the results demonstrate that (1) PARylation inhibits the binding of C/EBPβ to its cognate DNA response elements and (2) the DNA binding activity of the triple point mutant C/EBPβ protein is resistant to PARP-1-mediated PARylation.

2.4 Discussion

In the studies described herein, we identified amino acid residues in C/EBPβ, a pro-adipogenic transcription factor, that are PARylated by the NAD^+-dependent catalytic activity

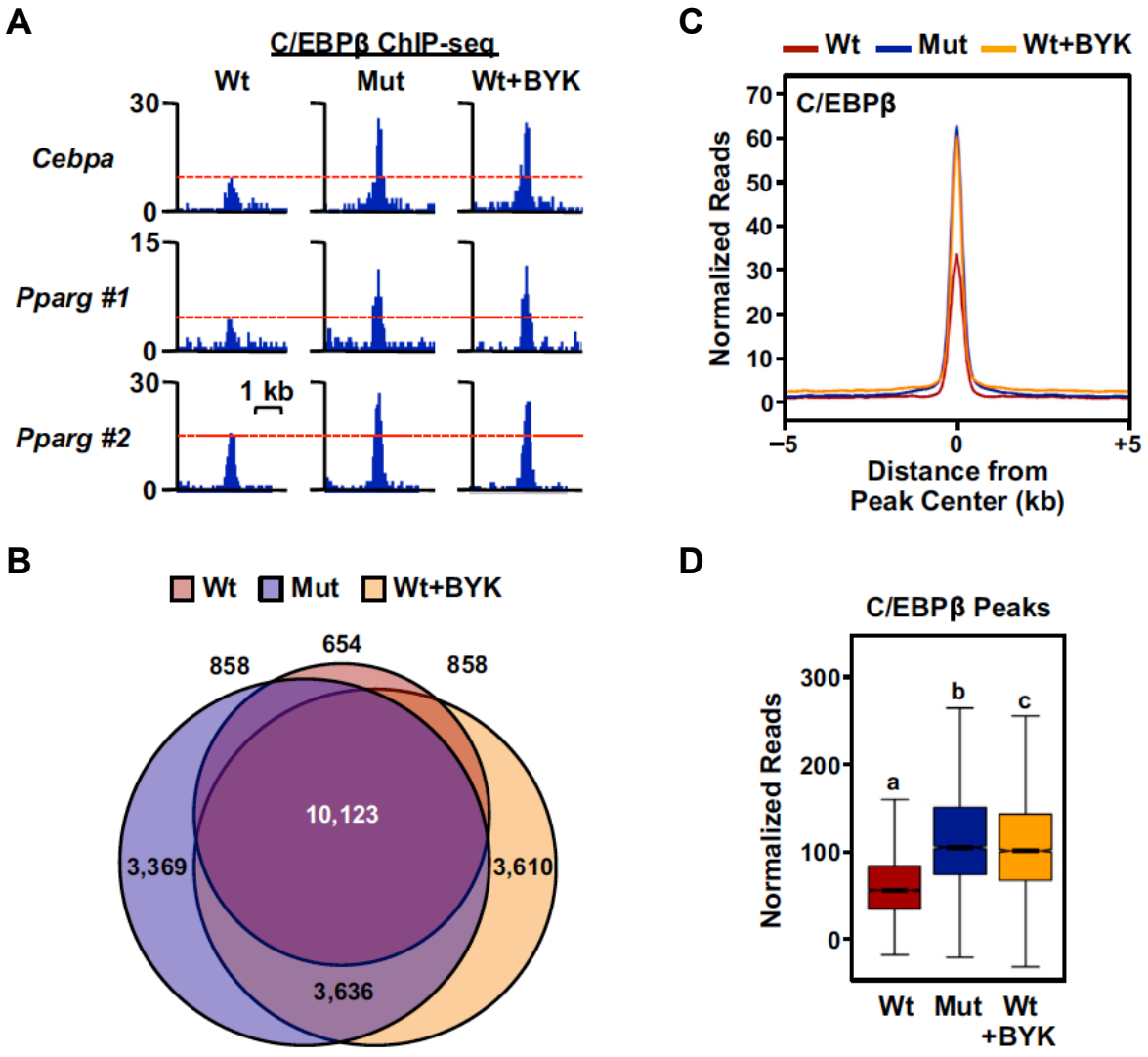

Figure 2.8. PARylation of C/EBPβ by PARP-1 at specific sites inhibits C/EBPβ binding to DNA in cells.

(**A – D**) Mutation of PARP-1-dependent sites of PARylation render C/EBPβ resistant to PARylation-induced decreases in chromatin binding in 3T3-L1 cells. Expression of HA-tagged wild-type (Wt) or PARylation site mutant (K133A/E135A/E139A; Mut) mouse C/EBPβ was induced from a transgene by treatment with Dox for 8 hours ± 20 μM BYK204165 (BYK). The cells were crosslinked and subjected to ChIP-seq for C/EBPβ. (A) ChIP-seq browser tracks for C/EBPβ in the three conditions tested (Wt, Mut, and Wt+BYK) at genomic loci with C/EBPβ enhancers near the *Cebpa* and *Pparg* genes. (B) Venn diagram showing the overlap of statistically significant peaks of C/EBPβ in the three conditions tested. (C) Metaplot and (D) box plot analyses of C/EBPβ binding in 3T3-L1 cells by ChIP-seq in the three conditions tested.

of PARP-1. In addition, we connected PARP-1-dependent PARylation of C/EBPβ at those residues to the regulation of adipogenesis in 3T3-L1 cells. Few examples of definitive biological roles for site-specific PARylation of proteins exist in the literature. In this regard, our results provide a clear example of how PARylation of specific amino acids in a key transcriptional regulatory protein can affect the molecular and biochemical functions of a protein, as well as the biological outcomes that it controls. More broadly, our results provide new insights into the NAD^+-dependent regulation of the transcriptional program controlling adipogenesis.

Site-specific PARylation by PARP-1 modulates the molecular functions of C/EBPβ

Our understanding of the biological roles of ADP-ribosylation has been hampered by the limited information available on the specific residues targeted by the catalytic activity of PARP family members in various biological contexts. Recent advances in mass spectrometry and proteomics have begun to address this issue, leading to the identification of PARP target proteins and the amino acids at which they are modified (reviewed in (Daniels et al., 2015)). In this regard, a previous unbiased mass spectrometry-based screen identified E175 in human C/EBPβ (homologous to E135 in mouse C/EBPβ) as a major site of ADP-ribosylation (Zhang et al., 2013b). We confirmed E135 in mouse C/EBPβ as a functional site of PARP-1-mediated PARylation. In addition, we identified two nearby residues (K133 and E139) that can also be PARylated by PARP-1. Together, these three amino acids account for the vast majority of PARP-1-dependent PARylation of C/EBPβ in cells (see Fig. 2C) and mediate PARP-1-dependent effects on C/EBPβ function (see Figs. 2.8).

Previous studies have demonstrated clear effects of PARylation of target proteins, although the sites of PARylation were not mapped in most cases. For example, we have shown that PARylation of KDM5B, a histone H3 lysine 4 demethylase, by PARP-1 prevents its binding to chromatin and blocks its enzymatic activity (Krishnakumar and Kraus, 2010b). Additional studies have shown that a number of DNA-binding transcription factors (e.g., Sox, YY1, and NFAT) are PARylated by PARP-1 (Gao et al., 2009; Oei and Shi, 2001; Olabisi et al., 2008). The few examples in the literature where the sites of PARylation on target proteins were identified are NFAT (increases DNA binding; (Olabisi et al., 2008)), p53 (inhibits nuclear export; (Kanai et al., 2007)), and NELF-E (inhibits RNA binding and NELF-dependent promoter-proximal pausing by RNA polymerase II; (Gibson et al., 2016)). Many of the molecular and biochemical effects of PARylation on these target proteins are likely due to the nature of PAR itself, namely a large charged polymer that can elicit both steric and charge effects on target protein functions (Gibson and Kraus, 2012).

Our results indicate that PARylation by PARP-1 can inhibit the sequence-specific binding of C/EBPβ to DNA and chromatin and, conversely, that inhibition of PARylation can enhance the binding of C/EBPβ to DNA and chromatin. Reduced binding of PARylated C/EBPβ to promoters is likely to account for the relatively low C/EBPβ-dependent transcription of target genes. We cannot, however, exclude additional effects on C/EBPβ transcriptional activity. C/EBPβ possesses both an amino-terminal activation domain and a central regulatory domain. The latter, which contains the sites of PARylation, functions as a bipartite regulatory domain that regulates DNA binding and supports C/EBPβ transcriptional activity under some cell types and promoter contexts (Abdou et al., 2013; Williams et al.,

1995). PARylation of this domain may directly inhibit or block intra- or intermolecular interactions required for the function of the regulatory domain. This possibility will require additional analysis in future studies.

Dual functions of PARP-1 in gene regulation

ChIP-based genome-wide localization studies have shown that PARP-1 is located at a large fraction of actively transcribed gene promoters (Krishnakumar et al., 2008b; Krishnakumar and Kraus, 2010b), although only a small subset of the genes transcribed from those promoters are affected by depletion or inhibition of PARP-1 (Frizzell et al., 2009; Krishnakumar et al., 2008b; Zhang et al., 2012). These seemingly paradoxical observations are consistent with an emerging view of dual roles for PARP-1 in gene regulation (Kraus and Hottiger, 2013; Krishnakumar and Kraus, 2010a), where it functions both as: (1) a nucleosome-binding chromatin regulator, which may function independently of its catalytic activity (Kim et al., 2004) and (2) a transcription factor-specific coregulator that may, in some cases, modify the transcription factors whose activities it modifies (Gao et al., 2009; Kanai et al., 2007; Krishnakumar and Kraus, 2010b; Olabisi et al., 2008). Our results with PARP-1 and C/EBPβ, which are a clear example of the latter, may serve as a useful model for understanding the role of PARP-1 in modulating signaling pathways that culminate in the modification of transcription factors.

A role for site-specific PARylation of C/EBPβ in adipogenesis

Adipogenesis is controlled by two sequential waves of transcription driven by two

distinct waves of transcription factor activation (C/EBPβ and C/EBPδ early, C/EBPα and PPARγ2 late) (Farmer, 2006; Siersbaek et al., 2012). Identifying the regulators that mediate the transition between these the two waves is key to understanding the process. Interestingly, the transition between the two waves of transcription, which occurs 24-48 hour post-differentiation, corresponds to a nadir of nuclear PAR levels, as well as the following effects on C/EBPβ: reduced PARylation, increased DNA binding, and enhanced transcriptional activity. Together, these results support a role for PARP-1 in the transcriptional switch during early adipogenesis through the modulation C/EBPβ transcriptional activity. How PARP-1 catalytic activity is regulated to control the timing and cessation of C/EBPβ PARylation during adipogenesis is currently unknown, but may involve cellular signaling directly to PARP-1 (Krishnakumar and Kraus, 2010a; Luo and Kraus, 2012) or possibly the availability of nuclear NAD^+ (Zhang et al., 2012).

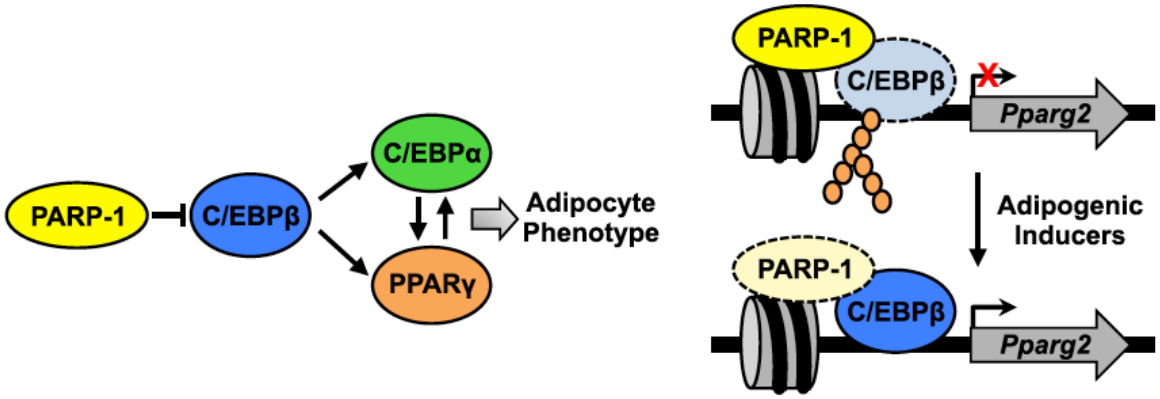

Figure 2.9. Model for the role of PARP-1 in attenuating adipogenesis, as described in the text.

Our results on the role of PARP-1 in adipogenesis different considerably from those reported previously by Hottiger and colleagues, who performed their studies using whole body *Parp1* null mice, as well as cell-based models (Erener et al., 2012a; Erener et al., 2012b; Lehmann et al., 2015). While we observed an inhibitory effect of PARP-1 on adipogenesis through PARylation of C/EBPβ at the early stages of adipogenesis that persists throughout differentiation, Hottiger et al. observed a stimulatory effect of PARP-1 on adipogenesis that occurs by enhancing the transcriptional activity of PPARγ (Erener et al., 2012a; Erener et al., 2012b; Lehmann et al., 2015). We have explored a number of possible causes for these discrepancies, but have not uncovered an obvious explanation. In this regard, we note the following: (1) our results were generated using three different model systems (i.e., SVF cells with conditional *Parp1* knockout, 3T3-L1 cells, and NIH/3T3 cells) and three different modes of PARP-1 inhibition (knockout, knockdown, PARP inhibitors), (2) our results with 3T3-L1 cells were replicated in two independent labs (W.L.K. and R.E.S.) using independent batches of cells purchased directly from the ATCC, and (3) we identified specific sites of PARylation on C/EBPβ that, when mutated, yielded predictable results that consistent with the rest of our studies.

We also note that conflicting results about the role of PARP-1 in adipogenesis and other metabolic processes have been reported by at least three different labs using whole body *Parp1* null mice (Asher et al., 2010; Bai et al., 2011; Devalaraja-Narashimha and Padanilam, 2010; Erener et al., 2012b; Luo and Kraus, 2011). As described above, PARP-1 contributes to overall metabolic outcomes by playing distinct (and sometimes opposing) roles in different metabolism-related tissues, including muscle, liver, pancreas, brain, and adipose,

with actions in one tissue presumably impacting actions in the other tissues (Luo and Kraus, 2011). As such, tissue-specific conditional *Parp1* knockout mice, like those we describe herein, are needed to unambiguously address questions about the role of PARP-1 in tissue-specific physiological outcomes. Studies with such genetic models should be coupled with assays using PARylation site point mutants of the target protein, the results of which should correspond logically with the results of assays using PARP-1 knockout, knockdown, or chemical inhibition.

2.5 Materials and Methods

Generation of *Parp1* conditional knockout mice

Parp1$^{tm1a(EUCOMM)Hmgu}$ embryonic stem (ES) cells on a C57BL/6N background were obtained from the International Mouse Phenotyping Consortium (IMPC; colony name G4786, colony number HEPD0555_6_C04). Chimeric mice were generated from the ES cells at UT Southwestern's Transgenic Core Facility. All mice were housed and maintained at UT Southwestern's Animal Resource Center. The chimeric mice were bred to C57BL/6 (*Parp1*$^{+/+}$) mice to generate *Parp1*$^{tm1a/+}$ heterozygous progeny (see Fig. S1A). The presence of the *Parp1*^{tm1a} cassette was determined using the short-range PCR primers listed below (see Fig. S1B). The *Parp1*$^{tm1a/+}$ mice were self-crossed to generate homozygous *Parp1*$^{tm1a/tm1a}$ progeny. The reporter cassette was excised by crossing the *Parp1*$^{tm1a/tm1a}$ mice with FLP recombinase-expressing B6.129S4-*Gt(ROSA)26Sor*$^{tm2(FLP*)Sor/J}$ mice (from The Jackson Laboratory, stock no. 012930) (see Fig. S1A). Removal of the reporter cassette was verified

by short-range qPCR using the *FRT* and *LacZ* primer pairs listed below (see Fig. S1B). Homozygous *Parp1*$^{loxP/loxP}$ mice were subsequently generated by self-crossing. To produce mice with a Tamoxifen-inducible conditional allele of *Parp1* (*Parp1*$^{loxP/loxP}$*;Pdgfra-cre/ERT*), *Parp1*$^{loxP/loxP}$ mice were crossed with transgenic mice expressing *Pdgfra-cre/ERT* [B6N.Cg-*Tg(Pdgfra-cre/ERT)467Dbe/J*; The Jackson Laboratory, stock no. 018280]. The presence of the *Pdgfra-cre/ERT* allele was determined using the short-range *Pdgfra* and *Cre* PCR primers listed below (see Fig. S1B).

The following short-range PCR primers used for genotyping:

Wild-type (Wt):

Forward: 5'-CTGTGGTCCTCTTGCCTCTG-3'

Reverse: 5'-ACTTCCCCAGGGATGGGTTA-3'

Mutant:

Forward: 5'-CTGTGGTCCTCTTGCCTCTG-3'

Reverse: 5'-TCGTGGTATCGTTATGCGCC-3'

FRT:

Forward: 5'-AGGCGCATAACGATACCACGAT-3'

Reverse: 5'- CCACAACGGGTTCTTCTGTT-3'

LacZ:

Forward: 5'-ATCACGACGCGCTGTATC-3'

Reverse: 5'-ACATCGGGCAAATAATATCG-3'

Pdgfra:

Forward: 5'- TCAGCCTTAAGCTGGGACAT-3'

Reverse 5'-ATGTTTAGCTGGCCCAAATG-3'

Cre:

Forward: 5'-GGACATGTTCAGGGATCGCCAGGCG-3'

Reverse: 5'- CCATGAGTGAACGAACCTGG-3'

Isolation and differentiation of stromal vascular fraction (SVF) cells

Isolation of SVF cells was performed as essentially as described previously (Gupta et al., 2012). Briefly, two 6-week-old male C57BL/6 mice were sacrificed and four pads of inguinal white adipose tissue were dissected and placed in sterile 1x PBS. The adipose tissue was minced with scissors until homogeneous, added to 10 mL of digestion solution [100 mM HEPES pH 7.4, 120 mM NaCl, 50 mM KCl, 5 mM glucose, 1 mM CaCl2, 1 mg/mL collagenase D (Roche, 11088858001), and 1.5% BSA], and incubated at 37°C with shaking for 2 hours, with gentle vortexing every 30 min. The digested tissue was mixed by pipetting up and down and then passed through a 100 μm cell strainer into a new 50 mL conical tube containing 30 mL of SVF cells culture medium [10% FBS in DMEM/F-12, GlutaMAX™ (Life Technologies, 10565-018)] to dilute the digestion buffer. The cells were collected by centrifugation at 600 x g for 5 min, resuspended in 10 mL of SVF culture medium, and passed through a 40 μm cell strainer. The cells were collected again by centrifugation at 600 x g for 5 min, resuspended in 5 mL of SVF culture medium, and plated onto a 6 cm diameter collagen-coated plate until well attached. The cells were grown to ~80 to 90% confluence, split and expanded, and frozen in aliquots for later use. To test the differentiation potential of

the SVF cells, they were seeded at ~5 x 10^4 cells per well in 12-well plates, grown to confluence, and then grown for another two days under contact inhibition. Induction of adipogenesis was achieved by the addition of a cocktail of differentiation agents (MDI), including 0.5 mM IBMX (3-isobutyl-1-methylxanthine; Calbiochem, 410957), 1 μM dexamethasone (Dex; Sigma, D4902), and 5 μg/mL insulin (Sigma, I-5500) for two days. Subsequently, the cells were grown in culture medium with 5 μg/mL insulin (Sigma, I-5500) for the indicated times before collection. In some cases, the cells were treated with vehicle, 20 μM BYK 204165, or 5 μM PJ34 for 2 days or as indicated. To assess adipogenesis, we performed RT-qPCR on total RNA isolated from the cells and staining of lipid droplets in intact cells using BODIPY 493/503 NHS Easter (Life Technologies, D2191).

Generation of *Parp1* knockout SVF cells

SVF cells were isolated from *Parp1*$^{loxP/loxP}$ or *Parp1*$^{loxP/loxP}$*;Pdgfra-cre/ERT* mice as described above for wild-type mice. For adenovirus-Cre mediated *Parp1* deletion, *Parp1*$^{loxP/loxP}$ SVF cells were grown to ~80 to 90% confluence, infected with adenovirus expressing GFP (ad-GFP; Vector Biolabs, 1060) or Cre-GFP (ad-Cre-GFP; Vector Biolabs, 1700) with a MOI of ~50 for two days. The cells were then cultured in fresh medium for two more days under contact inhibition before the induction of adipogenesis. For Tamoxifen-inducible Cre-mediated *Parp1* deletion, *Parp1*$^{loxP/loxP}$*;Pdgfra-Cre/ERT* SVF cells were cultured to ~80% confluence and then treated with 5 μm 4-Hydroxytamoxifen (4-OHT; Sigma, H7904) for four days before the induction of adipogenesis, as described above.

Cell culture and treatments

3T3-L1 cells (Green and Kehinde, 1975) were obtained from the American Type Cell Culture (ATCC, CL-173TM). The cells were maintained in DMEM (Cellgro, 10-017-CM) supplemented with 10% fetal bovine serum (Atlanta Biologicals, S11550). For induction of adipogenesis in 3T3-L1 cells, the cells were plated in 6-well plates, grown to confluence, and then grown for another two days under contact inhibition. Induction of adipogenesis was achieved by the addition of a cocktail of differentiation agents (MDI), including 0.25 mM IBMX (3-isobutyl-1-methylxanthine; Calbiochem, 410957), 1 μM dexamethasone (Dex; Sigma, D4902), and 10 μg/mL insulin (Sigma, I-5500) for two days. Subsequently, the cells were grown in culture medium with 10 μg/mL insulin (Sigma, I-5500) for the indicated times before collection. The induction of adipogenesis in NIH-3T3 cells was performed in a similar fashion by the addition of 5 μM of Rosiglitazone (Sigma, R2408) together with the MDI cocktail. For experiments with the PARP inhibitors BYK204165 (Eltze et al., 2008) (Tocris Bioscience, 1104546-89-5) and PJ34 (Jagtap et al., 2002) (Enzo Life Sciences, ALX-270-289), the cells were pretreated with the inhibitor at the indicated concentrations, or with DMSO vehicle, for 1 hour prior to the addition of the MDI cocktail and during the first two days of differentiation after adding the MDI cocktail. To assess adipogenesis, intact cells were stained with 5% Oil Red O (Sigma, O0625).

293T cells were purchased from the ATCC (CRL-3216) and maintained in DMEM (Cellgro, 10-017-CM) supplemented with 10% fetal bovine serum (Atlanta Biologicals, S11550).

Antibodies

The custom rabbit polyclonal antiserum against PARP-1 used for Western blotting and ChIP assays was generated by using an antigen comprising the amino-terminal half of PARP-1 (Kim et al., 2004) (now available from Active Motif; cat. no. 39559). The custom recombinant antibody-like anti-poly-ADP-ribose binding reagent (anti-PAR) and anti-pan-ADP-ribose binding reagent (anti-panADPR) were generated and purified in-house (now available from EMD Millipore; cat. nos. MABE1031 and MABE1016, respectively). The other antibodies used are as follows: mouse monoclonal PAR antibody (Trevigen, 4335-AMC-050), rabbit polyclonal ChIP-grade C/EBPβ antibody (Santa Cruz, sc-150X), mouse monoclonal ChIP-grade HA antibody (Abcam, ab9110), rabbit polyclonal PPARγ antibody (Santa Cruz, sc-7196), and SNRP70 (Abcam, ab51266), and rabbit IgG (Invitrogen, 10500C).

Cloning, mutagenesis, and generation of retroviral vectors for expression and knockdown

The following cloning strategies were used to make retroviral and lentiviral vectors for expressing C/EBPβ and knocking down C/EBPβ or PARP-1.

Generation of wild-type and PARylation mutant C/EBPβ cDNAs. pcDNA 3.1(-) mouse C/EBPβ (LAP isoform) and pcDNA 3.1(-) mouse C/EBPβ (LIP isoform) were purchased from Addgene (plasmids 12557 and 12561). A C/EBPβ-based DNA sequence encoding an HA tag was generated by PCR using the following primers:

Forward: 5'-acgcggccgcgaattcatgtacccatacgatgttccagattacgctgaagtggccaacttctactacgag-3'

Reverse: 5'-gcaagcttggatccctagcagtggcccgccgaggccag-3'

The PCR product was added at the 5' end of the cDNA (for an amino-terminal tag) using digestion with *NotI* and *HindIII*.

Mutant C/EBPβ (LAP) cDNAs encoding single, double, and triple point mutants of C/EBPβ were generated with the QuickChange Site-Directed Mutagenesis Kit from Stratagene using the following primers:

• Mutant 1 - C/EBPβ K133A (AAG to GCC) / E135A (GAG to GCC)

Forward: 5'-CGCTCgccGCGGccCCGGGCTTCGAAC-3'

Reverse: 5'-GTTCGAAGCCCGGggCCGCggcGAGCG-3'

• Mutant 2 - C/EBPβ E135A (GAG to GCC) / E139A (GAA to GCC)

Forward: 5'-GGccCCGGGCTTCGccCCCGCGGACTGCAAG-3'

Reverse: 5'-CTTGCAGTCCGCGGGggCGAAGCCCGGGggCC-3'

• Mutant 3 - C/EBPβ K133A (AAG to GCC) / E135A (GAG to GCC) / E139A (GAA to GCC)

Mutant 3 was generated with the Mutant 5 primers using the Mutant 3 cDNA as the template.

Generation of retroviral expression vectors for C/EBPβ and PARP-1. The wild-type and mutant HA-tagged mouse C/EBPβ cDNAs were cloned from the pcDNA 3.1(-) vectors described above into the pQCXIP retroviral expression vector (BD Biosciences; puromycin resistant) using *NotI* and *BamHI*. Flag-tagged human PARP-1 cDNA was cloned into pQCXIP as described previously (Frizzell et al., 2009).

Generation of retroviral expression vectors for shRNAs targeting PARP-1. Vectors for expression of shRNAs were generated by cloning double-stranded oligonucleotides

containing shRNA sequences targeting luciferase (Luc, as a control), PARP-1 into the pSUPER.retro vector (OligoEngine; puromycin or neomycin resistant). The oligonucleotide sequences are as follows:

Luc: 5' - gatatgggctgaatacaaa - 3' (Reynolds et al., 2004)

PARP-1: 5' - gggcaagcacagtgtcaaa - 3' (Frizzell et al., 2009)

C/EBPβ: 5' - ggccctgagtaatcacttaaa - 3' Dharmacon siDESIGN Center

Generation of doxycycline (Dox)-inducible lentiviral expression vectors for C/EBPβ. The wild-type and mutant HA-tagged mouse C/EBPβ cDNAs were cloned from the pcDNA 3.1(-) vectors described above into modified pINDUCER20 lentiviral expression vector (Addgene, plasmid no. 44012) (Meerbrey et al., 2011) using *XhoI*.

Generation of stable knockdown and ectopic expression cell lines

The retroviral and lentiviral expression vectors were used to generate stable cell lines, as described below.

Generation of stable cell lines using retroviral expression vectors. Retroviruses were generated by transfection of the pSUPER.retro or pQCXIP constructs described above, together with an expression vector for the VSV-G envelope protein, into Phoenix Ampho cells using GeneJuice transfection reagent (Novagen, 70967) according to the manufacturer's protocol. The resulting viruses were used to infect 3T3-L1 cells. Stably transduced cells were selected with puromycin (Sigma, P9620; 2 μg/mL) or G418 sulfate (Sigma, A1720; 1 mg/mL).

Generation of stable cell lines using lentiviral expression vectors. The pINDUCER20 vectors described above were transfected into 293T cells using GeneJuice transfection reagent (Novagen, 70967), together with an expression vector for the GAG-Pol-Rev, VSV-G envelope protein, and pAdvantage according to the manufacturer's protocol. The resulting viruses were then concentrated by using a Lenti-X concentrator (Clonetech, 631231) and used to infect 3T3-L1 cells. Stably transduced cells were selected with G418 sulfate (Sigma, A1720; 1 mg/mL). For experiments, the expression of C/EBPβ was achieved by treating the cells with 1 μg/ml Dox for 8 or 24 hours, as specified below.

Preparation of nuclear extracts and Western blotting

The 3T3-L1 stable cell lines described above were seeded at ~1.5 x 10^6 cells per 10 cm diameter plate and treated as described above. After collecting the cells, extracts of the cytoplasmic and nuclear fractions were made using the Sigma CelLytic NuCLEAR Extraction Kit according to the manufacturer's protocol. Specifically, the cells were incubated in isotonic buffer [10 mM Tris-HCl pH 7.5, 2 mM $MgCl_2$, 3 mM $CaCl_2$, 0.3 M sucrose, 1 mM DTT, 250 nM ADP-HPD (Sigma, A0627; a PARG inhibitor to prevent PAR chain cleavage during extraction), 10 μM PJ34 (a PARP inhibitor to prevent new PAR chain synthesis during extraction), and 1x complete protease inhibitor cocktail (Roche, 11697498001)] on ice for 15 minutes and lysed by the addition of 0.6% IGEPAL CA-630 detergent with vortexing. The lysates were centrifuged and the supernatants were collected as the cytoplasmic fraction. The crude nuclear pellet was washed once with isotonic buffer, resuspended in extraction buffer C (20 mM HEPES pH 7.9, 1.5 mM $MgCl_2$, 0.42 M NaCl,

0.2 mM EDTA, 25% v/v glycerol, 1 mM DTT, 250 nM ADP-HPD, 10 μM PJ34, and 1x complete protease inhibitor cocktail), and incubated for 20 minutes at 4°C with intermittent vigorous vortexing. The resuspended nuclear material was then clarified by centrifugation and the supernatant was collect as the nuclear extract. For each fraction under the indicated conditions, 20 μg of total protein were separated on an 8% polyacrylamide-SDS gel and transferred to a nitrocellulose membrane. Western blotting was performed with antibodies to the following: panADPR (1:3000), PARP-1 (1:2000), C/EBPβ (1:1000), PPARγ (1:1000), and SNRP70 (1:1000).

Immunofluorescent staining of cells

3T3-L1 cells were seeded at a density of ~3 x 10^4 per well on sterile cover slips in 24-well plates and differentiated as described above. The cells were rinsed twice with ice cold 1x PBS and fixed with ice cold methanol/acetone (7:3 ratio). The fixed cells were washed three times with ice cold 1x PBS and blocked with blocking solution (5% non-fat milk or 5% BSA, plus 0.05% Tween-20 in 1x PBS) for 30 minutes at room temperature. After blocking, the cells were incubated with anti-poly-ADP-ribose binding reagent (anti-PAR) or HA antibody (abcam, ab9110) overnight at 4°C. The cells were washed three times with ice cold 1x PBS and incubated with secondary antibody (Alexa fluor 488 goat anti-rabbit IgG (H+L) at 1:1000; Life Technologies, A-11034) for 30 minutes at room temperature in the dark. The cells were then washed three times with cold 1x PBS and stained with 1 μM TO-PRO-3 (Life Technologies, T3605) for 2 minutes at room temperature, followed by three washes with ice cold 1x PBS. The cover slips were then mounted onto glass slides with Vectashield HardSet

Mounting Medium (Vector Laboratories, H-1400). The slides were imaged using a Leica SP2 confocal microscope.

Immunoprecipitation of HA-tagged C/EBPβ

3T3-L1 cells expressing inducible HA-tagged wild-type or triple mutant (K133A, E135A, E139A) C/EBPβ were seeded at ~5 x 10^6 cells per 15 cm diameter plate and cultured, differentiated and treated as described above. For the induction of HA-tagged C/EBPβ expression, the cells were treated with 1 μg/ml of doxycycline (Dox) for 8 hours before collection. The cells were collected and the nuclei were isolated as described above. The nuclear pellet was resuspended in nuclear extraction buffer (50 mM Tris-HCl pH 7.5, 150 mM NaCl, 1 mM EDTA, 1 % IGEPAL CA-630, 250 nM ADP-HPD, 10 μM PJ34, 1 mM NaF, mM $NaVO_4$, and 1x complete protease inhibitor cocktail), incubated for 30 minutes at 4°C, and clarified by centrifugation. The supernatant was collected as the nuclear extract. Aliquots of nuclear extract containing 1 mg of total protein were used for each IP condition. The nuclear extracts were incubated with 30 μL of anti-HA magnetic beads (Thermo Fisher, 88836) at 4°C for 4 hours and then washed five times in nuclear extraction buffer for 10 minutes at 4°C with constant mixing. The beads were then heated to 100°C for 10 minutes in SDS-PAGE loading solution to release the bound proteins. The immunoprecipitated material was subjected to Western blotting as described above.

RNA isolation and RT-qPCR

RNA isolation and RT-qPCR were performed as described previously (Luo et al., 2014). Briefly, 3T3-L1 cells, or SVF cells were seeded at ~2 x 10^5 cells per well in 6-well plates and treated as described above. After collecting the cells, total RNA was isolated using Trizol Reagent (Invitrogen) according to the manufacturer's protocol. Total RNA was reverse transcribed using oligo (dT) primers and MMLV reverse transcriptase (Promega) and subjected to quantitative real-time PCR (qPCR) using gene-specific primers as described below. All target gene expression was normalized to the expression of the gene encoding TBP.

Chromatin immunoprecipitation-qPCR (ChIP-qPCR)

3T3-L1 cells were seeded at ~5 x 10^6 cells per 15 cm diameter plate and treated as described above. ChIP was performed as described previously (Kininis et al., 2007; Krishnakumar et al., 2008b), with a few modifications. The cells were cross-linked with 1% formaldehyde in PBS for 10 minutes at 37°C and quenched in 125 mM glycine in PBS for 5 minutes at 4°C. The cells were then collected and lysed in Farnham lysis buffer [5 mM PIPES pH 8.0, 85 mM KCl, 0.5% NP-40, 1 mM DTT, and 1x complete protease inhibitor cocktail (Roche)]. A crude nuclear pellet was collected by centrifugation, resuspended in lysis buffer (50 mM Tris-HCl pH 7.9, 1% SDS, 10 mM EDTA, 1 mM DTT, and 1x complete protease inhibitor cocktail), and incubated on ice for 10 minutes. The chromatin was sheared at 4°C by sonication using a Bioruptor UC200 at the highest setting for four 5-minute cycles of 30 seconds on and 60 seconds off to generate chromatin fragments of ~300 bp in length. The soluble chromatin was diluted 1:10 with dilution buffer (20 mM Tris-HCl pH 7.9, 0.5%

Triton X-100, 2 mM EDTA, 150 mM NaCl, 1 mM DTT, and 1x complete protease inhibitor cocktail) and pre-cleared with protein A agarose beads. The pre-cleared supernatant was used in immunoprecipitation reactions with antibodies against the factor of interest (PARP-1 or C/EBPβ) or with rabbit IgG as a control. The immunoprecipitated material was washed once with low salt wash buffer (20 mM Tris-HCl pH 7.9, 2 mM EDTA, 125 mM NaCl, 0.05% SDS, 1% Triton X-100, 1 μM aprotinin, and 1 μM leupetin), once with high-salt wash buffer (20 mM Tris-HCl pH 7.9, 2 mM EDTA, 500 mM NaCl, 0.05% SDS, 1% Triton X-100, 1 μM aprotinin, and 1 μM leupetin), once with LiCl wash buffer (10 mM Tris-HCl, pH 7.9, 1 mM EDTA, 250 mM LiCl, 1% NP-40, 1% sodium deoxycholate, 1 μM aprotinin, and 1 μM leupetin), and once with 1x Tris-EDTA (TE). The immunoprecipitated material was eluted in elution buffer (100 mM $NaHCO_3$, 1% SDS) and was then digested with proteinase K and RNase H to remove protein and RNA, respectively. The immunoprecipitated genomic DNA was then extracted with phenol:chloroform:isoamyl alcohol and precipitated with ethanol. The ChIPed genomic DNA was subjected to qPCR using gene-specific primers as described below.

Quantitative real-time PCR (qPCR) for gene expression and ChIP analyses

Reverse transcribed cDNA and ChIPed genomic DNA were analyzed by quantitative PCR (qPCR) as described previously (Luo et al., 2014). Briefly, cDNA or ChIPed genomic DNA, 1x SYBR Green PCR master mix, and forward and reverse primers (250 nM) were mixed and subjected to 45 cycles of amplification (95°C for 10 second, 60°C for 10 second, 72°C for 1 second) following an initial 5 minute incubation at 95°C using a Roche

LightCycler 480 384-well detection system. Melting curve analyses were performed to ensure that only the targeted amplicon was amplified. All experiments were performed on at least three separate biological replicates to ensure reproducibility. The sequences of the primers used for RT-qPCR and ChIP-qPCR are listed below.

• *mRNA expression primers*

TBP forward: 5'-TGCTGTTGGTGATTGTTGGT-3'

TBP reverse: 5'-CTGGCTTGTGTGGGAAAGAT-3'

PARP-1 forward: 5'-tggtttcaagtcccttgtcc-3'

PARP-1 reverse: 5'-tgctgtctatggagctgtgg-3'

CEBPA forward: 5'-gaacagcaacgagtaccgggta-3'

CEBPA reverse: 5'-gccatggccttgaccaaggag-3'

CEBPB forward: 5'-caagctgagcgacgagtaca-3'

CEBPB reverse: 5'-cagctgctccaccttcttct-3'

PPARG1 forward: 5'-CTGTGAGACCAACAGCCTGA-3'

PPARG1 reverse: 5'-CAGTGGTTCACCGCTTCTTT-3'

PPARG2 forward: 5'-TGCTGTTATGGGTGAAACTCT-3'

PPARG2 reverse: 5'-CGCTTGATGTCAAAGGAATGC-3'

CEBPD forward: 5'-TGCCCACCCTAGAGCTGTG-3'

CEBPD reverse: 5'-CGCTTTGTGGTTGCTGTTGA-3'

FABP4 forward: 5'-AAGTGGGAGTGGGCTTTGC-3'

FABP4 reverse: 5'-CCGGATGGTGACCAAATCC-3'

ADIPOQ forward: 5'-GACAAGGCCGTTCTCTTCAC-3'

ADIPOQ reverse: 5'-CAGACTTGGTCTCCCACCTC-3'

• *ChIP primers:*

CEBPA promoter forward: 5'-CTGGAAGTGGGTGACTTAGAGG-3'

CEBPA promoter reverse: 5'-GAGTGGGGAGCATAGTGCTAG-3'

PPARG2 promoter forward: 5'-GGCCAAATACGTTTATCTGGTG-3'

PPARG2 promoter reverse: 5'-GTGAGGGGCGTGAACTGTA-3'

C/EBPβ ChIP-seq

ChIP-seq for C/EBPβ in 3T3-L1 cells was performed as described below.

Generation of C/EBPβ ChIP-seq libraries. 3T3-L1 cells expressing inducible HA-tagged wild-type or triple mutant (K133A, E135A, E139A) C/EBPβ were seeded at ~5 x 10^6 cells per 15 cm plate and treated as described above. Inducible expression of C/EBPβ was achieved by treating the cells with 1 μg/ml of doxycycline for 8 hours. For some experiments, the cells were treated with the PARP inhibitor BYK204165 during induction of C/EBPβ. ChIP was performed as described above using a C/EBPβ antibody or rabbit IgG, and the resulting immunoprecipitated genomic DNA was purified using AMPure XP beads (Beckman Coulter, A63881). After purification, 5 to 10 ng of ChIPed genomic DNA per condition were used to generate ChIP-seq libraries. For the spike-in control, 20 pg of phiX DNA was added to each condition. ChIP-seq libraries were generated as described previously (Franco et al., 2015) with some modifications. Briefly, the ChIPed DNA was end-repaired using an end repair kit (Enzymatics, Y9140-LC-L) and a single "A"-base overhang was added using the Klenow DNA polymerase (Enzymatics, P7010-HC-L). The A-modified

DNA was ligated to Illumina sequencing adaptors using T4 DNA ligase (Enzymatics, L6030-HC-L). The ligated DNA was amplified using Kapa HiFi Hot Start Ready Mix (KAPA Biosystems, KK2612), size-selected (250 - 300 bp) by agarose gel electrophoresis, and purified using a QIAquick Gel Extraction Kit (Qiagen, 28706). The size-selected fragments were further amplified using Illumina TruSeq P5 and P7 PCR primers and subjected to another round of agarose gel electrophoresis. Quality control was performed to determine the size, concentration, and purity of the final libraries. The libraries were sequenced using an Illumina Next seq 500 per the manufacturer's instructions.

ChIP-seq data analyses. ChIP-seq data analyses were performed largely as described previously (Franco et al., 2015). The ChIP-seq libraries containing phiX spike-in controls were first aligned to the mouse genome (mm10) using Bowtie ver. 2 with default parameters (Langmead and Salzberg, 2012). The libraries were then aligned to phiX DNA to estimate the spike in levels in each individual condition. Uniquely mapped reads from the alignment were converted to bigWig files using BEDTools for visualization in the UCSC genome browser (Quinlan and Hall, 2010). The inputs for each condition were used as controls to call peaks using MACS software (Zhang et al., 2008).

Venn diagrams: We used the mergePeaks function in the HOMER software suite (Heinz et al., 2010) to determine the overlap of peaks between conditions.

Metagene analyses: We used metagene representations to illustrate the distribution of reads near the C/EBPβ binding sites. To compare different conditions by metagene analyses, the total reads in each condition were scaled to 62 million reads and then divided by the individual read depth of each condition. The spike in reads were also used to normalize the

final read counts. The signals from the corresponding conditions without doxycycline were then subtracted to remove the background signal from endogenous C/EBPβ. For some analyses, we calculated the fold change between the wild-type and mutant C/EBPβ with doxycycline treatment, and then extracted the top 50 percent of C/EBPβ peaks for analysis and representation.

Box plots: For quantitatively assessing the read distribution in a fixed window around each binding site under various conditions, we generated box plots for the data. The read distribution surrounding the C/EBPβ peaks was calculated and plotted using the box plot function in R. The reads were normalized in a similar manner as described for the metagene analyses. Wilcoxon rank sum tests were performed to determine the statistical significance of all comparisons. For some analyses, we used the reads around the top 50 percent of C/EBPβ peaks extracted from the metagene analysis, which were then normalized and plotted using the box plot function in R.

2.6 References

Abdou, H.S., Atlas, E., and Hache, R.J. (2013). A positive regulatory domain in CCAAT/enhancer binding protein beta (C/EBPBeta) is required for the glucocorticoid-mediated displacement of histone deacetylase 1 (HDAC1) from the C/ebpalpha promoter and maximum adipogenesis. Endocrinology *154*, 1454-1464.

Altmeyer, M., Messner, S., Hassa, P.O., Fey, M., and Hottiger, M.O. (2009). Molecular mechanism of poly(ADP-ribosyl)ation by PARP1 and identification of lysine residues as ADP-ribose acceptor sites. Nucleic acids research *37*, 3723-3738.

Asher, G., Reinke, H., Altmeyer, M., Gutierrez-Arcelus, M., Hottiger, M.O., and Schibler, U. (2010). Poly(ADP-ribose) polymerase 1 participates in the phase entrainment of circadian clocks to feeding. Cell *142*, 943-953.

Bai, P., Canto, C., Oudart, H., Brunyanszki, A., Cen, Y., Thomas, C., Yamamoto, H., Huber, A., Kiss, B., Houtkooper, R.H.*, et al.* (2011). PARP-1 inhibition increases mitochondrial metabolism through SIRT1 activation. Cell metabolism *13*, 461-468.

Daniels, C.M., Ong, S.E., and Leung, A.K. (2015). The promise of proteomics for the study of ADP-ribosylation. Molecular cell *58*, 911-924.

Devalaraja-Narashimha, K., and Padanilam, B.J. (2010). PARP1 deficiency exacerbates diet-induced obesity in mice. The Journal of endocrinology *205*, 243-252.

Eltze, T., Boer, R., Wagner, T., Weinbrenner, S., McDonald, M.C., Thiemermann, C., Burkle, A., and Klein, T. (2008). Imidazoquinolinone, imidazopyridine, and isoquinolindione derivatives as novel and potent inhibitors of the poly(ADP-ribose) polymerase (PARP): a comparison with standard PARP inhibitors. Molecular pharmacology *74*, 1587-1598.

Erener, S., Hesse, M., Kostadinova, R., and Hottiger, M.O. (2012a). Poly(ADP-ribose)polymerase-1 (PARP1) controls adipogenic gene expression and adipocyte function. Mol Endocrinol *26*, 79-86.

Erener, S., Mirsaidi, A., Hesse, M., Tiaden, A.N., Ellingsgaard, H., Kostadinova, R., Donath, M.Y., Richards, P.J., and Hottiger, M.O. (2012b). ARTD1 deletion causes increased hepatic lipid accumulation in mice fed a high-fat diet and impairs adipocyte function and differentiation. FASEB journal : official publication of the Federation of American Societies for Experimental Biology *26*, 2631-2638.

Farmer, S.R. (2006). Transcriptional control of adipocyte formation. Cell metabolism *4*, 263-273.

Franco, H.L., Nagari, A., and Kraus, W.L. (2015). TNFalpha signaling exposes latent estrogen receptor binding sites to alter the breast cancer cell transcriptome. Molecular cell *58*, 21-34.

Frizzell, K.M., Gamble, M.J., Berrocal, J.G., Zhang, T., Krishnakumar, R., Cen, Y., Sauve, A.A., and Kraus, W.L. (2009). Global analysis of transcriptional regulation by poly(ADP-

ribose) polymerase-1 and poly(ADP-ribose) glycohydrolase in MCF-7 human breast cancer cells. The Journal of biological chemistry *284*, 33926-33938.

Gao, F., Kwon, S.W., Zhao, Y., and Jin, Y. (2009). PARP1 poly(ADP-ribosyl)ates Sox2 to control Sox2 protein levels and FGF4 expression during embryonic stem cell differentiation. The Journal of biological chemistry *284*, 22263-22273.

Gibson, B.A., and Kraus, W.L. (2012). New insights into the molecular and cellular functions of poly(ADP-ribose) and PARPs. Nature reviews Molecular cell biology *13*, 411-424.

Gibson, B.A., Zhang, Y., Jiang, H., Hussey, K.M., Shrimp, J.H., Lin, H., Schwede, F., Yu, Y., and Kraus, W.L. (2016). Chemical genetic discovery of PARP targets reveals a role for PARP-1 in transcription elongation. Science *353*, 45-50.

Green, H., and Kehinde, O. (1975). An established preadipose cell line and its differentiation in culture. II. Factors affecting the adipose conversion. Cell *5*, 19-27.

Gupta, R.K., Mepani, R.J., Kleiner, S., Lo, J.C., Khandekar, M.J., Cohen, P., Frontini, A., Bhowmick, D.C., Ye, L., Cinti, S.*, et al.* (2012). Zfp423 expression identifies committed preadipocytes and localizes to adipose endothelial and perivascular cells. Cell metabolism *15*, 230-239.

Heinz, S., Benner, C., Spann, N., Bertolino, E., Lin, Y.C., Laslo, P., Cheng, J.X., Murre, C., Singh, H., and Glass, C.K. (2010). Simple combinations of lineage-determining transcription factors prime cis-regulatory elements required for macrophage and B cell identities. Molecular cell *38*, 576-589.

Jagtap, P., Soriano, F.G., Virag, L., Liaudet, L., Mabley, J., Szabo, E., Hasko, G., Marton, A., Lorigados, C.B., Gallyas, F., Jr.*, et al.* (2002). Novel phenanthridinone inhibitors of poly (adenosine 5'-diphosphate-ribose) synthetase: potent cytoprotective and antishock agents. Critical care medicine *30*, 1071-1082.

Janssen, O.E., and Hilz, H. (1989). Differentiation of 3T3-L1 pre-adipocytes induced by inhibitors of poly(ADP-ribose) polymerase and by related noninhibitory acids. European journal of biochemistry / FEBS *180*, 595-602.

Kanai, M., Hanashiro, K., Kim, S.H., Hanai, S., Boulares, A.H., Miwa, M., and Fukasawa, K. (2007). Inhibition of Crm1-p53 interaction and nuclear export of p53 by poly(ADP-ribosyl)ation. Nature cell biology *9*, 1175-1183.

Kim, M.Y., Mauro, S., Gevry, N., Lis, J.T., and Kraus, W.L. (2004). NAD+-dependent modulation of chromatin structure and transcription by nucleosome binding properties of PARP-1. Cell *119*, 803-814.

Kininis, M., Chen, B.S., Diehl, A.G., Isaacs, G.D., Zhang, T., Siepel, A.C., Clark, A.G., and Kraus, W.L. (2007). Genomic analyses of transcription factor binding, histone acetylation, and gene expression reveal mechanistically distinct classes of estrogen-regulated promoters. Molecular and cellular biology *27*, 5090-5104.

Kraus, W.L., and Hottiger, M.O. (2013). PARP-1 and gene regulation: progress and puzzles. Molecular aspects of medicine *34*, 1109-1123.

Krishnakumar, R., Gamble, M.J., Frizzell, K.M., Berrocal, J.G., Kininis, M., and Kraus, W.L. (2008). Reciprocal binding of PARP-1 and histone H1 at promoters specifies transcriptional outcomes. Science *319*, 819-821.

Krishnakumar, R., and Kraus, W.L. (2010a). The PARP side of the nucleus: molecular actions, physiological outcomes, and clinical targets. Molecular cell *39*, 8-24.

Krishnakumar, R., and Kraus, W.L. (2010b). PARP-1 regulates chromatin structure and transcription through a KDM5B-dependent pathway. Molecular cell *39*, 736-749.

Langmead, B., and Salzberg, S.L. (2012). Fast gapped-read alignment with Bowtie 2. Nature methods *9*, 357-359.

Lehmann, M., Pirinen, E., Mirsaidi, A., Kunze, F.A., Richards, P.J., Auwerx, J., and Hottiger, M.O. (2015). ARTD1-induced poly-ADP-ribose formation enhances PPARgamma ligand binding and co-factor exchange. Nucleic acids research *43*, 129-142.

Luo, X., Chae, M., Krishnakumar, R., Danko, C.G., and Kraus, W.L. (2014). Dynamic reorganization of the AC16 cardiomyocyte transcriptome in response to TNFalpha signaling revealed by integrated genomic analyses. BMC genomics *15*, 155.

Luo, X., and Kraus, W.L. (2011). A one and a two ... expanding roles for poly(ADP-ribose) polymerases in metabolism. Cell metabolism *13*, 353-355.

Luo, X., and Kraus, W.L. (2012). On PAR with PARP: cellular stress signaling through poly(ADP-ribose) and PARP-1. Genes & development *26*, 417-432.

Meerbrey, K.L., Hu, G., Kessler, J.D., Roarty, K., Li, M.Z., Fang, J.E., Herschkowitz, J.I., Burrows, A.E., Ciccia, A., Sun, T.*, et al.* (2011). The pINDUCER lentiviral toolkit for inducible RNA interference in vitro and in vivo. Proceedings of the National Academy of Sciences of the United States of America *108*, 3665-3670.

Nerlov, C. (2008). C/EBPs: recipients of extracellular signals through proteome modulation. Current opinion in cell biology *20*, 180-185.

Oei, S.L., and Shi, Y. (2001). Poly(ADP-ribosyl)ation of transcription factor Yin Yang 1 under conditions of DNA damage. Biochemical and biophysical research communications *285*, 27-31.

Olabisi, O.A., Soto-Nieves, N., Nieves, E., Yang, T.T., Yang, X., Yu, R.Y., Suk, H.Y., Macian, F., and Chow, C.W. (2008). Regulation of transcription factor NFAT by ADP-ribosylation. Molecular and cellular biology *28*, 2860-2871.

Pekala, P.H., Lane, M.D., Watkins, P.A., and Moss, J. (1981). On the mechanism of preadipocyte differentiation. Masking of poly(ADP-ribose) synthetase activity during differentiation of 3T3-L1 preadipocytes. The Journal of biological chemistry *256*, 4871-4876.

Quinlan, A.R., and Hall, I.M. (2010). BEDTools: a flexible suite of utilities for comparing genomic features. Bioinformatics *26*, 841-842.

Reynolds, A., Leake, D., Boese, Q., Scaringe, S., Marshall, W.S., and Khvorova, A. (2004). Rational siRNA design for RNA interference. Nature biotechnology *22*, 326-330.

Rodeheffer, M.S., Birsoy, K., and Friedman, J.M. (2008). Identification of white adipocyte progenitor cells in vivo. Cell *135*, 240-249.

Ryu, K.W., Kim, D.S., and Kraus, W.L. (2015). New facets in the regulation of gene expression by ADP-ribosylation and poly(ADP-ribose) polymerases. Chemical reviews *115*, 2453-2481.

Siersbaek, R., Nielsen, R., and Mandrup, S. (2012). Transcriptional networks and chromatin remodeling controlling adipogenesis. Trends in endocrinology and metabolism: TEM *23*, 56-64.

Todaro, G.J., and Green, H. (1963). Quantitative studies of the growth of mouse embryo cells in culture and their development into established lines. The Journal of cell biology *17*, 299-313.

Van, R.L., Bayliss, C.E., and Roncari, D.A. (1976). Cytological and enzymological characterization of adult human adipocyte precursors in culture. The Journal of clinical investigation *58*, 699-704.

Vyas, S., Chesarone-Cataldo, M., Todorova, T., Huang, Y.H., and Chang, P. (2013). A systematic analysis of the PARP protein family identifies new functions critical for cell physiology. Nature communications *4*, 2240.

Williams, S.C., Baer, M., Dillner, A.J., and Johnson, P.F. (1995). CRP2 (C/EBP beta) contains a bipartite regulatory domain that controls transcriptional activation, DNA binding and cell specificity. The EMBO journal *14*, 3170-3183.

Zhang, T., Berrocal, J.G., Yao, J., DuMond, M.E., Krishnakumar, R., Ruhl, D.D., Ryu, K.W., Gamble, M.J., and Kraus, W.L. (2012). Regulation of poly(ADP-ribose) polymerase-1-dependent gene expression through promoter-directed recruitment of a nuclear NAD+ synthase. The Journal of biological chemistry *287*, 12405-12416.

Zhang, Y., Liu, T., Meyer, C.A., Eeckhoute, J., Johnson, D.S., Bernstein, B.E., Nusbaum, C., Myers, R.M., Brown, M., Li, W*., et al.* (2008). Model-based analysis of ChIP-Seq (MACS). Genome Biol *9*, R137.

Zhang, Y., Wang, J., Ding, M., and Yu, Y. (2013). Site-specific characterization of the Asp- and Glu-ADP-ribosylated proteome. Nature methods *10*, 981-984.

CHAPTER THREE

Metabolic Regulation of Transcription through Compartmentalized NAD^+ Biosynthesis

The study was conducted in collaboration with Tulip Nandu, M.S., Ji Yeon Kim, Ph.D.. I initiated the study, designed and performed all the molecular biology experiments herein except for the glucose flux analysis, which was performed by J.Y.K.. T.N. performed bioinformatics analysis on the RNA-seq dataset.

3.1 Summary

Extracellular signaling and nutrient availability are major factors for cell fate decision (Lu and Thompson, 2012). Responds to extracellular information requires metabolic alterations and differential gene expression (Boukouris et al., 2016). Recent evidence suggests that many enzymes involved in gene regulation requires substrate or cofactors that are intermediate cell metabolism, providing a direct link between metabolism and transcription (Lu and Thompson, 2012). However, how cells integrate extracellular signals (e.g. hormones) and cellular metabolic status to coordinate transcriptional outcome is poorly understood. I hypothesized that fluctuations in nuclear metabolite levels adds an additional layer of regulation to integrate metabolic status and signal-dependent gene expression. Here, I report that changes in nuclear nicotinamide adenine dinucleotide (NAD^+) levels act as a signal to integrate cellular glucose metabolism and transcription program during adipocyte differentiation. Regulation of nuclear NAD^+ levels is achieved by the rapid induction of the cytoplasmic NAD^+-synthesizing enzyme, nicotinamide mononucleotide adenylyl transferase-2 (NMNAT-2), which concomitantly increases with glucose metabolism during differentiation. Competition for the common substrate, nicotinamide mononucleotide (NMN), between nuclear (NMNAT-1) and cytoplasmic (NMNAT-2) NAD^+ synthesizing enzymes leads to decreased NMN availability for NMNAT-1 and the subsequent decrease in nuclear NAD^+. Reduction of nuclear NAD^+ decreases the enzymatic activity of poly(ADP-ribose) polymerase 1 (PARP-1), which leads to enhanced binding of the key adipogenic transcription factor, C/EBPβ, to target genes that initiate differentiation. Notably, alterations in glucose metabolism during differentiation inhibits induction of NMNAT-2 and sustains

PARP-1 enzymatic activity, which leads to inhibition of transcription factor binding even in the presence of differentiation signals. These results indicate that the compartmentalized regulation of NAD^+ synthesis is a key regulator of integrating cellular metabolic status and signal-dependent transcriptional programs.

3.2 Introduction

NAD^+ is an essential small molecule cofactor in metabolic redox reactions as well as a substrate for many NAD^+-dependent enzymes, such as poly(ADP-ribose) polymerases (PARPs; e.g., PARP-1) or sirtuins (SIRTs; e.g., SIRT-1), many of which are known to play important roles in gene regulation (Canto et al., 2012; Chiarugi et al., 2012; Gibson and Kraus, 2012; Ryu et al., 2015). Unlike metabolic redox reactions, which reversibly oxidize or reduce NAD^+, NAD^+-dependent enzymes cleave NAD^+ into nicotinamide (NAM) and ADP-ribose, resulting the irreversible consumption of NAD^+. Thus, the regeneration and maintenance of NAD^+ is crucial for preserving cellular function. In mammalian cells, NAD^+ is synthesized from NMN and ATP, by the family of enzymes known as NMNATs (Chiarugi et al., 2012; Ryu et al., 2015). NMNATs exhibit unique subcellular localizations: NMNAT-1 in the nucleus NMNAT-2 in the cytosol and Golgi, and NMNAT-3 in the mitochondria (Figure 3.2A), suggesting the spatial-specific regulation of NAD^+ biosynthesis within the cell. However, the biological role of this compartment-specific NAD^+ synthesis is largely unknown. Interestingly, NMNATs localize at the subcellular compartment where the transcription (nucleus) or the cellular metabolism (cytoplasm and mitochondria) occurs. Considering the dual role of NAD^+ as a metabolic cofactor and a substrate for enzymes

involved in gene regulation, I hypothesized that compartmentalized synthesis of NAD^+ could be a link connecting cellular metabolism and gene regulation.

To address these issues, I identified a biological system that requires both dynamic transcriptional regulation and active cellular metabolism. Adipose tissue is an important regulator of energy balance and glucose homeostasis (Cristancho and Lazar, 2011). The formation of functional adipocytes is achieved by the differentiation of preadipocytes into mature adipocytes (i.e. adipogenesis), which is tightly controlled by the sequential expression of key adipogenic transcription factors (Rosen and MacDougald, 2006; Siersbaek et al., 2012) as well as the diverse range of metabolic pathways (Lu and Thompson, 2012; Wellen et al., 2009). Both NMNAT-1 and NMNAT-2 are expressed in adipose tissue (Figure 3.1A), indicating potential crosstalk between the nuclear and cytoplasmic NAD^+ synthesis pathways. Interestingly, I previously observed dynamic regulation of PARP-1 enzymatic activity during adipogenesis (Luo et al., 2017) (Extended Data Figure 1b), suggesting a role for nuclear NAD^+ during the adipocyte differentiation.

3.3 Results

NMNAT-1 regulates adipogenic transcriptional program through PARP-1 and C/EBPβ

To test the effect of nuclear NAD^+ biosynthesis on adipogenesis, I used shRNA to knockdown NMNAT-1 in 3T3-L1 preadipocytes. Depletion of NMNAT-1 dramatically reduced PARP-1 enzymatic activity, which continued to decrease during the early phase of differentiation (Figure 3.1B and Figure 3.2B). Previously, inhibition of PARP-1 enzymatic activity during the early phase of adipogenesis has been shown to enhance

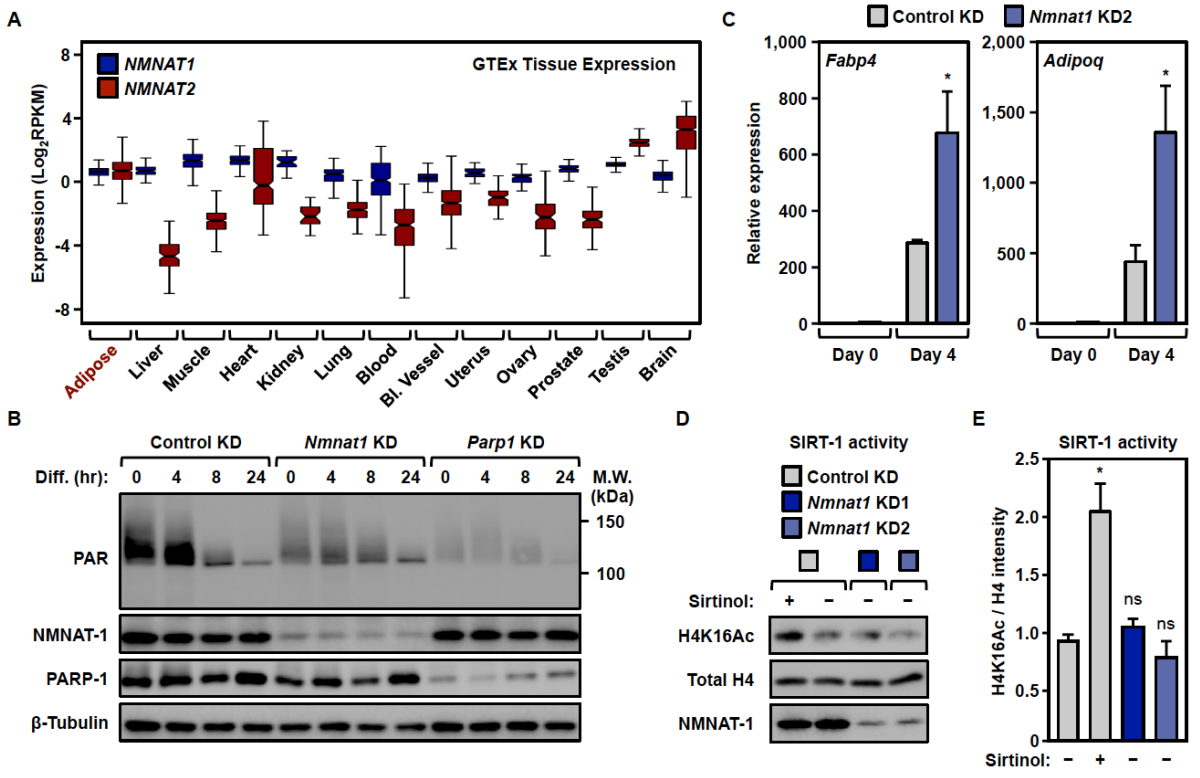

Figure 3.1. NMNAT-1 regulates PARP-1 enzymatic activity.
(A) Expression of *NMNAT1* and *NMNAT2* in various human tissues. mRNA expression of *NMNAT1* and *NMNAT2* were obtained from GTEx RNA-seq data (http://gtexportal.org/home).
(B) Westernblot showing the regulation of PARP-1 enzymatic activity upon NMNAT-1 or PARP-1 depletion during early phase of adipogenesis. PAR levels indicate enzymatic activity of PARP-1.
(C) Effect of *Nmnat1* knockdown on 3T3-L1 differentiation . Different shRNA (*Nmnat1* KD2) were used to confirm the result in Figure 1e. mRNA expression of adipocyte marker genes *Fabp4* and *Adipoq* were used to determine the levels of differentiation. Bars represent the mean ± SEM, n = 3 and the asterisks shows the statistical differences (Student's t-test; * $p < 0.05$).
(D and E) SIRT-1 activity upon *Nmnat1* depletion. Western blots of known SIRT-1 substrate histone H4 lysine 16 acetylation (H4K16Ac) were used to measure SIRT-1 activity (D), and a SIRT-1 inhibitor (sirtinol) treatment was used as a positive control. Quantification of the relative H4K16Ac (E) were from n = 3 experiments and western blot intensity of H4K16Ac and H4 were used to quantify the SIRT-1 activity. Each bar represents the mean ± SEM, n = 3. The asterisks show significant differences from the corresponding control while ns indicate no differences (Student's t-test; ns = $p > 0.05$, * $p < 0.05$).

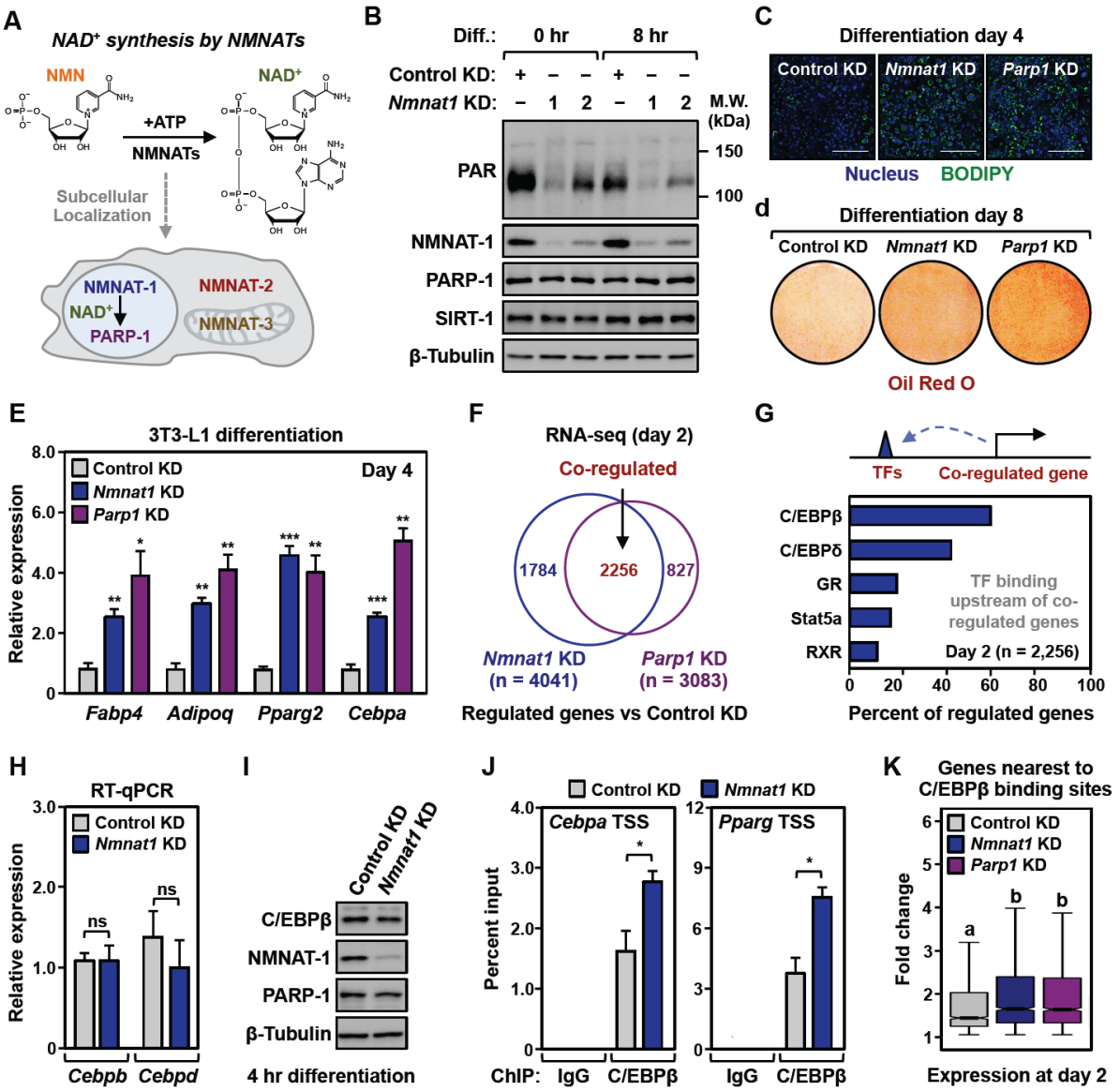

Figure 3.2. See the next page for the figure legend.

[See the previous page for the image for Figure 3.2]

Figure 3.2. NMNAT-1 regulates adipogenic transcriptional program through PARP-1 and C/EBPβ.
(A) Schematic representation of NAD^+ biosynthesis by NMNATs and their subcellular localization.
(B) Western blot showing the level of PAR upon NMNAT-1 depletion during early phase of adipogenesis. PAR level represents the enzymatic activity of PARP-1.
(C and D) Accumulation of lipid droplets at 4 (C) and 8 (D) days of differentiation in *Nmnat1* and *Parp1* knockdown (KD) 3T3-L1 cells. Lipids were stained using BODIPY 493/503 (green, C) or oil red o (D) and nuclei were stained using TO-PRO-3 (blue, C).
(E) mRNA expression of adipocyte marker genes at 4 days of differentiation. Each bar represents the mean ± SEM, n = 3 and the asterisks indicate significant differences from the corresponding control (Student's t-test; * $p < 0.05$, ** $p < 0.01$, *** $p < 0.001$).
(F) Differentially regulated genes upon *Nmnat1* and *Parp1* knockdown compare to control knockdown at 2 days of differentiation. Overlapping region indicates co-regulated genes.
(G) Numbers of NMNAT-1 and PARP-1 co-regulated genes bound by transcription factors. Co-regulated genes with ChIP-seq peaks within -50 kb upstream of the transcription start sites were defined as a transcription factor bound genes.
(H and I) Expression of C/EBPβ mRNA (H) and protein (I) upon silencing NMNAT-1. Each bar represents the mean ± SEM, n = 3 (Student's t-test; ns $p > 0.05$).
(J) Results from ChIP-qPCR assays for C/EBPβ at 4 hours after MDI-induced differentiation. Each bar represents the mean ± SEM, n = 3. Bars marked with asterisks are significantly different from the control (Student's t-test; * $p < 0.05$).
(K) Expression of genes nearest to C/EBPβ binding sites upon NMNAT-1 or PARP-1 depletion. C/EBPβ ChIP-seq peak at 4 hours post differentiation were used to define genes nearest to C/EBPβ binding sites. Bars marked with different letters are significantly different from each other (Wilcoxon rank sum test; $p < 0.0001$).

differentiation (Luo et al., 2017). Indeed, depletion of NMNAT-1 in 3T3-L1 facilitates differentiation, increases lipid accumulation (Figure 3.2C and 2D), and induces adipocyte marker genes (*Fabp4*, *Adipoq*) as well as transcription factors responsible for maintaining adipocyte function (*Pparg*, *Cebpa*), thus phenocopying PARP-1 knockdown 3T3-L1 (Figure 3.1C and Figure 3E). SIRT-1 is another major NAD^+-dependent enzyme in the nucleus (Houtkooper et al., 2012; Ryu et al., 2015). However, depletion of NMNAT-1 did not affect SIRT-1 enzymatic activity (Figure 3.1D and 1E), indicating that the observed phenotype upon NMNAT-1 knockdown is the result of decreased PARP-1 activity.

To further confirm that enhanced adipocyte differentiation upon depletion of nuclear NAD^+ synthesis occurs via PARP-1, I performed RNA-seq using NMNAT-1 or PARP-1 knockdown 3T3-L1. At 2 days post-differentiation, I observed that significant overlap between the genes regulated upon NMNAT-1 or PARP-1 knockdown (Figure 3.2F), further supporting the notion that NMNAT-1 regulates differentiation through PARP-1. To determine the mechanism underlying NMNAT-1/PARP-1-dependent transcriptional regulation during adipogenesis, I took all NMNAT-1 and PARP-1 co-regulated genes and assessed which transcription factor binds upstream of these genes. Interestingly, most of the differentially regulated genes upon NMNAT-1 and PARP-1 knockdown were bound by C/EBPβ (Figure 3.2G and Figure 3.3C), a key adipogenic transcription factor during the early phase of differentiation (Rosen and MacDougald, 2006; Siersbaek et al., 2012). Similar results were observed at 4 days post-differentiation (Figure 3.3A and 3B), indicating that regulation of C/EBPβ upon NMNAT-1 and PARP-1 depletion leads to enhance adipocyte

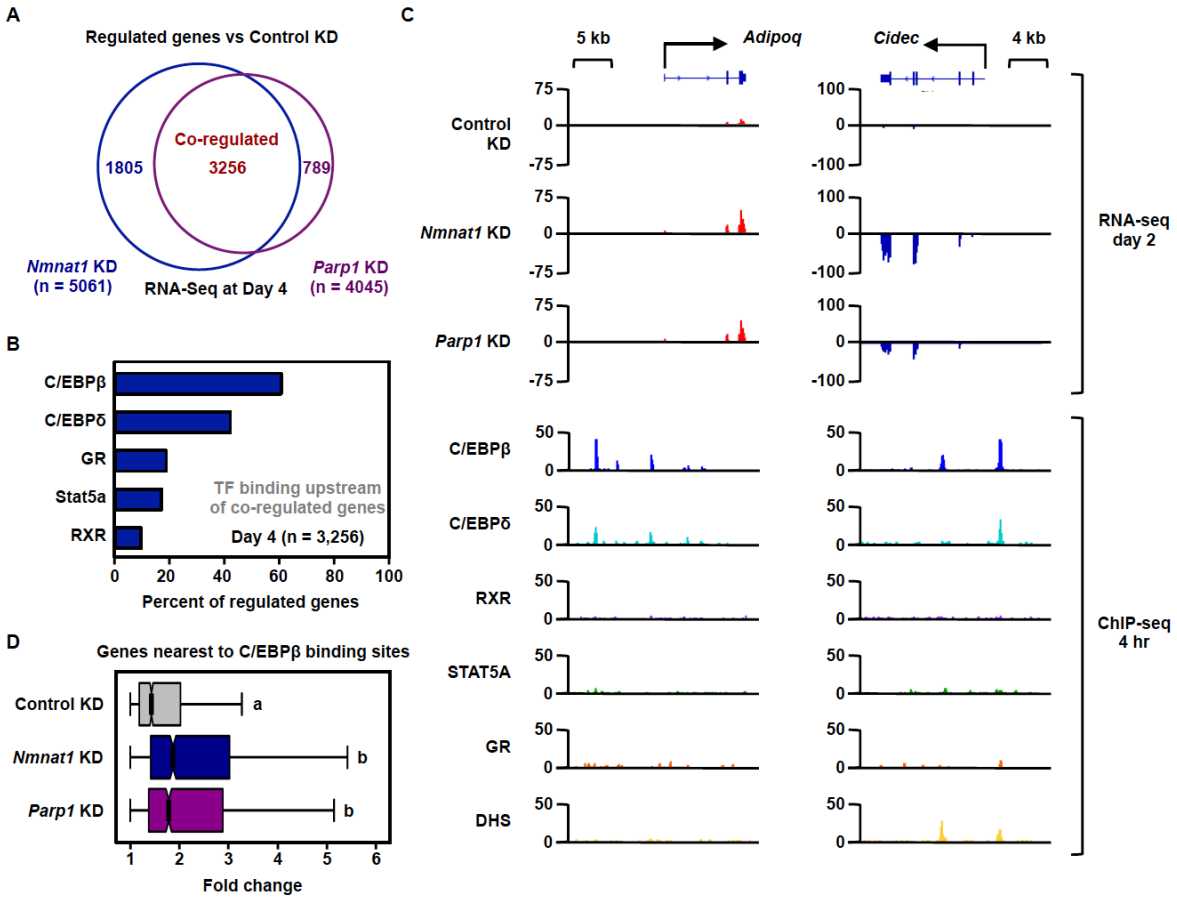

Figure 3.3. NMNAT-1 regulates C/EBPβ-dependent adipogenic gene expression through PARP-1.

(A) Differentially regulated genes upon *Nmnat1* and *Parp1* knockdown compare control at 4 days of differentiation. Overlapping region indicates co-regulated genes.

(B) Transcription factor binding upstream of NMNAT-1 and PARP-1 co-regulated genes. ChIP-seq peaks of listed transcription factors at 4 hours post differentiation were compared to NMNAT-1 and PARP-1 regulated genes at 4 days of differentiation. Percent of regulated genes containing ChIP-seq peaks within -50kb upstream of transcription start sites were plotted.

(C) Example browser tracks of the genes regulated upon *Nmnat1* and *Parp1* knockdown and transcription factor binding at upstream of these genes. mRNA expression of genes was measured using RNA-seq (*Top*) and transcription factor binding was measured using ChIP-seq (*Bottom*).

(D) Expression of NMNAT-1 and PARP-1 co-regulated genes nearest to C/EBPβ binding sites at 4 days post differentiation. Genes that are nearest to C/EBPβ binding sites were defined using C/EBPβ ChIP-seq peak at 4 hours post differentiation. Within these genes, genes that are regulated upon NMNAT-1/PARP-1 depletion were analyzed to measure the expression. Bars marked with different letters are significantly different from each other (Wilcoxon rank sum test; $p < 0.0001$).

differentiation. However, C/EBPβ expression, both in mRNA and protein levels, was not altered upon NMNAT-1 knockdown in 3T3-L1 cells (Figure 3.2H and 2I), suggesting that enhanced differentiation was not due to increased transcription factor expression. It has been previously shown that PARP-1 PARylates C/EBPβ during the early phase of adipogenesis, thereby inhibiting DNA binding (Luo et al., 2017). Indeed, depletion of NMNAT-1 significantly induced C/EBPβ binding to target gene promoters (Figure 3.2J). In addition, genes nearest to C/EBPβ binding sites were significantly induced upon NMNAT-1 or PARP-1 knockdown (Figure 3.2K). These results demonstrate that nuclear NAD^+ synthesis by NMNAT-1 regulates PARP-1 enzymatic activity to modulate the adipogenic transcription program through regulation of C/EBPβ binding to target genes.

Nuclear NAD^+ is regulated by compartmentalized biosynthesis of NAD^+

Since PAR levels rapidly decrease during differentiation and nuclear NAD^+ synthesis is required for maintaining PARP-1 enzymatic activity, I hypothesized that NAD^+ levels may decrease during the early phase of adipogenesis. To our surprise, however, I did not observe changes in total intracellular NAD^+ during differentiation (Figure 3.4A). I then postulated that nuclear NAD^+ could be differentially regulated from total intracellular NAD^+. To test this hypothesis, I used an NAD^+ biosensor generated by Cambronne et al. that utilizes a cpVenus-derived fluorescent protein that exhibits reduced fluorescence upon binding to NAD^+ (Cambronne et al., 2016)(Figure 3.5A – C). I expressed either nuclear or cytoplasmic-localized sensors and a corresponding cpVenus control in 3T3-L1 cells.

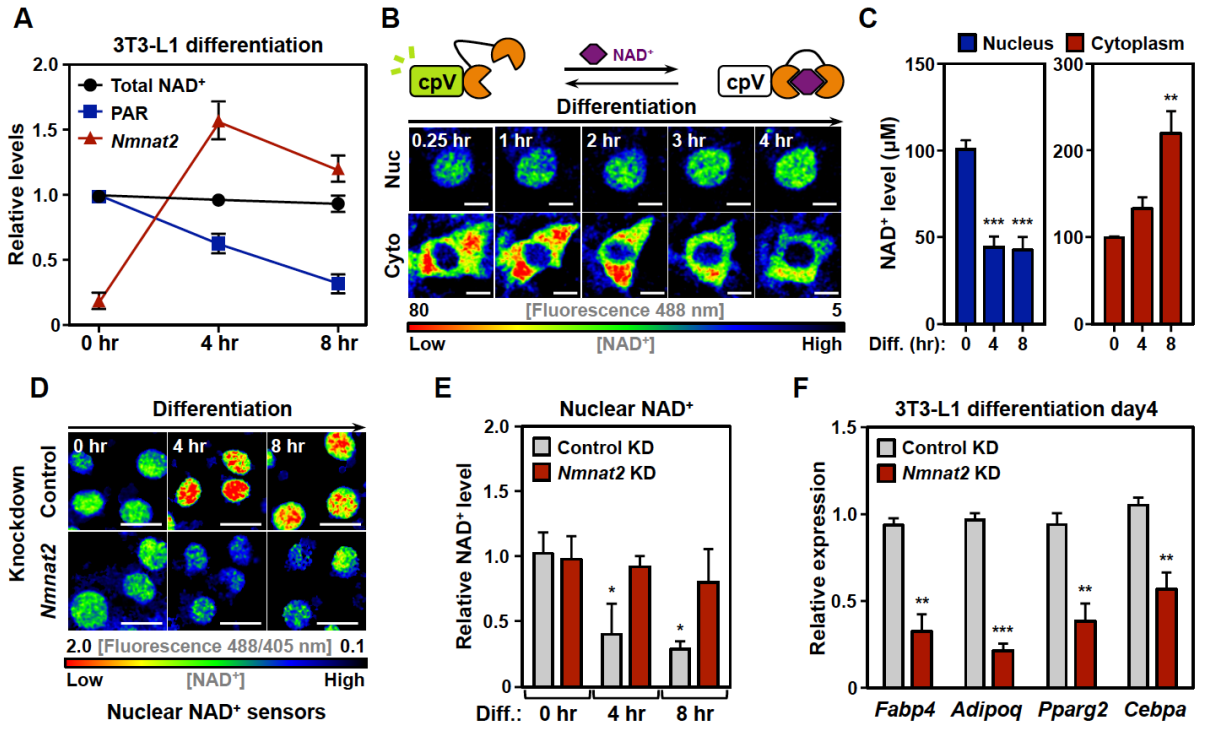

Figure 3.4. Nuclear NAD$^+$ is regulated by compartmentalized biosynthesis of NAD$^+$.
(A) Total intracellular NAD$^+$, PAR, and *Nmnat2* mRNA were measured at indicated time points. PAR represents PARP-1 enzymatic activity and was quantified from western blot signal.
(B) Representative images of nuclear (Nuc) and cytoplasmic (Cyto) NAD$^+$ sensor fluorescence during differentiation.
(C) Changes in subcellular NAD$^+$ level during differentiation. NAD$^+$ levels were calculated from Sensor/cpVenus (488/405 nm) and the fluorescence ratios were measured by flowcytometry. Each bar represents the mean ± SEM, n = 5. Bars marked with asterisks are significantly different from the undifferentiated (0 hr) control (ANOVA; ** $p < 0.01$, *** $p < 0.001$).
(D) Representative images of nuclear sensor (488/405 nm) during differentiation upon *Nmnat2* knockdown.
(E) Effect of *Nmnat2* knockdown on nuclear NAD$^+$ levels. Nuclear NAD$^+$ levels were determined from the fluorescence ratio of Sensor/cpVenus (488/405 nm) using flowcytometry. Bar graphs represents ± SEM, n = 3 and the bars with asterisks are significantly different from control KD at 0 hour (ANOVA; $p < 0.05$).
(F) Effect of *Nmnat2* depletion on differentiation of 3T3-L1. Differentiation was assessed by the expression of adipocyte marker genes. Each bar in the bar graphs represents the mean ± SEM, n = 3 and the asterisks indicate significant difference from the control (Student's t-test; ** $p < 0.01$, *** $p < 0.001$).

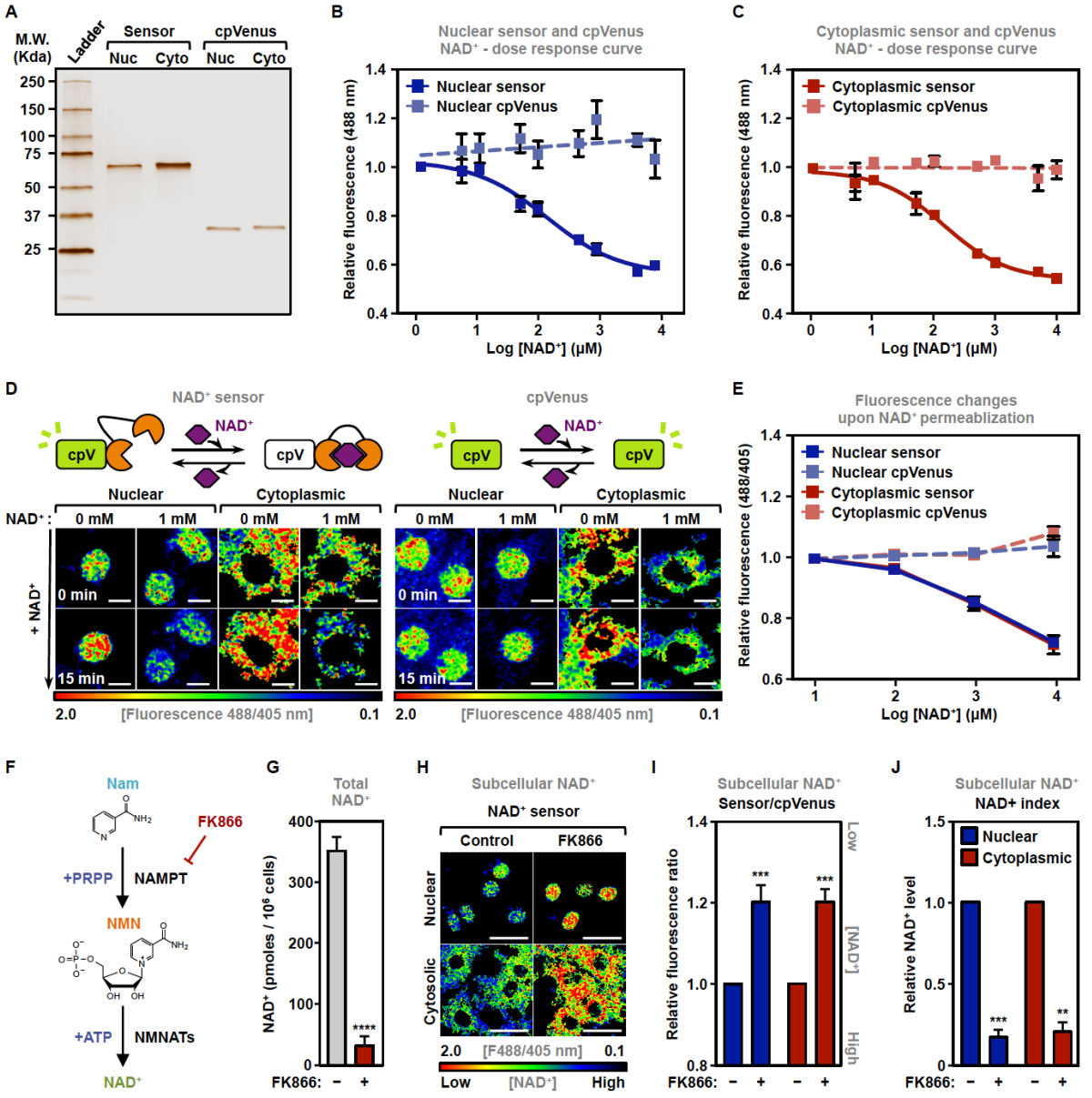

Figure 3.5. See the next page for the figure legend.

[See the previous page for the image for Figure 3.5]

Figure 3.5. NAD^+ sensor reveals changes in subcellular NAD^+ levels.
(A) Purification of nuclear and cytoplasmic NAD^+ sensor and corresponding cpVenus control.
(B and C) Fluorescence (488 nm) of purified NAD^+ sensor and cpVenus at indicated NAD^+ concentration. Fluorescence levels were plotted relative to 1 μM NAD^+. *In vitro* titration curve were generated using values obtain from these dose-response curves (Sensor/cpVenus).
(D) (Top) Schematics of NAD^+ sensors. NAD^+ sensor contains cpVenus fluorescence protein and NAD^+ binding domain modeled from bacterial (*E. faecalis*) DNA ligase. Upon NAD^+ binding, sensor decreases its fluorescence (488 nm), while fluorescence of corresponding cpVenus protein lacking NAD^+ binding domain is not affected. Expression of sensor or cpVenus was normalized with fluorescence emitted from 405 nm excitation, neither were affected by the levels of intracellular NAD^+ concentration. (Bottom) Representative images showing changes in fluorescence upon NAD^+ permeablization. 3T3-L1 cells expressing NAD^+ sensors or cpVenus controls were permeablized with 0.001% digitonin in the presence of indicated amounts of NAD^+ for 15 to 30 minutes and changes in the fluorescence ratio (488/405 nm) were measured.
(E) Dose-response curve of sensors and cpVenus upon NAD^+ permeablization. Fluorescence ratio (488/405 nm) was measured by flowcytometry and the values were plotted relative to 10 μM NAD^+.
(F) schematic representation of NAMPT inhibition by FK866.
(G) Total intracellular NAD^+ levels upon FK866 treatment (mean ± SEM, n = 3, Student's t-test; **** $p < 0.0001$).
(H – J) Representative images showing changes in NAD^+ sensor fluorescence upon 48 hours of FK866 treatment (H) and quantification of fluorescence ratio of sensor/cpVenus (488/405 nm) measured by flowcytometry (I). Fluorescence ratio of sensor/cpVenus was then interpolated onto *in vitro* titration curve to determine relative NAD^+ level (J). Each bar represents mean ± SEM, n = 4 and the asterisk indicates significant difference (Student's t-test; ** $p < 0.01$, *** $p < 0.001$).

Intracellular NAD^+ levels were equilibrated by normalizing the external NAD^+ concentration and permeablizing cells with digitonin. As previously reported, NAD^+ decreased the fluorescent signal from the sensors in a dose-dependent manner but had no affect on the cpVenus control (Cambronne et al., 2016) (Figure 3.5D and 5E). When treated with an NAMPT inhibitor, FK866, that depletes intracellular NAD^+ levels in all subcellular compartments, both 3T3-L1 cells expressing either the nuclear or cytoplasmic NAD^+ sensor exhibited a strong increase in NAD^+ sensor fluorescence (Figure 3.5F – I), indicating that these sensors are capable of measuring changes in subcellular NAD^+. When interpolated to a dose-response curve generated by NAD^+ permeablization, I estimated subcellular NAD^+ levels to be approximately 100 μM (100.5 μM in the nucleus and 101.6 μM in the cytoplasm), consistent with previous observations in HEK293T and HeLa cells (Cambronne et al., 2016).

Using 3T3-L1 cells expressing the nuclear localized NAD^+ sensor, I found that the nuclear NAD^+ sensor signal increases during early time points in differentiation, indicating a decrease in nuclear NAD^+ (Figure 3.4B). Decreases in nuclear NAD^+ level concurrent with the decrease in PARP-1 enzymatic activity. Interestingly, at 8 hours post-differentiation, the estimated nuclear NAD^+ level was near 40 μM (42.1 μM)—below PARP-1's Km towards NAD^+ (86.5 – 109.5 μM)—suggesting that decreases in nuclear NAD^+ regulate PARP-1 enzymatic activity during differentiation. Changes in nuclear NAD^+ level were also confirmed by using Peredox-mCherry-NLS, a nuclear localized NADH/NAD^+ ratiometric sensor (Hung et al., 2011) (Figure 3.6).

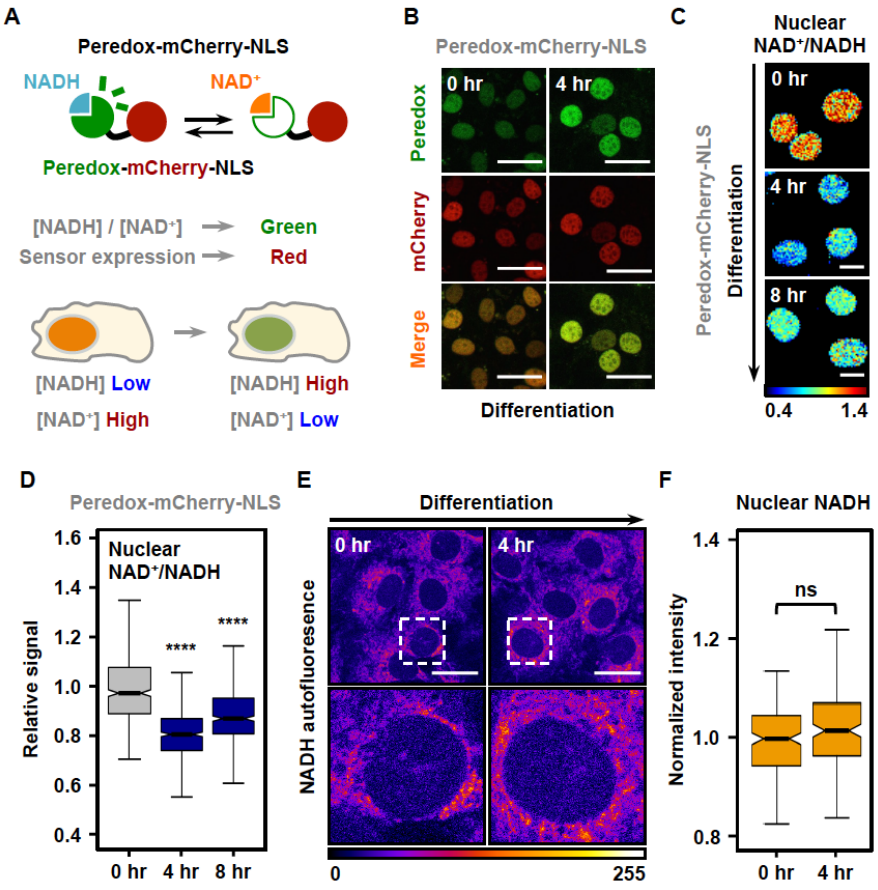

Figure 3.6. Measurement of changes in nuclear NAD$^+$ level during adipogenesis using Peredox-mCherry-NLS sensor.

(A) Schematic representation of nuclear NAD$^+$/NADH ratiometric sensor Peredox-mCherry-NLS. Peredox emits green fluorescence upon NADH binding, while signal is inhibited upon NAD$^+$ binding. mCherry signal represents expression level of the sensor.

(B) Representative images of changes in Peredox-mCherry-NLS signal during 3T3-L1 differentiation.

(C – F) During the early phase of differentiation (4 hours and 8 hours), nuclear NAD$^+$/NADH ratio was decreased (C and D) without altering the nuclear NADH level (E and F), indicating decreased level of nuclear NAD$^+$. Ratiometric image of Peredox and mCherry signal were used to represent changes in nuclear NAD$^+$/NADH (C). For quantification, n ≥ 400 nuclei were measured (D). Bars marked with asterisks indicate significant differences from the corresponding control (ANOVA; **** $p < 0.0001$). NADH auto fluorescence was measured using two-photon microscope (E) and measurement from n = 100 cells were used for the quantification (F). No significant difference in NADH auto fluorescence was observed between the nuclei of undifferentiated (0 hr) and 4 hour differentiated cells (Student's t-test; ns = $p > 0.01$).

During differentiation, the nuclear NAD^+/NADH ratio decreased without altering the nuclear NADH levels (Extended Data Figure 3.6C – E), consistent with a decrease in nuclear NAD^+ during differentiation.

Given that nuclear NAD^+ decreases while total intracellular NAD^+ remains unchanged, I hypothesized that alterations in other subcellular compartment may compensate for the decreased nuclear NAD^+, thus disguising changes in nuclear level when total intracellular NAD^+ is measured. Interestingly, I found that the cytosolic NAD^+ synthase, NMNAT-2, is rapidly induced within 8 hours of differentiation (Figure 3.4A and Figure 3.7). Moreover, I observed increased cytoplasmic NAD^+ during differentiation (Figure 3.4B and 4C), suggesting that a rapid induction of cytoplasmic NAD^+ synthesis may cause temporal compartmentalized regulation of NAD^+. To test if this rapid induction of NMNAT-2 is responsible for the regulation of nuclear NAD^+, I measured changes in nuclear NAD^+ upon NMNAT-2 knockdown (Figure 3.8A and 8B). Surprisingly, depletion of NMNAT-2 inhibits changes in nuclear NAD^+ during differentiation (Figure 3.4D and 4E), suggesting that increased cytoplasmic NAD^+ synthesis may be responsible for the nuclear NAD^+ regulation. Moreover, NMNAT-2 depletion increases nuclear PARP-1 enzymatic activity (Figure 3.8B), and inhibits adipogenesis (Figure 3.4F) without altering the total intracellular NAD^+ level (Figure 3.8C). I also confirmed these results with the Peredox-mCherry-NLS system. Consistent with our observations using the NAD^+ sensor, I found that depletion of NMNAT-2 abolishes changes in the nuclear NAD^+/NADH ratio (Figure 3.8D and 8E).

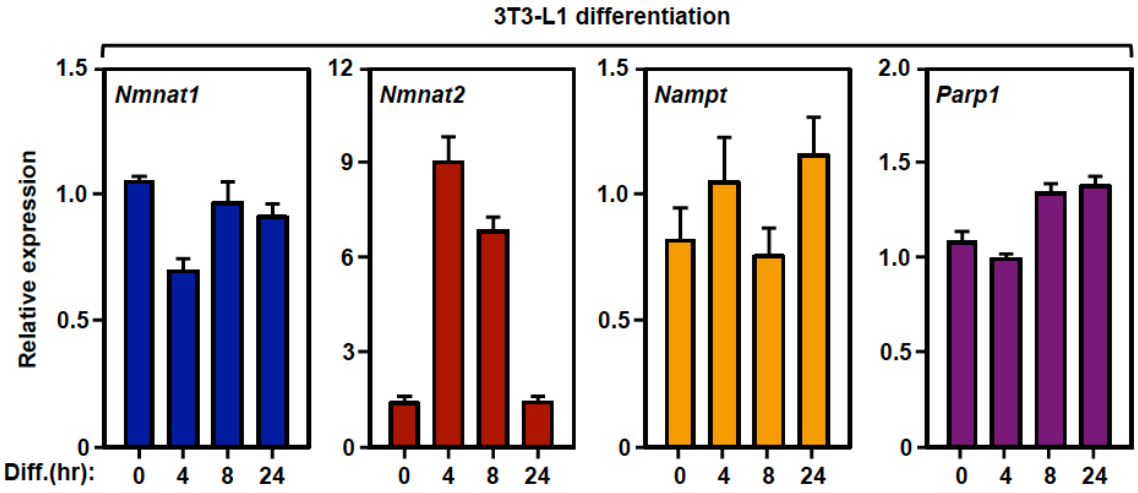

Figure 3.7. Expression of the genes involved in NAD^+ biosynthesis and NAD^+ consumption. mRNA expression level of genes involved in NAD^+ biosynthesis (*Nmnat1*, *Nmnat2,* and *Nampt*) and major nuclear NAD^+-consuming enzyme, *Parp1* were measured during the early phase of adipogenesis.

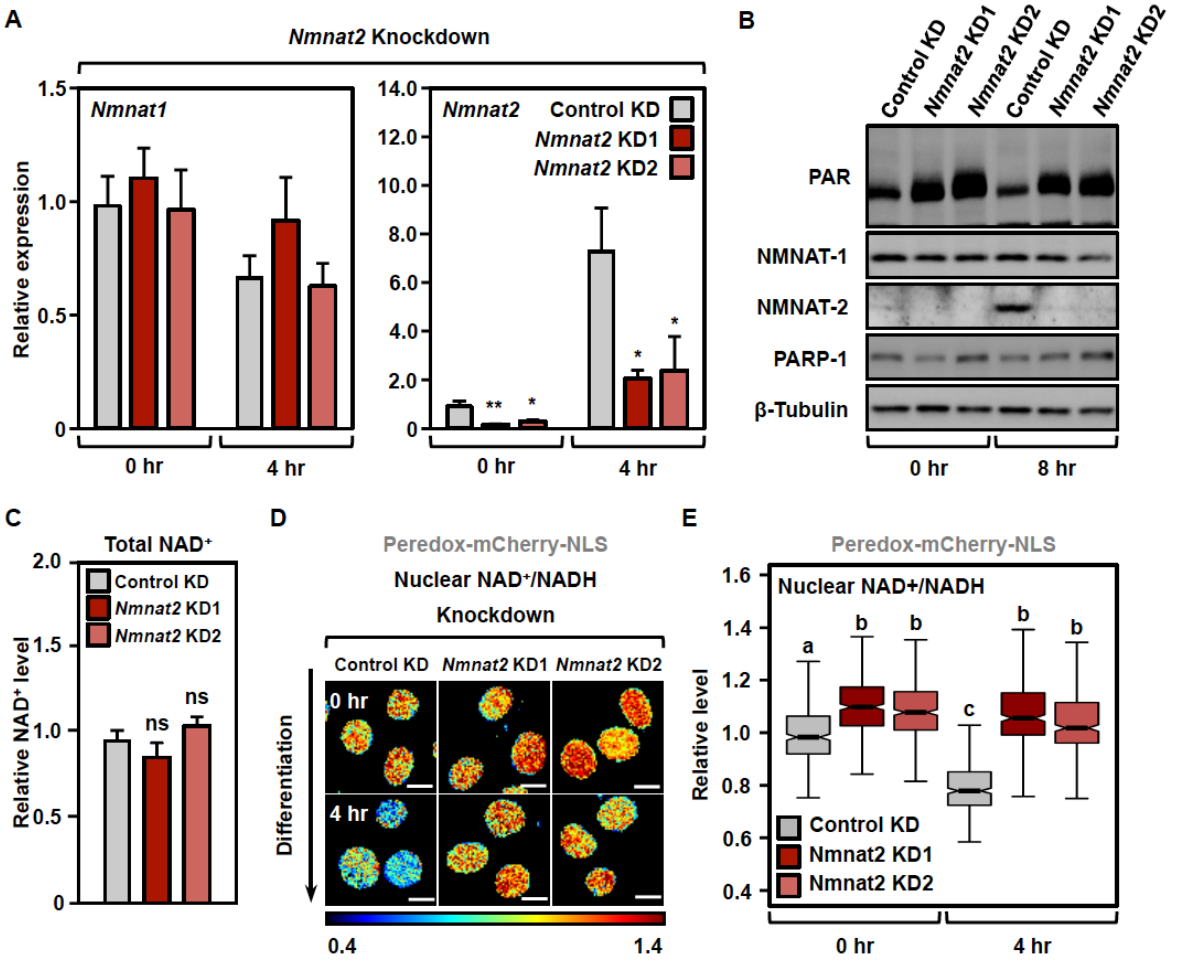

Figure 3.8. NMNAT-2 induction reduces nuclear NAD^+ and regulates PARP-1 enzymatic activity during adipogenesis.

(A) Expression of *Nmnat1* and *Nmnat2* mRNA upon *Nmnat2* knockdown. Bars marked with asterisks indicate significant difference (mean ± SEM, n = 3, Student's t-test; * $p < 0.05$, ** $p < 0.01$).

(B) Western blot showing the enzymatic activity of PARP-1 during early phase of differentiation upon *Nmnat2* depletion. PAR levels were used as a surrogate for the PARP-1 enzymatic activity.

(C) Total intracellular NAD^+ levels upon *Nmnat2* knockdown compare to the control (mean ± SEM, n = 3, Student's t-test; ns = $p > 0.05$).

(D and E) Ratiometric images (D) and the quantification (E) of Peredox-mCherry-NLS signals during differentiation upon *Nmnat2* knockdown. For the nuclear NAD^+/NADH ratio, $n \geq 380$ nuclei were analyzed and the bars marked with different letters are significantly different from each other (ANOVA; $p < 0.0001$).

Substrate competition between NMNAT-1 and NMNAT-2

How does induction of cytoplasmic NAD^+ synthesis affect nuclear events? One reasonable explanation can be that NMNAT-2 competes with NMNAT-1 for their common substrate NMN or ATP, limiting substrate availability in the nucleus for NMNAT-1 to synthesize nuclear NAD^+. In cells, NMN concentration is considerably lower than ATP(Sasaki et al., 2016) and NMNATs are endowed with affinities for ATP that are significantly lower than the intracellular ATP concentration (Revollo et al., 2004). Moreover, NMN has been reported as a rate-limiting factor for NAD^+ synthesis(Chiarugi et al., 2012; Revollo et al., 2004). Therefore, I hypothesized that rapid induction of NMNAT-2 will deprive NMN from the nucleus and decrease nuclear NAD^+ concentration during differentiation (Figure 3.9A). To test this hypothesis, I exogenously provided NMN to culture media. Consistent with previous reports, NMN supplementation increased total intracellular NAD^+ (Figure 3.9B). Interestingly, providing sufficient amounts of NMN could inhibit the decline of nuclear NAD^+ during differentiation (Figure 3.9C and 9D), which results in increased PARP-1 enzymatic activity (Figure 3.9E), implying that NMN availability in the nucleus may be initiating reduction of nuclear NAD^+. Furthermore, maintaining high nuclear NAD^+ levels by NMN supplementation inhibits adipogenesis in both 3T3-L1 and primary SVF cells (Figure 3.9F), indicating that high nuclear NAD^+ levels act as an inhibitory signal for adipocyte differentiation by regulating PARP-1 activity. This inhibitory effect of NMN supplementation was abolished upon knockdown of NMNAT-1 or PARP-1 (Figure 3.9G), further supporting that nuclear NAD^+ levels regulate adipocyte differentiation.

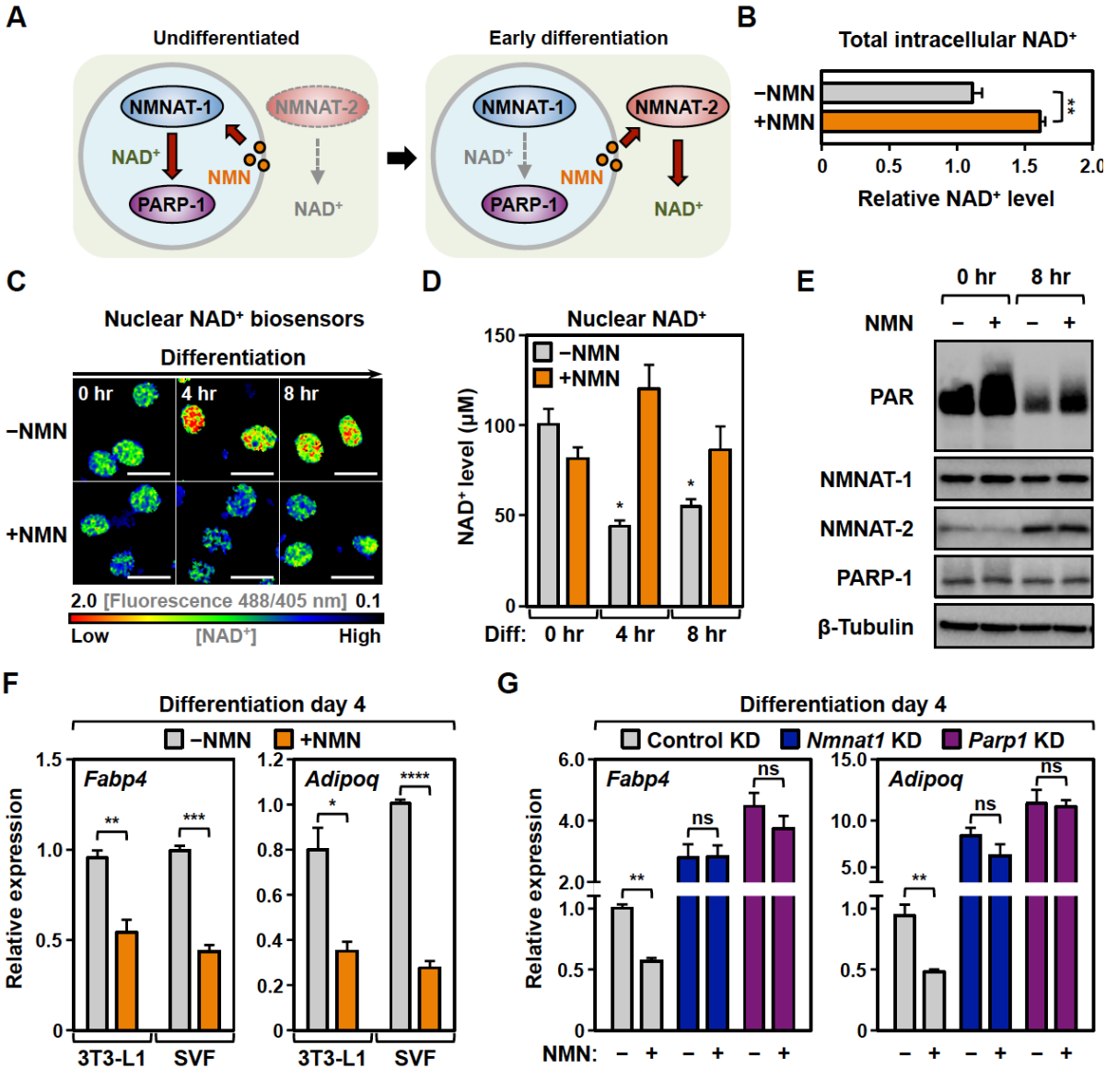

Figure 3.9. See the next page for the figure legend.

[See the previous page for the image for Figure 3.9]

Figure 3.9. Substrate competition between NMNAT-1 and NMNAT-2 regulates nuclear NAD^+ during differentiation.
(A) Schematic representation of substrate competition between NMNAT-1 and NMNAT-2.
(B – D) Regulation of total intracellular NAD^+ (B) and nuclear NAD^+ levels (C, D) upon 1mM NMN supplementation. Bar graphs represents the mean ± SEM, n = 3. Representative images shows changes in nuclear NAD^+ sensor fluorescence ratio (488/405 nm) during differentiation (C). Nuclear NAD^+ levels were determined by measuring fluorescence ratio of Sensor/cpVenus (488/405 nm) with flowcytometry. Bars marked with asterisks are significantly different from the undifferentiated (0 hr) control (ANOVA; * $p < 0.05$) (D).
(E) Western blots showing the rescue of PARP-1 enzymatic activity during early phase of differentiation upon 5mM NMN supplementation. PAR levels were used as a surrogate for the PARP-1 enzymatic activity.
(F – G) NMN supplements inhibits adipocyte differentiation in 3T3-L1 and SVF cells (F) but not in NMNAT-1 and PARP-1 depleted cells (G). During differentiation, cells were supplemented with 5mM NMN. mRNA Expressions of adipocyte marker genes were used to measure the differentiation. Each bar represents the mean ± SEM, n = 3 and the bars marked with asterisks indicate significant difference while ns are not significant (Student's t-test; ns = $p > 0.05$, * $p < 0.05$, ** $p < 0.01$, *** $p < 0.001$, **** $p < 0.0001$).

Glucose-dependent regulation of nuclear NAD^+ levels by NMNAT-2

It was unclear as to why cells require induction of cytoplasmic NAD^+ synthesis to regulate nuclear events during differentiation. Considering the role of NAD^+ as a metabolic cofactor, I hypothesized that NMNAT-2 induction may support increased glucose metabolism during differentiation by providing NAD^+ required for the process (Figure 3.10A). Interestingly, I observed a rapid induction of the genes involved in glycolysis within 8 hours of differentiation, indicating increased glucose metabolism during the early phase of adipogenesis (Figure 3.11A). To confirm these results, I differentiated 3T3-L1 cells in medium containing D[U-^{13}C]glucose (U indicates uniformly labeled) and measured ^{13}C enrichment of intracellular metabolites by mass spectrometry (Figure 3.11B). Consistent with gene expression, glycolytic intermediate metabolites containing glucose-derived ^{13}C, as well as citrate m+2 (citrate containing two additional mass unit from ^{13}C) rapidly increased upon differentiation (Figure 3.11C and D), indicating an increased glucose flux during the early phase of adipogenesis. Depletion of NMNAT-2 did not affect the expression of genes involved in glycolysis (Figure 3.10B), however, it decreased the level of glucose-derived citrate m+2, suggesting that NMNAT-2 induction during differentiation occurs to supports increased glucose metabolism (Figure 3.10C).

I further tested whether NMNAT-2 induction is dependent on changes in glucose flux by altering glucose levels in the differentiation medium. Surprisingly, NMNAT-2 induction was completely abolished when 3T3-L1 cells were differentiated with the medium containing low levels of glucose (Figure 3.10D). PAR levels remained high during differentiation when glucose was deprived, suggesting that the absence of NMNAT-2 induction leads to the

sustained levels of nuclear NAD^+ and PARP-1 enzymatic activity. Similar results were observed when cells were differentiated in the presence of glycolysis inhibitor, 2-deoxyglycose (2-DG), indicating that NMNAT-2 induction depends on glucose metabolism (Figure 3.10E). However, Nmnat2 mRNA induction was not affected by the glucose level or the glycolysis inhibition (Figure 3.12A), suggesting that the glucose-dependent modulation of NMNAT-2 levels occurs via post-translational regulation.

Since PARP-1 PARylates C/EBPβ and inhibits its DNA binding(Luo et al., 2017), I hypothesized that impeded NMNAT-2 induction upon glucose deprivation alters C/EBPβ DNA binding. Expression of C/EBPβ was not affected by the glucose metabolism, both in mRNA as well as protein levels (Figure 3.12A and B). However, binding of C/EBPβ to target gene promoters was dramatically reduced when glycolysis was inhibited during differentiation (Figure 3.10F), suggesting that adipogenic transcription is regulated by the glucose metabolism through PARP-1.

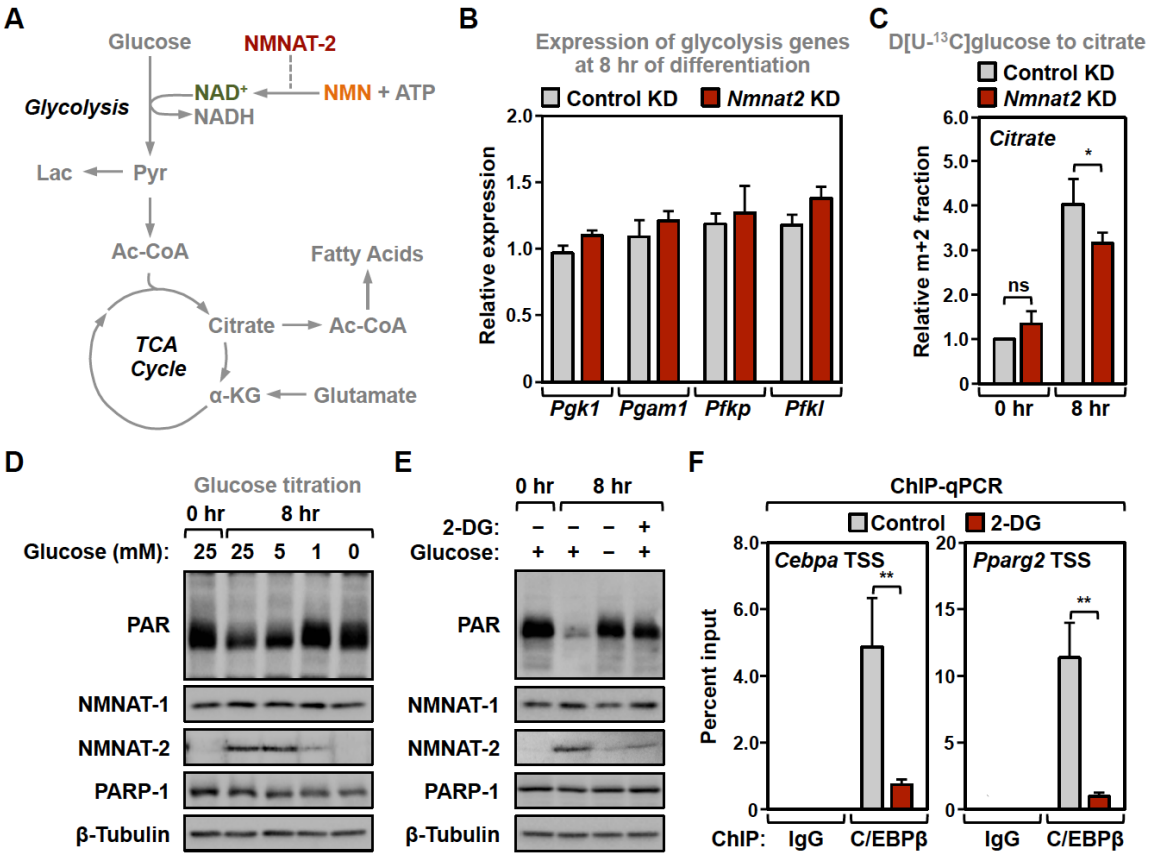

Figure 3.10. NMNAT-2 senses enhanced glucose metabolism during early phase of adipogenesis.

(A) Schematic representation of glucose metabolism and potential role of NMNAT-2.

(B) Expression of genes involved in glucose metabolism upon *Nmnat2* depletion after 8 hours of differentiation.

(C) Mass isotopomer analysis of citrate in *Nmnat2* knockdown cells. m+2 citrate were used to measure glucose influx during differentiation. Bars marked with ns are not statistically different while asterisks indicate statistical differences from the corresponding control (Student's t-test; ns = $p > 0.05$, * $p < 0.05$).

(D and E) Expression of NMNAT-2 in cells differentiated with various extracellular glucose level (D) or cells differentiated with glycolysis inhibitor (2-DG, E). PAR level indicates enzymatic activity of PARP-1.

(F) Regulation of C/EBPβ binding to its target gene promoters upon inhibition of glycolysis. Assays were done after 8-hour post MDI-induced differentiation. Bars marked with asterisks are significantly different from the control (Student's t-test; ** $p < 0.01$).

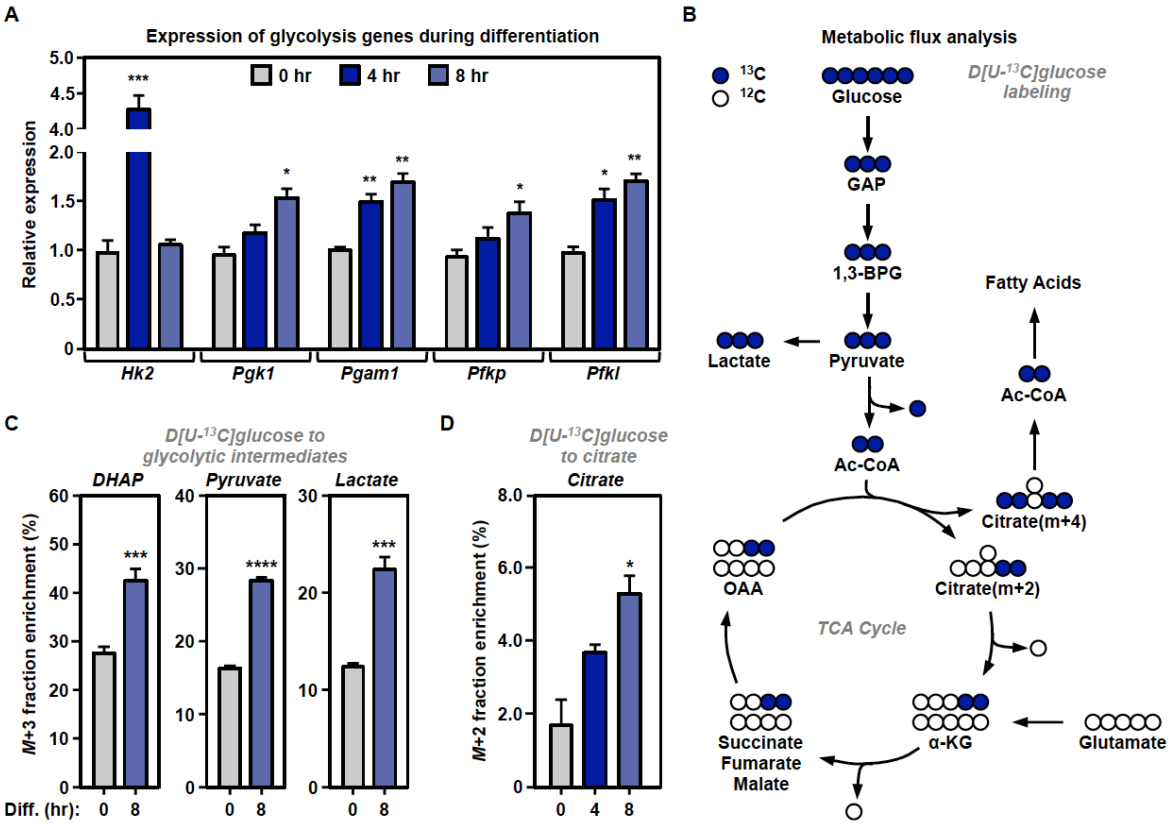

Figure 3.11. Enhanced glucose metabolism during early phase of adipogenesis.
(A) mRNA expression of genes involved in glycolysis were measured at the indicated time after the differentiation. Expression of mRNAs at the indicated time points were compare to undifferentiated (0 hr) cells.
(B) Schematic outlining of D[U-13C]glucose metabolism.
(C and D) Mass isotopomer analysis of glycolytic intermediate (C) and citrate (D) during early phase of adipogenesis. Cells were differentiated until indicated time and cultured with D[U-^{13}C]glucose and unlabeled glutamine. In all panels, each bar represents the mean ± SEM, n = 3 and the asterisks indicate significant differences from the corresponding control (Student's t-test; * $p < 0.05$, **** $p < 0.0001$).

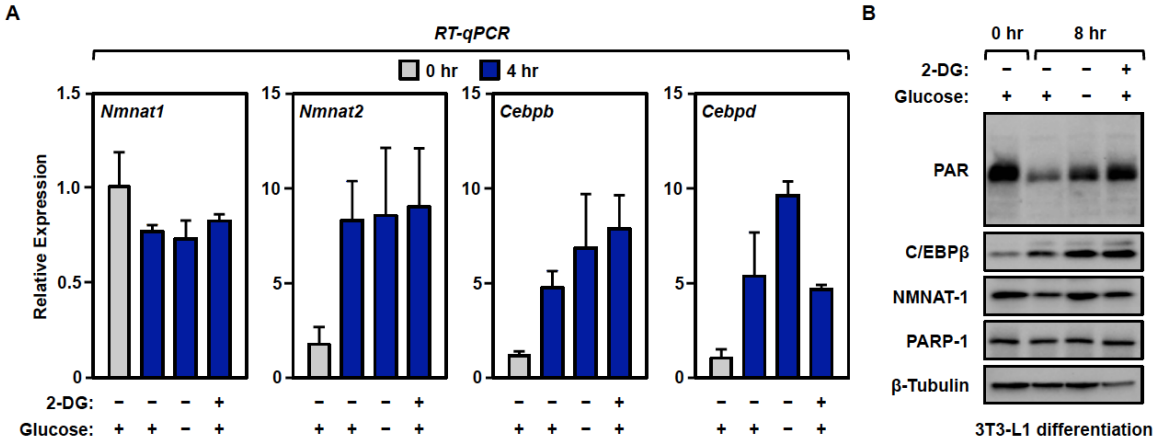

Figure 3.12. C/EBPβ expression is not affected by glucose metabolism.
(A and B) Effects of glucose metabolism in mRNA (A) and protein (B) expression levels of *Nmnat1*, *Nmnat2* and the adipogenic transcription factors (*Cebpb*, *Cebpd*) controlling the early phase of adipogenesis. Glucose metabolism was altered by depriving extracellular glucose or inhibiting glycolysis (2-DG). mRNA levels of the listed genes were compare to undifferentiated (0 hr) cells. Each bar represents the mean ± SEM, n = 3.

3.4. Conclusion

In summary, I have shown that compartmentalized NAD^+ biosynthesis is crucial for regulating transcription during adipocyte differentiation. Proper regulation of nuclear NAD^+ levels is achieved by the rapid induction of cytosolic NAD^+ synthesizing enzyme, NMNAT-2, which consumes NMN in cytoplasm, thereby limiting \ NMN availability in the nucleus for NMNAT-1 to use. Nuclear NAD^+ levels dictate PARP-1 enzymatic activity and affects chromatin binding of the major adipogenic transcription factor C/EBPβ. Decreasing nuclear NAD^+ synthesis by NMNAT-1 knockdown rapidly enhances differentiation, whereas increasing nuclear NAD^+ by NMN supplementation or NMNAT-2 knockdown inhibits adipogenesis. Compartmentalized NAD^+ biosynthesis is tightly linked to glucose metabolism, where enhanced glucose metabolism is required for the rapid induction of NMNAT-2, thus integrating cellular metabolism and the adipogenic transcription program. These data suggest that compartmentalized NAD^+ biosynthesis can be a key to orchestrate intracellular metabolism and signal-regulated transcription.

3.5 Materials and Methods

Generation of *Nmnat1* conditional knockout mice

Frozen *Nmnat1*$^{tm1a(EUCOMM)Wtsi}$ embryos with a C57BL/6N background were obtained from the International Mouse Phenotyping Consortium (IMPC; MGI ID 1913704) and were recovered at UT Southwestern's Transgenic Core Facility. All mice were housed and maintained at UT Southwestern's Animal Resource Center. The reporter cassette was removed by crossing *Nmnat1*$^{tm1a/tm1a}$ mice with FLP recombinase-expressing B6.129S4-

Gt(ROSA)26Sor$^{tm2(FLP*)Sor}$/J mice (The Jackson Laboratory, stock no. 012930). After removing the reporter cassette, the resulting *Nmnat1*$^{loxP/+}$ mice were self-crossed to generate homozygous *Nmnat1*$^{loxP/loxP}$ progeny. To produce mice with a Tamoxifen-inducible conditional allele of *Nmnat1* (*Nmnat1*$^{loxP/loxP}$*;CAG-cre/ERT2*), *Nmnat1*$^{loxP/loxP}$ mice were crossed with transgenic mice containing a *CAG-cre/ERT2* cassette [B6.Cg-Tg(CAG-cre/Esr1*)5Amc/J; The Jackson Laboratory, stock no. 004682]. All of the mouse genotypes were confirmed by short-range PCR, using PCR primers listed below.

The following short-range PCR primers used for genotyping:

Wild-type (Wt):

Forward: 5'- TCATGTAGGGAACTCAGAGCTGGT -3'

Reverse: 5'- GTTCTGTAGTGTGGAGCTCATGCA -3'

LoxP:

Forward: 5'- AAGGCGCATAACGATACCAC -3'

Reverse: 5'- CCGCCTACTGCGACTATAGAGA -3'

FRT:

Forward: 5'-AGGCGCATAACGATACCACGAT-3'

Reverse: 5'- CCACAACGGGTTCTTCTGTT-3'

LacZ:

Forward: 5'-ATCACGACGCGCTGTATC-3'

Reverse: 5'-ACATCGGGCAAATAATATCG-3'

Cre:

Forward: 5'-GGACATGTTCAGGGATCGCCAGGCG-3'

Reverse: 5'- CCATGAGTGAACGAACCTGG-3'

Isolation of stromal vascular fraction (SVF) cells from white adipose tissue

SVF cells were isolated as described previously (Gupta et al., 2012). Briefly, 4 to 6 week old male mice (2 mice per condition) were sacrificed and the inguinal white adipose tissue (WAT) was collected. The WAT was washed, pooled, minced, and digested for 2 hours at 37°C in 10 mL of digestion solution [100 mM HEPES pH 7.4, 120 mM NaCl, 50 mM KCl, 5 mM glucose, 1 mM $CaCl_2$, 1 mg/mL collagenase D (Roche, 11088858001), and 1.5% BSA]. The digested WAT tissue was filtered through a 100 μm cell strainer to remove undigested tissue, and 30 mL of SVF cell culture medium [10% FBS, 1% penicillin/streptomycin in DMEM/F12, GlutaMAX (Life Technologies, 10565-018)] was added to dilute the digestion buffer. The flow-through was centrifuged for 5 minutes at 600 x *g* to collect the SVF cells. The cell pellet was resuspended in 10 mL of SVF culture medium, and passed through a 40 μm cell strainer to remove clumps of cells and large adipocytes. The cells were collected again by centrifugation at 600 x *g* for 5 minutes, resuspended in SVF culture medium (5 mL per 2 mouse equivalents), and plated in a 6 cm diameter collagen-coated culture dish until well attached.

Culture and differentiation of 3T3-L1 cells and SVF cells

SVF cells were grown in SVF culture medium until confluent and were then cultured for two more days under contact inhibition. The cells were then treated for two days with an adipogenic cocktail (MDI), including 0.5 mM IBMX (3-isobutyl-1-methylxanthine; Calbiochem, 410957), 1 μM dexamethasone (Sigma, D4902), and 5 μg/mL insulin (Sigma, I-5500). Subsequently, the cells were cultured in medium containing 5 μg/mL insulin for the indicated times before collection.

3T3-L1 cells were obtained from the American Type Cell Culture (ATCC, CL-173) and maintained in DMEM (Cellgro, 10-017-CM) supplemented with 10% fetal bovine serum (Atlanta Biologicals, S11550) and 1% penicillin/streptomycin. For the glucose titration experiments, the 3T3-L1 cells were grown in DMEM without glucose (Life Technologies, 11966-025). For the induction of adipogenesis, the 3T3-L1 cells were grown to confluence and then cultured for two more days under contact inhibition. The cells were then treated for two days with an MDI adipogenic cocktail containing 0.25 mM IBMX, 1 μM dexamethasone, and 10 μg/mL insulin. Subsequently, the cells were cultured in medium containing 10 μg/mL insulin for the indicated times before collection.

293T cells were obtained from the ATCC (CRL-3216) and maintained in DMEM (Cellgro, 10-017-CM) supplemented with 10% fetal bovine serum and 1% penicillin/streptomycin.

Cell treatments

3T3-L1 or SVF were exposed to various treatments and culture conditions for the experiments described herein. For treatment with NMN (1 mM or 5 mM; Sigma, N3501) or

2-deoxy-D-glucose (5 mM; Sigma, D8375), the cells were grown until confluent and then pretreated with either compound for 2 hours prior to the addition of the MDI cocktail. The cells were then differentiated in medium with MDI in the presence of NMN or 2-deoxy-D-glucose for the indicated times before collection. For differentiation longer than two days, the compounds were added to the medium with MDI for two days, then removed when changing culture medium. For SIRT1 inhibition, the cells were treated with 10 μM sirtinol (Calbiochem, 566320) for 48 hours before collection. For the doxycycline inducible system, the cells were treated with 1 μg/mL of doxycycline (Dox) for 48 hours. For NAMPT inhibition, the cells were treated with 50 nM FK866 (Sigma, F8557) for 48 hours. For the Tamoxifen-inducible, Cre-mediated *Nmnat1* deletion, *Nmnat1*$^{loxP/loxP}$*;CAG-CreERT2* SVF cells were cultured until confluent and were then treated with 1 μm 4-Hydroxytamoxifen (4-OHT; Sigma, H7904) for two days before the induction of adipogenesis, as described above.

Antibodies

The custom rabbit polyclonal antiserum against PARP-1 used for Western blotting and ChIP assays was generated by using an purified recombinant antigen comprising the amino-terminal half of PARP-1 (Kim et al., 2004) (now available from Active Motif; cat. no. 39559). The custom rabbit polyclonal antiserum against NMNAT-1 was raised against purified recombinant human and mouse NMNAT-1 (Pocono Rabbit Farm and Laboratory). The custom recombinant antibody-like anti-poly(ADP-ribose) binding reagent (anti-PAR) was generated and purified in-house (now available from EMD Millipore, MABE1031). The other antibodies used were as follows: C/EBPβ (Santa Cruz, sc-150X), NMNAT-2 (Abcam,

ab56980), β-Tubulin (Abcam, ab6046), rabbit IgG (Invitrogen, 10500C), goat anti-rabbit HRP-conjugated IgG (Pierce, 31460), and goat anti-mouse HRP-conjugated IgG (Pierce, 31430).

Molecular cloning to generate expression and knockdown vectors

shRNAs targeting Nmnat1 and Parp1 mRNAs. shRNA constructs targeting mouse Nmnat1 (TRCN0000111435, TRCN0000335596) and control shRNA (SHC002) were purchased from Sigma. An shRNA construct targeting mouse PARP-1 was generated by cloning a double-stranded oligonucleotide (5'-GGGCAAGCACAGTGTCAAA-3') into the pLKO.1 vector (SHC001), which confers puromycin resistance.

Peredox-mCherry constructs. pMSCV-Peredox-mCherry-NLS (Addgene plasmid no. 32385) and pcDNA3.1-Peredox-mCherry (Addgene plasmid no. 32383), described previously (Hung et al., 2011), were kindly provided by Dr. Gary Yellen.

NAD^+ sensor constructs. Nuclear and cytoplasmic NAD^+ sensor expression constructs and the corresponding cpVenus control expression construct (Cambronne et al., 2016) were kindly provided by Dr. Michael Cohen and Dr. Richard Goodman. The expression cassettes were amplified using the primers listed below and cloned into pINDUCER20 dox-inducible lentiviral expression vector (Addgene, plasmid no. 44012)(Meerbrey et al., 2011) using Gibson assembly (NEB, E2621).

Primers to amplify the NAD^+sensors and cpVenus

Forward: 5'- TCCGCGGCCCCGAACTAGTGATCTGCCACCATGACCGG -3'

Reverse: 5'-

GTTTAATTAATCATTACTACCAAGAAAGCTGGGTCTAGATATCTC-3'

Generation of cell lines with stable knockdown and ectopic expression

Cells were transduced with either lentiviruses or retroviruses for stable knockdown or ectopic expression. We generated lentiviruses by transfection of the pLKO.1 constructs described above, together with: (1) an expression vector for the VSV-G envelope protein (pCMV-VSV-G, Addgene plasmid no. 8454), an expression vector for GAG-Pol-Rev (psPAX2, Addgene plasmid no. 12260), and a vector to aid with translation initiation (pAdVAntage, Promega) into 293T cells using GeneJuice transfection reagent (Novagen, 70967) according to the manufacturer's protocol. The resulting viruses were collected in the culture medium, concentrated by using a Lenti-X concentrator (Clontech, 631231), and used to infect 3T3-L1 cells.

Retroviruses were generated by transfection of the pMSCV constructs described above, together with an expression vector for the VSV-G envelope protein (pCMV-VSV-G), into Phoenix Ampho cells using GeneJuice transfection reagent (Novagen, 70967) according to the manufacturer's protocol. The resulting viruses were used to infect 3T3-L1 cells.

Stably transduced cells were selected with puromycin (Sigma, P9620; 2 μg/mL) or G418 sulfate (Sigma, A1720; 1 mg/mL).

Knockdown of *Nmnat2* using siRNAs

Commercially available siRNA oligos targeting *Nmnat2* (Sigma, SASI_Mm01_00083355 and SASI_Mm01_00083356) were transfected at a final concentration of 20 nM using Lipofectamine RNAiMAX reagent (Invitrogen, 13778150) according to the manufacturer's instructions. All experiments were performed 48 hours after siRNA transfection.

Preparation of cell lysates and Western blotting

3T3-L1 ands SVF cells were cultured and differentiated as describe above. The cells were then washed twice with ice-cold PBS and lysed with Lysis Buffer (20 mM Tris-HCl pH 7.5, 150 mM NaCl, 1 mM EDTA, 1 mM EGTA, 1% NP-40, 1% sodium deoxycholate, 0.1% SDS) containing 1 mM DTT, 250 nM ADP-HPD (Sigma, A0627; a PARG inhibitor to prevent PAR chain cleavage during extraction), 10 μM PJ34 (a PARP inhibitor to prevent new PAR chain synthesis during extraction), and 1x complete protease inhibitor cocktail (Roche, 11697498001). For the chromatin fractions, lysed cells were sonicated in Lysis Buffer to solubilize the chromatin. The lysates were incubated on ice for 30 minutes and then centrifuged to clarify. The supernatants were collected, run on a 6% polyacrylamide-SDS gel (for PARP-1 and PAR analyses) or a 10% polyacrylamide-SDS gel (for NMNAT-1, C/EBPβ, NMNAT-2, β-tubulin), and transferred to a nitrocellulose membrane. The membranes were blocked with 5% non-fat milk in TBST and incubated with the primary antibodies described above in 1% non-fat milk in TBST, followed by anti-rabbit HRP-conjugated IgG (1:5000) or anti-mouse HRP-conjugated IgG (1:3000). Western blot signals were detected using an ECL detection reagent (Thermo Fisher, 34077, 34095).

GTEx tissue expression analyses

The expression profiles of *NMNAT1* and *NMNAT2* in different human tissues was determined based on RPKM values using GTEx ((Consortium, 2015); http://www.gtexportal.org/home/) with dbGaP Study Accession phs000424.v6.p1.(http://www.ncbi.nlm.nih.gov/projects/gap/cgi-bin/study.cgi?study_id=phs000424.v6.p1).

RNA isolation and reverse transcription-quantitative real-time PCR (RT-qPCR)

3T3-L1 cells or SVF cells were seeded at ~2 x 10^5 cells per well in 6-well plates and treated as described above. The cells were collected and total RNA was isolated using Trizol Reagent (Invitrogen) according to the manufacturer's protocols. Total RNA was reverse transcribed using oligo (dT) primers and MMLV reverse transcriptase (Promega) to generate cDNA. The cDNA samples were subjected to quantitative real-time PCR (qPCR) using gene-specific primers, as described below. Target gene expression was normalized to the expression of *Tbp* mRNA.

Chromatin immunoprecipitation-qPCR (ChIP-qPCR)

3T3-L1 cells were cultured, differentiated, and treated as described above in 15 cm diameter plates. ChIP was performed as described previously (Kininis et al., 2007; Krishnakumar et al., 2008a), with slight modifications. Briefly, the cells were cross-linked with 1% formaldehyde in PBS for 10 minutes at 37°C and quenched in 125 mM glycine in PBS for 5 minutes at 4°C. Cross-linked cells were then collected by centrifugation and lysed

in Farnham Lysis Buffer (5 mM PIPES pH 8.0, 85 mM KCl, 0.5% NP-40, 1 mM DTT, and 1x complete protease inhibitor cocktail). A crude nuclear pellet was collected by centrifugation, resuspended in Sonication Buffer (50 mM Tris-HCl pH 7.9, 1% SDS, 10 mM EDTA, 1 mM DTT, and 1x complete protease inhibitor cocktail), and sonicated to generate chromatin fragments of ~300 bp in length. The soluble chromatin was clarified by centrifugation, diluted 1:10 with Dilution Buffer (20 mM Tris-HCl pH 7.9, 0.5% Triton X-100, 2 mM EDTA, 150 mM NaCl, 1 mM DTT, and 1x complete protease inhibitor cocktail) and pre-cleared with protein A agarose beads.

The pre-cleared samples were used in immunoprecipitation reactions with antibodies against C/EBPβ or with rabbit IgG (as a control) with incubation overnight at 4°C. The samples were washed with Low Salt Wash Buffer (20 mM Tris-HCl pH 7.9, 2 mM EDTA, 125 mM NaCl, 0.05% SDS, 1% Triton X-100, 1 μM aprotinin, and 1 μM leupetin), High Salt Wash Buffer (20 mM Tris-HCl pH 7.9, 2 mM EDTA, 500 mM NaCl, 0.05% SDS, 1% Triton X-100, 1 μM aprotinin, and 1 μM leupetin), LiCl Wash Buffer (10 mM Tris-HCl, pH 7.9, 1 mM EDTA, 250 mM LiCl, 1% NP-40, 1% sodium deoxycholate, 1 μM aprotinin, and 1 μM leupetin), and 1x Tris-EDTA (TE). The immunoprecipitated genomic DNA was eluted in Elution Buffer (100 mM NaHCO3, 1% SDS), digested with proteinase K and RNase H to remove protein and RNA, respectively, and then extracted with phenol:chloroform:isoamyl alcohol. The ChIPed genomic DNA was subjected to qPCR using gene-specific primers, as described below. The immunoprecipitation of genomic DNA was normalized to the input.

Quantitative real-time PCR (qPCR)

Quantitative PCR (qPCR) was performed as described previously (Luo et al., 2014). Briefly, the cDNA or ChIPed DNA samples were mixed with 1x SYBR Green PCR master mix and primers (forward and reverse, 250 nM), and were then subjected to 45 cycles of amplification (95°C for 10 second, 60°C for 10 second, 72°C for 1 second) following an initial 5 minute incubation at 95°C using a Roche LightCycler 480 384-well detection system. Melting curve analyses were performed to ensure that only the targeted amplicon was amplified. All experiments were performed a minimum of three times with independent biological replicates to ensure reproducibility. Statistical differences between control and experimental samples were determined using the Student's t-test. The sequences of the primers are listed below.

RT-qPCR primers

TBP forward:	5'- TGCTGTTGGTGATTGTTGGT -3'
TBP reverse:	5'- CTGGCTTGTGTGGGAAAGAT -3'
Nmnat1 forward:	5'- GTGCCCAACTTGTGGAAGAT -3'
Nmnat1 reverse:	5'- CAGCACATCGGACTCGTAGA -3'
Nmnat2 forward:	5'- CCGTCTCATCATGTGTCAGC -3'
Nmnat2 reverse:	5'- ACACACTGCAGGTTGTCTGC -3'
Parp1 forward:	5'- TGGTTTCAAGTCCCTTGTCC -3'
Parp1 reverse:	5'- TGCTGTCTATGGAGCTGTGG -3'
Nampt forward:	5'- ATCCAGGAGGCCAAAGAAGT -3'
Nampt reverse:	5'- ATCGGGAGATGACCATCGTA -3'

Cebpb forward:	5’- CAAGCTGAGCGACGAGTACA -3’
Cebpb reverse:	5’- CAGCTGCTCCACCTTCTTCT -3’
Cebpd forward:	5’- TGCCCACCCTAGAGCTGTG -3’
Cebpd reverse:	5’- CGCTTTGTGGTTGCTGTTGA -3’
Cebpa forward:	5’- GAACAGCAACGAGTACCGGGTA -3’
Cebpa reverse:	5’- GCCATGGCCTTGACCAAGGAG -3’
Pparg2 forward:	5’- TGCTGTTATGGGTGAAACTCT -3’
Pparg2 reverse:	5’- CGCTTGATGTCAAAGGAATGC -3’
Fabp4 forward:	5’- AAGTGGGAGTGGGCTTTGC -3’
Fabp4 reverse:	5’- CCGGATGGTGACCAAATCC -3’
Adipoq forward:	5’- GACAAGGCCGTTCTCTTCAC -3’
Adipoq reverse:	5’- CAGACTTGGTCTCCCACCTC -3’
Hk2 forward:	5’- TGATCGCCTGCTTATTCACGG -3’
Hk2 reverse:	5’- AACCGCCTAGAAATCTCCAGA-3’
Pgk1 forward:	5’- ATGTCGCTTTCCAACAAGCTG -3’
Pgk1 reverse:	5’- GCTCCATTGTCCAAGCAGAAT -3’
Pgam1 forward:	5’- TCTGTGCAGAAGAGAGCAATCC -3’
Pgam1 reverse:	5’- CTGTCAGACCGCCATAGTGT -3’
Pfkp forward:	5’- GAAACATGAGGCGTTCTGTGT -3’
Pfkp reverse:	5’- CCCGGCACATTGTTGGAGA -3’
Pfkl forward:	5’- GGAGGCGAGAACATCAAGCC -3’
Pfkl reverse:	5’- CGGCCTTCCCTCGTAGTGA -3’

ChIP-qPCR primers

Cebpa promoter forward: 5'- CTGGAAGTGGGTGACTTAGAGG -3'

Cebpa promoter reverse: 5'- GAGTGGGGAGCATAGTGCTAG -3'

Pparg2 promoter forward: 5'- GGCCAAATACGTTTATCTGGTG -3'

Pparg2 promoter reverse: 5'- GTGAGGGGCGTGAACTGTA -3'

RNA-seq

Generation of RNA-seq libraries. Two biological replicates of control, *Nmnat1*, and *Parp1* knockdown 3T3-L1 cells were differentiated as described above. Total RNA was isolated using the RNeasy kit (Qiagen) according to the manufacturer's instructions. The total RNA was then enriched for polyA+ RNA using Dynabeads Oligo(dT)25 (Invitrogen). The polyA+ RNA was then used to generate strand-specific RNA-seq libraries as described previously (Zhong et al., 2011). The RNA-seq libraries were subjected to QC analyses (i.e., number of PCR cycles required to amplify each library, the final library yield, and the size distribution of final library DNA fragments) and sequenced using an Illumina HiSeq 2000.

Analysis of RNA-seq data. The raw data were subjected to QC analyses using the FastQC tool (Andrews, 2015). The reads were then mapped to mouse genome (mm10) using the spliced reader aligner TopHat version.2.0.13 (Kim et al., 2013). Transcriptome assembly was performed using cufflinks v.2.2.1 (Trapnell et al., 2010) with default parameters. The transcripts were merged into two distinct, non-overlapping sets using cuffmerge, followed by cuffdiff to call the differentially regulated transcripts. The significantly ($p < 0.05$) regulated

genes upon Nmnat1 or Parp1 knockdown compared to control knockdown at the indicated time points were used to find the commonly regulated gene set.

Linking TFs to gene regulation. In order to determine the transcription factors that bind upstream of the Nmnat1 and Parp1 commonly regulated genes, we queried publicly available ChIP-seq data sets for C/EBPβ, STAT5A, RXRα, C/EBPδ, and GR (NCBI GEO accession number GSE27826) and the called peaks from these data sets were lifted over to mm10. A genomic region 50 kb upstream of the transcription start site (TSS, +1) of each Nmnat1 and Parp1 commonly regulated gene at day 2 and day 4 was extracted. We then determined the binding of each of the transcription factors within the 50 kb upstream regions using the coordinates from the ChIP-seq peak files. To determine the expression of the nearest neighboring genes to sites of transcription factor binding, we (1) used Homer (http://homer.salk.edu/homer/) to find the genes located nearest to the transcription factor binding sites of interest and (2) determined their expression (FPKM > 1) in various conditions compared to the control knockdown cells at day 0 of differentiation to calculate the fold change for each gene.

Staining of intracellular lipids

BODIPY staining. 3T3-L1 cells were seeded on sterile cover slips in 24-well plates and differentiated as described above. The cells were rinsed twice with 1x PBS and fixed with 4% paraformaldehyde. The fixed cells were washed twice with 1x PBS and stained with 1 μg/ml of BODIPY 493/503 (Life Technologies, D3922) for 10 minutes. The cells were then washed three times with 1x PBS and counterstained with 1 μM TO-PRO-3 (Life

Technologies, T3605) for 2 minutes. The cover slips were then mounted onto glass slides with VECTASHIELD Mounting Medium (Vector Laboratories, H-1000). Confocal images were acquired using a Leica SP2 confocal microscope.

Oil Red O staining. 3T3-L1 cells were cultured in 6 well plates and differentiated as described above. After 8 days of differentiation, the cells were rinsed twice with 1x PBS and fixed with 4% paraformaldehyde. The fixed cells were washed with water and incubated in 60% isopropanol for 5 minutes. After incubation, the isopropanol was removed and replaced with a 0.3% Oil Red O working solution [prepared by diluting a stock solution (0.5% in isopropanol; Sigma, O1391) with water (3:2)] for an additional 5 minute incubation. Visible light images were acquired by digital photography.

Measurement of total intracellular NAD^+ levels

3T3-L1 cells were cultured and differentiated as described above. For NAD^+ measurements, the cells were harvested with 0.5 M perchloric acid and neutralized with and equal volume of 0.55 M of K_2CO_3. The samples were then centrifuged and the supernatants were collected for metabolite measurement. Total intracellular NAD^+ or NADH levels were measured using an NAD^+/NADH colorimetric assay kit (Cyclex, CY-1253) following the manufacturer's instructions.

Determination of intracellular NAD^+/NADH ratios using a ratiometric sensor

Intracellular NAD^+/NADH ratios in 3T3-L1 cells were determined using the Peredox-mCherry system (Hung et al., 2011), modified for nuclear imaging as described above. 3T3-

L1 cells expressing Peredox-mCherry-NLS were seeded on chambered cover slips (Thermo Fisher, 155411) and cultured in DMEM without phenol red (Life Technology, 21063029) supplemented with 10% fetal bovine serum (Atlanta Biologicals, S11550) and 1% penicillin/streptomycin. Before imaging, adipogenesis was induced for indicated times, as described above. In each condition, more than 300 nuclei were imaged for quantification.

Confocal images were acquired on an inverted Leica LSM 780 affixed with a 37°C, 5% CO_2 incubator. Images were taken as described previously (Hung et al., 2011), with modifications. The excitation wavelength for Peredox and mCherry were 405 nm and 594 nm, respectively, with emission at 490 -553 nm and 597 - 695 nm, respectively. Images were acquired with ~10 μm thickness using a Plan-Apochromat 20x/0.8 M27 objective. Green fluorescence from Peredox was used to measure the relative NADH/NAD^+ ratio and red fluorescence from mCherry was used to normalize sensor expression. We used ImageJ software (Collins, 2007; Schneider et al., 2012) or a custom MATLAB program to subtract background, set thresholds to avoid artifacts from the ratiometric analysis, and generate a pixel-by-pixel green to red ratio image for each time point. To derive the relative NAD^+/NADH ratio, we took the inverse of the ratiometric values. Fluorescence values for undifferentiated 3T3-L1 cells were defined as 1, and the rest of the data were normalized accordingly. Normalized values were mapped back to the image using a custom MATLAB program.

Determination of relative NADH levels using autofluorescence

Intracellular NADH autofluorescence was measured by using two-photon microscopy. 3T3-L1 cells were cultured on chambered cover slips (Thermo Fisher, 155411) and were differentiation as described above. Experiments were performed as described previously (Zhang et al., 2012) with modifications. The excitation and emission wavelengths were 740 nm and 410-553 nm, respectively. Images were acquired using an inverted Leica LSM 780 affixed with a 37°C, 5% CO_2 incubator. All images were obtained using the same imaging conditions (e.g. detector gain, etc.) for signal comparison. Nuclear and cytoplasmic regions were selected from the images based on intensity threshold and the morphology of the cells, and the average intensities were calculated using ImageJ.

Measurement of nuclear and cytoplasmic NAD^+ levels using cellular NAD^+ sensors

3T3-L1 cells expressing nuclear or cytoplasmic NAD^+ sensors, as well as corresponding cpVenus control (see above), were used to measure NAD^+ levels in the different subcellular compartments. The cells were treated with 1 μg/mL of doxycycline for 48 hours prior to the experiment to induce the expression of the censors and the cpVenus control. NAD^+ sensor experiments were performed as described previously (Cambronne et al., 2016), with details described below.

Protein purification. The sensors and cpVenuses were transfected into 293T cells with lipfectamine 3000 (Thermo Fisher, L3000015) following the manufacturer's protocol. After 48 hours, cells were washed twice with ice-cold PBS and collected via centrifugation. Cytoplasmic sensor and cpVenus were lysed using lysis buffer (50 mM Tris-HCl pH 7.4, 150 mM NaCl, 1 mM EDTA, 0.5% IGEPAL CA-630, 1 mM DTT and 1x complete protease

inhibitor cocktail), incubated for 30 minutes at 4°C, and clarified by centrifugation. For the nuclear sensor and cpVenus, cells were incubated in isotonic buffer (10 mM Tris-HCl pH 7.5, 2 mM $MgCl_2$, 3 mM $CaCl_2$, 0.3 M sucrose, 1 mM DTT, and 1x complete protease inhibitor cocktail) on ice for 15 minutes and lysed by the addition of 0.6% IGEPAL CA-630 detergent. Nuclei were pelleted by the centrifugation and resuspended in nuclear extraction buffer (50 mM Tris-HCl pH 7.4, 150 mM NaCl, 1 mM EDTA, 1 % IGEPAL CA-630, 1 mM DTT, and 1x complete protease inhibitor cocktail). Nuclear extract was incubated for 30 minutes 4°C, and clarified by centrifugation. Both lysate and nuclear extract were incubated with anti-FLAG M2 affinity gel (Sigma, A2220) at 4°C for 4 hours and then washed five times in either the lysis buffer or the nuclear extraction buffer, respectively, for 10 minutes at 4°C with constant mixing. Proteins were eluted with 500 μg/mL of 3x FLAG peptide (Sigma, F4799) and dialyzed in the buffer containing 100 mM Tris-HCl pH 7.4, 150 mM NaCl, 1 mM EDTA, 0.5 mM DTT, 100 μM PMSF, and 20% glycerol. Concentrations of the proteins were measured by Bradford assays. Purity of the sensors and cpVensuses were confirmed by silver staining using Pierce silver staining kit (Thermo Fisher, 24600) following the manufacturer's protocol.

Measurement of in vitro fluorescence changes using spectroscopy. Purified sensors and cpVenuses (250 nM) were incubated with indicated amount of NAD^+ in a total 75 μL of the reaction volume. Samples were incubated in RT for 15 minutes and the fluorescence were measured using a TECAN spark 20M plate reader. Excitation and emission spectra were 488 nm and 530 nm, respectively, with slit widths of 5 nm band pass for the excitation and 10 nm band pass for the emission. *In vitro* standard curve were generated using the ratio of obtained

fluorescence values ($\frac{Sensor\ fluorescence}{cpVenus\ fluorescence}$) and were fitted to a sigmoidal regression model using GraphPad Prism 7.

Imaging. 3T3-L1 cells were seeded on chambered cover slips (Thermo Fisher, 155411) and cultured in FluoroBrite medium (Thermo Fisher, A1896701) supplemented with 10% FBS (TET tested; Atlanta Biologicals, S103050) and 1% penicillin/streptomycin. Confocal images were acquired on an inverted Leica LSM 780 microscope affixed with a 37°C, 5% CO_2 incubator. To measure NAD^+-dependent changes in fluorescence, both the sensors and the cpVenus control were imaged with excitation at 488 nm and emission at 525 nm. The expression levels of the sensors and cpVenus were measured using excitation at 405 nm and emission at 525 nm.

Image analysis. We used ImageJ to subtract background, set thresholds, select regions of interest (ROI), and quantify fluorescence intensities. Ratiometric measurements (488/405 nm) of the sensors and cpVenus were used to normalize sensor expression levels and to analyze the changes in subcellular NAD^+ levels. To generate a pixel-by-pixel ratiometric image, a custom MATLAB program was used. Average ratiometric values for the undifferentiated 3T3-L1 cells were defined as 1, and the rest of the data were normalized accordingly.

Flow cytometry. 3T3-L1 cells were cultured and differentiated as described above. For flow cytometry analysis, the cells were trypsinized and resuspended in FluoroBrite medium containing 10% FBS and 1% penicillin/streptomycin. The data were collected on a BD LSR II flow cytometer (BD Biosciences). The cells were gated using forward scatter (FSC) and side scatter (SSC) for the live cells and then further gated for both SSC and FSC

width to ensure that individual cells were analyzed. FITC (excitation 488 nm, emission 530/30 nm) and BV510 (excitation 405 nm, emission 525/50 nm) were used to measure the sensor and the cpVenus fluorescence. Samples of $1x10^4$ cells each were evaluated for the nuclear cpVenus, cytoplasmic sensor, and cytoplasmic cpVenus. A sample of $5x10^4$ cells was evaluated for the nuclear sensor due to relatively low expression of the sensor. 3T3-L1 cells without fluorescent protein were used as a negative control to set a threshold for the analysis. The data were analyzed with FlowJo software (https://www.flowjo.com) and ratiometric analyses were performed using the derived function in the software. Cells expressing high levels of sensor or cpVenus were subjected to ratiometric analysis (488/405 nm) to obtain values. Geometric mean fluorescence intensity of the ratio was determined in each conditions and the ratiometric values of the sensor were divided by the ratiometric values of cpVenus to account for the pH effect ($\frac{Sensor\ (488/405)}{cpVenus(488/405)}$). Changes in subcellular NAD^+ levels were analyzed by normalizing the values relative to the undifferentiated or control 3T3-L1 cells.

Cell permeablization and treatment with NAD$^+$. 3T3-L1 cells expressing the sensors and cpVenus were cultured as described above. To generate a dose-response curve for NAD^+ detection, the cells were trypsinized and suspended with FluoroBrite medium containing 10% FBS and 1% penicillin/streptomycin. The cells were then permeablized with 0.001% digitonin and the indicated amount of NAD^+ with subsequent incubation at RT for 15 minutes. The samples were subjected to flow cytometry and analyzed as described above. All the values were plotted relative to the values obtained from 10 μM NAD^+ treatment and the values from 8 biological replicates were used to generate the standard curve. For imaging

analyses, cells were cultured on chambered cover slips as described above. After acquiring images for the untreated condition, 0.001% digitonin and the indicated amount of NAD^+ were added to the medium and equilibrated for 15 minutes to obtain NAD^+-dependent changes in signal. Images were analyzed as described above.

Calculation of the free intracellular NAD$^+$. To determine the free intracellular NAD^+ level, the standard curve generated from the NAD^+ permeablization assays above were fitted into a sigmoidal regression model using GraphPad Prism 7 ($y = min + [\frac{max-min}{1+10^{(logIC50-\chi)\times Hillslope}}]$). Ratiometric values relative to 10 μM NAD^+ treatment were subjected the equation as an y value to calculate free intracellular (nuclear or cytoplasmic) NAD^+ level. Due to the variability of the measurement, average of 32 biological replicates from 11 independent experiments were interpolated to obtain values for x. To measure the changes in NAD^+ level, fluorescence ratio was measured using flowcytometry as described above and normalized to the control conditions (e.g. undifferentiated 3T3-L1). Relative ratiometric values were then interpolated onto *in vitro* standard curve to obtain NAD^+ concentration.

Analysis of metabolic flux

3T3-L1 cells were grown to confluence, and then grown for another two days under contact inhibition. Induction of adipogenesis was achieved as described above until indicated time points. To quantify different mass isotopomers of intracellular citrate by GC/MS (Mullen et al., 2012), the cells were washed with PBS and incubated in medium containing an isotopically enriched nutrient (i.e., D[U-^{13}C]glucose and unlabeled glutamine

for measuring glucose flux) for 1 minute or 5 minutes. Labeled cells were then rinsed with ice-cold normal saline and lysed with three freeze-thaw cycles in cold 50% methanol/50% water. The lysates were centrifuged to remove precipitated proteins and a standard (50 nmols of sodium 2-oxobutyrate) was added. The samples were then evaporated and derivatized using tertbutyldimethylsilyl (TBDMS). Five microliters of the derivatized sample was injected into an Agilent 6970 gas chromatograph equipped with a fused silica capillary GC column and networked to an Agilent 5973 mass selective detector. Retention times of citrate were validated using pure standards. The abundance of the citrate ions was monitored at m/z 459, pyruvate at m/z 174-177, and lactate at m/z 261-264. The measured distribution of mass isotopomers was corrected for the natural abundance of ^{13}C. M+2 indicates the percent abundance of citrate, two carbons of which were ^{13}C-labeled, providing a measure of glucose flux through the TCA cycle. M+4 indicates the percent abundance of citrate, four carbons of which were ^{13}C-labeled, providing a measure of glutamine flux through TCA cycle.

3.6 References

Andrews, S. (2015). FastQC: A quality control tool for high throughput sequence data.

Boukouris, A.E., Zervopoulos, S.D., and Michelakis, E.D. (2016). Metabolic Enzymes Moonlighting in the Nucleus: Metabolic Regulation of Gene Transcription. Trends in biochemical sciences *41*, 712-730.

Cambronne, X.A., Stewart, M.L., Kim, D., Jones-Brunette, A.M., Morgan, R.K., Farrens, D.L., Cohen, M.S., and Goodman, R.H. (2016). Biosensor reveals multiple sources for mitochondrial NAD(+). Science *352*, 1474-1477.

Canto, C., Houtkooper, R.H., Pirinen, E., Youn, D.Y., Oosterveer, M.H., Cen, Y., Fernandez-Marcos, P.J., Yamamoto, H., Andreux, P.A., Cettour-Rose, P.*, et al.* (2012). The NAD(+) precursor nicotinamide riboside enhances oxidative metabolism and protects against high-fat diet-induced obesity. Cell metabolism *15*, 838-847.

Chiarugi, A., Dolle, C., Felici, R., and Ziegler, M. (2012). The NAD metabolome--a key determinant of cancer cell biology. Nature reviews Cancer *12*, 741-752.

Collins, T.J. (2007). ImageJ for microscopy. BioTechniques *43*, 25-30.

Consortium, G.T. (2015). Human genomics. The Genotype-Tissue Expression (GTEx) pilot analysis: multitissue gene regulation in humans. Science *348*, 648-660.

Cristancho, A.G., and Lazar, M.A. (2011). Forming functional fat: a growing understanding of adipocyte differentiation. Nature reviews Molecular cell biology *12*, 722-734.

Gibson, B.A., and Kraus, W.L. (2012). New insights into the molecular and cellular functions of poly(ADP-ribose) and PARPs. Nature reviews Molecular cell biology *13*, 411-424.

Gupta, R.K., Mepani, R.J., Kleiner, S., Lo, J.C., Khandekar, M.J., Cohen, P., Frontini, A., Bhowmick, D.C., Ye, L., Cinti, S.*, et al.* (2012). Zfp423 expression identifies committed preadipocytes and localizes to adipose endothelial and perivascular cells. Cell metabolism *15*, 230-239.

Houtkooper, R.H., Pirinen, E., and Auwerx, J. (2012). Sirtuins as regulators of metabolism and healthspan. Nature reviews Molecular cell biology *13*, 225-238.

Hung, Y.P., Albeck, J.G., Tantama, M., and Yellen, G. (2011). Imaging cytosolic NADH-NAD(+) redox state with a genetically encoded fluorescent biosensor. Cell metabolism *14*, 545-554.

Kim, D., Pertea, G., Trapnell, C., Pimentel, H., Kelley, R., and Salzberg, S.L. (2013). TopHat2: accurate alignment of transcriptomes in the presence of insertions, deletions and gene fusions. Genome biology *14*, R36.

Kim, M.Y., Mauro, S., Gevry, N., Lis, J.T., and Kraus, W.L. (2004). NAD+-dependent modulation of chromatin structure and transcription by nucleosome binding properties of PARP-1. Cell *119*, 803-814.

Kininis, M., Chen, B.S., Diehl, A.G., Isaacs, G.D., Zhang, T., Siepel, A.C., Clark, A.G., and Kraus, W.L. (2007). Genomic analyses of transcription factor binding, histone acetylation, and gene expression reveal mechanistically distinct classes of estrogen-regulated promoters. Molecular and cellular biology *27*, 5090-5104.

Krishnakumar, R., Gamble, M., Frizzell, K., Berrocal, J., Kininis, M., and Kraus, W. (2008). Reciprocal binding of PARP-1 and histone H1 at promoters specifies transcriptional outcomes. Science *319*, 819-821.

Lu, C., and Thompson, C.B. (2012). Metabolic regulation of epigenetics. Cell metabolism *16*, 9-17.

Luo, X., Chae, M., Krishnakumar, R., Danko, C.G., and Kraus, W.L. (2014). Dynamic reorganization of the AC16 cardiomyocyte transcriptome in response to TNFalpha signaling revealed by integrated genomic analyses. BMC genomics *15*, 155.

Luo, X., Ryu, K.W., Kim, D.S., Nandu, T., Medina, C.J., Gupte, R., Gibson, B.A., Soccio, R.E., Yu, Y., Gupta, R.K.*, et al.* (2017). PARP-1 Controls the Adipogenic Transcriptional Program by PARylating C/EBPbeta and Modulating Its Transcriptional Activity. Molecular cell *65*, 260-271.

Meerbrey, K.L., Hu, G., Kessler, J.D., Roarty, K., Li, M.Z., Fang, J.E., Herschkowitz, J.I., Burrows, A.E., Ciccia, A., Sun, T.*, et al.* (2011). The pINDUCER lentiviral toolkit for inducible RNA interference in vitro and in vivo. Proceedings of the National Academy of Sciences of the United States of America *108*, 3665-3670.

Mullen, A.R., Wheaton, W.W., Jin, E.S., Chen, P.H., Sullivan, L.B., Cheng, T., Yang, Y., Linehan, W.M., Chandel, N.S., and DeBerardinis, R.J. (2012). Reductive carboxylation supports growth in tumour cells with defective mitochondria. Nature *481*, 385-388.

Revollo, J.R., Grimm, A.A., and Imai, S. (2004). The NAD biosynthesis pathway mediated by nicotinamide phosphoribosyltransferase regulates Sir2 activity in mammalian cells. The Journal of biological chemistry *279*, 50754-50763.

Rosen, E.D., and MacDougald, O.A. (2006). Adipocyte differentiation from the inside out. Nature reviews Molecular cell biology *7*, 885-896.

Ryu, K.W., Kim, D.S., and Kraus, W.L. (2015). New facets in the regulation of gene expression by ADP-ribosylation and poly(ADP-ribose) polymerases. Chemical reviews *115*, 2453-2481.

Sasaki, Y., Nakagawa, T., Mao, X., DiAntonio, A., and Milbrandt, J. (2016). NMNAT1 inhibits axon degeneration via blockade of SARM1-mediated NAD+ depletion. eLife *5*.

Schneider, C.A., Rasband, W.S., and Eliceiri, K.W. (2012). NIH Image to ImageJ: 25 years of image analysis. Nature methods *9*, 671-675.

Siersbaek, R., Nielsen, R., and Mandrup, S. (2012). Transcriptional networks and chromatin remodeling controlling adipogenesis. Trends in endocrinology and metabolism: TEM *23*, 56-64.

Trapnell, C., Williams, B.A., Pertea, G., Mortazavi, A., Kwan, G., van Baren, M.J., Salzberg, S.L., Wold, B.J., and Pachter, L. (2010). Transcript assembly and quantification by RNA-Seq reveals unannotated transcripts and isoform switching during cell differentiation. Nat Biotechnol *28*, 511-515.

Wellen, K.E., Hatzivassiliou, G., Sachdeva, U.M., Bui, T.V., Cross, J.R., and Thompson, C.B. (2009). ATP-citrate lyase links cellular metabolism to histone acetylation. Science *324*, 1076-1080.

Zhang, T., Berrocal, J.G., Yao, J., DuMond, M.E., Krishnakumar, R., Ruhl, D.D., Ryu, K.W., Gamble, M.J., and Kraus, W.L. (2012). Regulation of poly(ADP-ribose) polymerase-1-dependent gene expression through promoter-directed recruitment of a nuclear NAD+ synthase. The Journal of biological chemistry *287*, 12405-12416.

Zhong, S., Joung, J.G., Zheng, Y., Chen, Y.R., Liu, B., Shao, Y., Xiang, J.Z., Fei, Z., and Giovannoni, J.J. (2011). High-throughput illumina strand-specific RNA sequencing library preparation. Cold Spring Harb Protoc *2011*, 940-949.